Title

The calcium-activated chloride channel ANOl regulates gastrointestinal motility, mammary growth and sperm physiology

Author

Pardo, David M.

Publication Date

2016

Peer reviewed|Thesis/dissertation

The calcium-activated chloride channel ANO1 regulates gastrointestinal motility, mammary growth and sperm physiology

by

David M Pardo

DISSERTATION

Submitted in partial satisfaction of the requirements for the degree of

DOCTOR OF PHILOSOPHY

in

Biomedical Sciences

in the

GRADUATE DIVISION

of the

UNIVERSITY OF CALIFORNIA, SAN FRANCISCO

Acknowledgments

My projects involved the help of many colleagues, friends and mentors. Firstly, I would like to thank my advisor Jason Rock for his continuous support and guidance. I would like to thank Jayanta Debnath and Jeroen Roose for serving on my thesis committee and providing valuable feedback during my studies. I would also like to express my gratitude to Sean Ward and the members of his laboratory at the University of Nevada in Reno for collaborating with us and sharing their expertise in gastrointestinal physiology. I give my thanks to Polina Lishko from the University of California in Berkeley for providing advice with my sperm physiology project. I would like to thank Paolo Rinaudo and the members of his laboratory for providing training in mouse IVF techniques and guidance with my experiments. Lastly, I would like to thank the other members of the Rock lab including Matthew Donne, Ian Driver, Gorica Amidzic and Andrew Lechner for their suggestions and help with my projects. I especially would like to thank Sonali Verma for assisting with mouse colony responsibilities and experiments.

My research was supported by a National Science Foundation Graduate Research Fellowhsip.

Abstract

ANO1 was recently shown to be a critical component of the calcium-activated chloride conductance that regulates numerous physiological processes including epithelial secretion, smooth muscle contraction and tumor growth. Previous studies have also suggested that chloride currents regulate mammary branching morphogenesis and sperm activation during fertilization. However, the premature mortality of *Ano1*$^{n/n}$ mice has hindered characterization of the diverse roles of ANO1 in adult mouse physiology. In the current studies, *Ano1*$^{f/f}$ mice were used in combination with two different Cre recombinase alleles (*c-Kit*^{CreERT2} and *MMTV-Cre*) to specifically disrupt ANO1 expression in adult gastrointestinal tissues and mammary gland. The results show that ANO1-mediated slow waves regulate gastrointestinal motility in adult mice and loss of ANO1 delays mammary development during puberty. We also show that ANO1 promotes *MMTV-PyMT* mammary tumor growth *in vitro* and *in vivo*. Finally, using *Ano1*$^{n/+}$ mice we demonstrate a novel role for ANO1 in the regulation of sperm capacitation and fertilization *in vitro* and *in vivo*.

Table of Contents

List of Figures:

Chapter 1: Introduction

1.1 ANO1 is a calcium-activated chloride channel

The calcium-activated chloride conductance (CaCC) was first described more than 25 years ago, but its genetic identity was unknown until recently[1–3]. In 2008, several groups independently discovered that Anoctamin 1 (ANO1) mediates a component of the calcium-induced chloride current[4–6] and demonstrates the properties of native CaCCs including activation at positive membrane potentials, deactivation at negative membrane potentials and activation by Ca^{2+} in the cytosol with an increased affinity for Ca^{2+} at more positive membrane potentials[1].

The current model for the function of ANO1 during epithelial secretion in secretory acini is outlined in Figure 1. NKCC1 cotransporter, found in the basolateral membrane of acinar cells, maintains intracellular chloride at a higher concentration than outside of the cell. Activation of g-protein coupled receptors (GPCRs) stimulates IP_3-mediated release of Ca^{2+} from intracellular stores, which bind to and open ANO1 channels leading to the efflux of Cl^- anions and the generation of an osmotic driving force for the luminal secretion of water through aquaporin channels.[7] In addition to epithelial secretion, CaCC currents regulate a number of physiological processes including cell volume changes, proliferation, migration, and smooth muscle contraction[1]. Accordingly, since its identification as the source of CaCC activity, ANO1 expression has been confirmed in a variety of organs in which calcium-induced chloride currents had been previously described including salivary glands, lung airways, testis, gastrointestinal smooth muscle and pancreas[8–10].

1.1 Mouse studies on physiological functions of ANO1

To determine the functional importance of ANO1 expression across organ systems, a mouse homozygous for a null allele (*Ano1*$^{n/n}$) was generated[11]. *Ano1*$^{n/n}$ mice do not survive beyond the first month of postnatal life as a result of several defects including tracheal malformations[11], impaired gastrointestinal pacemaker activity[12] and reduced epithelial secretion[13]. The lethality of ANO1 loss highlights its importance in mouse physiology during development and early neonatal life. Consequently, since the animals do not survive beyond several weeks, investigation of the role of ANO1 in adult organ function and physiology was not possible.

To characterize the functional importance of ANO1 in adult tissues and organs, transgenic mice carrying *ANO1* flanked by loxP sites (*Ano1*$^{f/f}$) were generated[14]. This enabled the genetic disruption of ANO1 expression in a tissue-specific manner through crossing *Ano1*$^{f/f}$ animals with animals expressing Cre recombinase. Experiments utilizing ANO1 conditional knockout mouse models have shown that ANO1-mediated chloride currents regulate diverse physiological processes in adult mice including salivary[15] and kidney[16] epithelial secretion, and sensory transduction[17]. However, the precise role of ANO1 in the development and function of other secretory acini and the regulation of smooth muscle contraction in adult mice remains to be explored.

1.2 ANO1 regulates gastrointestinal motility in neonates

Prior to the identification of the molecular source of CaCC activity, the conductance had been detected throughout the gastrointestinal (GI) tract[18,19]. Interstitial cells of Cajal (ICCs) found within the *tunica muscularis* provide a CaCC-mediated pacemaker mechanism to GI smooth muscle contractions[19]. Specifically, ICCs actively and continuously generate calcium-

induced chloride currents, which trigger membrane potential oscillations called slow waves, whereby the membrane potential shifts between negative and more positive values[19]. The close proximity of ICCs to smooth muscle cells and their connection by gap junctions, enables the propagation of slow waves from ICCs to adjacent smooth muscle cells where the slow waves regulate activation of voltage-gated calcium channels and thereby control excitation-contraction coupling[19]. In this way, ICC-generated slow waves organize the contractile behavior of smooth muscle cells to control gastrointestinal motility and transit.

Previous experiments using *Ano1*$^{n/n}$ animals have demonstrated that ANO1 is required for the generation of slow waves in the small intestine and antrum of the stomach[12]. Microelectrode recordings were performed on intact muscle strips isolated from *Ano1*$^{n/n}$ animals and slow waves were absent in gastric antrum and small intestines from these mice[12]. In contrast, *Ano1*$^{n/+}$ littermates displayed normal slow wave activity. While this study demonstrated that ANO1-mediated currents are responsible for the generation of gastrointestinal slow waves, the physiological consequences of their loss in adult mice could not be assessed. A number of impairments in *Ano1*$^{n/n}$ animals could be contributing to their morbidity, since CaCC activity has been implicated in the function of a diversity of organs. It is therefore difficult to ascertain whether defects in GI motility are specifically causing the early mortality of *Ano1*$^{n/n}$ animals. The importance of ANO1 in generating slow waves and regulating intestinal motility in adult mice is also currently unknown.

1.2 Investigating the role of ANO1 in regulating slow waves and gastrointestinal motility in adult mice

To determine whether ANO1 expression in adult ICCs is required for GI slow wave production and motility, animals expressing inducible Cre recombinase under the control of the c-Kit promoter (*c-Kit*^{CreERT2}) were crossed with those harboring ANO1 flanked by loxP sites (*Ano1*$^{f/f}$). After confirming effective recombination within ICCs following tamoxifen treatment, the reduction in ANO1 expression in ICCs was analyzed using confocal microscopy of whole mount preparations and qPCR analysis. Then *in vivo* motility experiments were performed to quantify total gastrointestinal transit time, small intestine transit and gastric emptying. Microelectrode recordings were also used to analyze slow wave activity within gastric antrum and small intestine smooth muscles. The results of the study showed that reducing ANO1 expression within adult GI organs reproducibly abrogated slow waves in gastric antrum but not the small intestine. This loss of slow waves in gastric antrum was sufficient to delay total transit time for orally administered semi-solid food. It also reduced gastric emptying in the animals.

1.3 Mammary gland ductal cells exhibit CaCC activity

A previous study suggested that ANO1 is responsible for a calcium-induced chloride conductance in mammary epithelial cells from a lactating mouse[20]. There is also evidence that in addition to controlling epithelial secretion, chloride transport regulates mammary gland (MG) development[21], but the role of ANO1 in mammary branching morphogenesis and physiology is an unexplored question.

1.3 Investigating the role of ANO1 in mouse mammary gland development

To determine the functional importance of ANO1 in mouse MG development, animals expressing Cre recombinase under the control of the MMTV promoter (*MMTV-Cre*^{D}; herafter

referred to as *M-Cre*) were crossed with *Ano1*$^{f/f}$ animals. Adult control mice demonstrate localized ANO1 expression in the luminal facing membrane of MG ducts, which is reduced in *M-Cre*; *Ano1*$^{f/f}$ mammary glands. Analysis of mammary whole mounts from these animals showed that loss of ANO1 during puberty delays MG development in 8 week old mice, but is ultimately dispensable for complete maturation.

1.4 ANO1 amplification and overexpression in various cancer subtypes promotes tumor growth

Preceding the identification of ANO1 as the source of calcium-induced chloride currents, its upregulation in a variety of cancers led to the gene being known under several names including tumor-amplified and overexpressed sequence 2 (*TAOS2*), discovered on gastrointestinal stromal tumors protein 1 (*DOG1*), oral cancer overexpressed 2 (*ORAOV2*)[22–24]. ANO1 is encoded by the 11q13 chromosomal region, which is frequently amplified in human cancers. It was recently shown that overexpression and amplification of ANO1 correlates with worse survival and prognosis in breast cancer and knocking down ANO1 expression in 11q13-amplified human breast cancer cells decreased their growth *in vitro* and *in vivo*[25]. Studies in squamous cell carcinoma of the head and neck (HNSCC) and breast cancer have demonstrated that ANO1 promotes tumor growth through activation of EGFR and CAMKII-dependent signaling pathways and stimulation of EGF secretion[26–28]. ANO1 was also shown to directly interact with and stabilize EGFR to promote growth of HNSCC cells[26]. While these experiments and others have established the importance of ANO1 in supporting tumor growth through activation of EGFR-mediated signaling pathways, the functional roles of ANO1 during various

stages of tumor progression *in vivo* including initiation, invasion and metastasis are currently unknown.

Genetically engineered mice have been invaluable tools for studying the roles of oncogenes and tumor suppressors in breast cancer initiation and progression in the context of intact immune environments[29,30]. One such model is the *MMTV-PyMT* allele that spontaneously induces formation of metastatic breast cancer in mice and has been used to determine the functions of specific proteins in distinct stages of tumorigenesis[30]. Since 11q13 amplification is often associated with the luminal subtype of breast cancer[31,32], the MMTV-PyMT mouse model could be useful for studying the role of ANO1 during various stages of cancer progression *in vivo*[33].

1.4 Investigating the role of ANO1 in MMTV-PyMT tumor growth

The goal of the study was to determine whether ANO1 promotes growth of MMTV-PyMT mammary tumors and establish whether this model can be used to study the functional role of ANO1 in specific stages of tumor growth *in vivo*. The results show that ANO1 is expressed in both primary and lung metastatic tumors in the MMTV-PyMT mouse model and a MMTV-PyMT cell line exhibits a calcium-induced chloride conductance. Disrupting ANO1 in the cell line reduced growth *in vitro* and i*n vivo*. The mechanism of ANO1-mediated tumor growth appeared to be through an EGFR-dependent signaling pathway, since blocking EGFR and ANO1 did not have a synergistic effect. The results establish that the MMTV-PyMT model could be used for testing the functional role of ANO1 expression during different stages of spontaneous tumor growth *in vivo.*

1.5 Chloride transport regulates sperm physiology during fertilization

Upon ejaculation into the female reproductive tract, sperm encounter a different ionic composition than that of the seminal fluid[34]. Ion channels are involved in coordinating the biochemical changes that lead to the hyperactivation of sperm during the process of capacitation, which confers sperm the capacity to undergo the acrosome reaction during fertilization[35]. It has been shown that chloride transport is required for capacitation-associated processes and the acrosome reaction but the mechanism and required ion channels have not been fully characterized[34]. A previous study demonstrated that human sperm have a calcium-induced chloride conductance that is blocked with an ANO1-specific inhibitor. The ANO1 inhibitor also reduces *in vitro* ZP3-induced acrosome reaction [36]. However, the localization and functions of ANO1 in sperm during capacitation and fertilization have not been determined.

1.5 Investigating the role of ANO1 in sperm capacitation, acrosome reaction and fertilization

The goal of the study was to determine the localization of ANO1 in mouse sperm and its role in capacitation, the acrosome reaction and fertilization. Wild-type mice express ANO1 in the acrosome region of sperm heads and it is reduced in sperm from *Ano1*$^{n/+}$ animals. Isolated *Ano1*$^{n/+}$ sperm showed increased frequencies of capacitation-associated processes including tyrosine phosphorylation and spontaneous acrosome reaction, which impaired *in vitro* fertilization ability. When bred conventionally, *Ano1*$^{n/+}$ males produced less offspring per litter than control males. These results suggest that ANO1 plays important roles during capacitation, the acrosome reaction and fertilization.

References

1. Pedemonte, N. & Galietta, L. J. V. Structure and function of TMEM16 proteins (anoctamins). *Physiol. Rev.* **94,** 419–59 (2014).
2. Hartzell, C., Putzier, I. & Arreola, J. Calcium-activated chloride channels. *Annu. Rev. Physiol.* **67,** 719–758 (2005).
3. Duran, C., Thompson, C. H., Xiao, Q. & Hartzell, H. C. *Chloride channels: often enigmatic, rarely predictable. Annual review of physiology* **72,** (2010).
4. Caputo, A. *et al.* TMEM16A, a membrane protein associated with calcium-dependent chloride channel activity. *Science* **322,** 590–594 (2008).
5. Schroeder, B. C., Cheng, T., Jan, Y. N. & Jan, L. Y. Expression cloning of TMEM16A as a calcium-activated chloride channel subunit. *Cell* **134,** 1019–1029 (2008).
6. Yang, Y. D. *et al.* TMEM16A confers receptor-activated calcium-dependent chloride conductance. *Nature* **455,** 1210–1215 (2008).
7. Lee, M. G., Ohana, E., Park, H. W., Yang, D. & Muallem, S. Molecular mechanism of pancreatic and salivary gland fluid and HCO3 secretion. *Physiol Rev* **92,** 39–74 (2012).
8. Huang, F. *et al.* Studies on expression and function of the TMEM16A calcium-activated chloride channel. (2009).
9. Ousingsawat, J. *et al.* Loss of TMEM16A causes a defect in epithelial Ca2+-dependent chloride transport. *J. Biol. Chem.* **284,** 28698–703 (2009).
10. Romanenko, V. G. *et al.* Tmem16A Encodes the Ca 2 ⁄ -activated Cl ⁄ Channel in Mouse Submandibular Salivary Gland Acinar Cells * □. (2010). doi:10.1074/jbc.M109.068544
11. Rock, J. R., Futtner, C. R. & Harfe, B. D. The transmembrane protein TMEM16A is

required for normal development of the murine trachea. *Dev Biol* **321,** 141–149 (2008).

12. Hwang, S. J. *et al.* Expression of anoctamin 1/TMEM16A by interstitial cells of Cajal is fundamental for slow wave activity in gastrointestinal muscles. *J Physiol* **587,** 4887–4904 (2009).
13. Ousingsawat, J. *et al.* Loss of TMEM16A causes a defect in epithelial Ca2+-dependent chloride transport. *J. Biol. Chem.* **284,** 28698–28703 (2009).
14. Faria, D. *et al.* The calcium-activated chloride channel Anoctamin 1 contributes to the regulation of renal function. *Kidney Int.* 1369–1381 (2014). doi:10.1038/ki.2013.535
15. Catalan, M. A. *et al.* A fluid secretion pathway unmasked by acinar-specific Tmem16A gene ablation in the adult mouse salivary gland. *Proc. Natl. Acad. Sci. U. S. A.* **112,** 2263–2268 (2015).
16. Faria, D. *et al.* The calcium-activated chloride channel Anoctamin 1 contributes to the regulation of renal function. *Kidney Int.* 1369–1381 (2014). doi:10.1038/ki.2013.535
17. Cho, H. *et al.* The calcium-activated chloride channel anoctamin 1 acts as a heat sensor in nociceptive neurons. *Nat. Neurosci.* **15,** 1015–1021 (2012).
18. Blair, P. J., Rhee, P. L., Sanders, K. M. & Ward, S. M. The significance of interstitial cells in neurogastroenterology. *J. Neurogastroenterol. Motil.* **20,** 294–317 (2014).
19. Sanders, K. M., Ward, S. M. & Koh, S. D. Interstitial cells: regulators of smooth muscle function. *Physiol Rev* **94,** 859–907 (2014).
20. Kamikawa, A., Ichii, O., Sakazaki, J. & Ishikawa, T. Ca^{2+} -activated Cl^{-} channel currents in mammary secretory cells from lactating mouse. *Am. J. Physiol. - Cell Physiol.* ajpcell.00050.2016 (2016). doi:10.1152/ajpcell.00050.2016
21. Shillingford, J. M., Miyoshi, K., Flagella, M., Shull, G. E. & Hennighausen, L. Mouse

mammary epithelial cells express the Na-K-Cl cotransporter, NKCC1: characterization, localization, and involvement in ductal development and morphogenesis. *Mol Endocrinol* **16,** 1309–1321 (2002).

22. Huang, X., Gollin, S. M., Raja, S. & Godfrey, T. E. High-resolution mapping of the 11q13 amplicon and identification of a gene, TAOS1, that is amplified and overexpressed in oral cancer cells. *Proc. Natl. Acad. Sci. U. S. A.* **99,** 11369–11374 (2002).

23. West, R. B. *et al.* The novel marker, DOG1, is expressed ubiquitously in gastrointestinal stromal tumors irrespective of KIT or PDGFRA mutation status. *Am. J. Pathol.* **165,** 107–13 (2004).

24. Kashyap, M. K. *et al.* Genomewide mRNA profiling of esophageal squamous cell carcinoma for identification of cancer biomarkers. *Cancer Biol. Ther.* **8,** 34–46 (2009).

25. Britschgi, A. *et al.* Calcium-activated chloride channel ANO1 promotes breast cancer progression by activating EGFR and CAMK signaling. *Proc. Natl. Acad. Sci. U. S. A.* **110,** E1026-34 (2013).

26. Bill, A. *et al.* ANO1 interacts with EGFR and correlates with sensitivity to EGFR-targeting therapy in head and neck cancer. *Oncotarget* **6,** 9173–9188 (2015).

27. Duvvuri, U. *et al.* TMEM16A induces MAPK and contributes directly to tumorigenesis and cancer progression. *Cancer Res.* **72,** 3270–81 (2012).

28. Britschgi, A. *et al.* Calcium-activated chloride channel ANO1 promotes breast cancer progression by activating EGFR and CAMK signaling. **110,** (2013).

29. Nash, C. & Speirs, V. Pre-Clinical Modeling of Breast Cancer: Which Model to Choose? 161–175 (2013). doi:10.1007/978-1-4614-5647-6_9

30. Vargo-Gogola, T. & Rosen, J. M. Modelling breast cancer: one size does not fit all. *Nat*

Rev Cancer **7,** 659–672 (2007).

31. Cerami, E. *et al.* The cBio cancer genomics portal: an open platform for exploring multidimensional cancer genomics data. *Cancer Discov* **2,** 401–404 (2012).

32. Gao, J. *et al.* Integrative analysis of complex cancer genomics and clinical profiles using the cBioPortal. *Sci Signal* **6,** pl1 (2013).

33. Lin, E. Y. *et al.* Progression to malignancy in the polyoma middle T oncoprotein mouse breast cancer model provides a reliable model for human diseases. *Am J Pathol* **163,** 2113–2126 (2003).

34. Buffone, M. G. *et al.* Heads or tails? Structural events and molecular mechanisms that promote mammalian sperm acrosomal exocytosis and motility. *Mol. Reprod. Dev.* **79,** 4–18 (2012).

35. Bailey, J. L. Factors Regulating Sperm Capacitation. *Syst. Biol. Reprod. Med.* **56,** 334–348 (2010).

36. Orta, G. *et al.* Human spermatozoa possess a calcium-dependent chloride channel that may participate in the acrosomal reaction. *J. Physiol.* **590,** 2659–75 (2012).

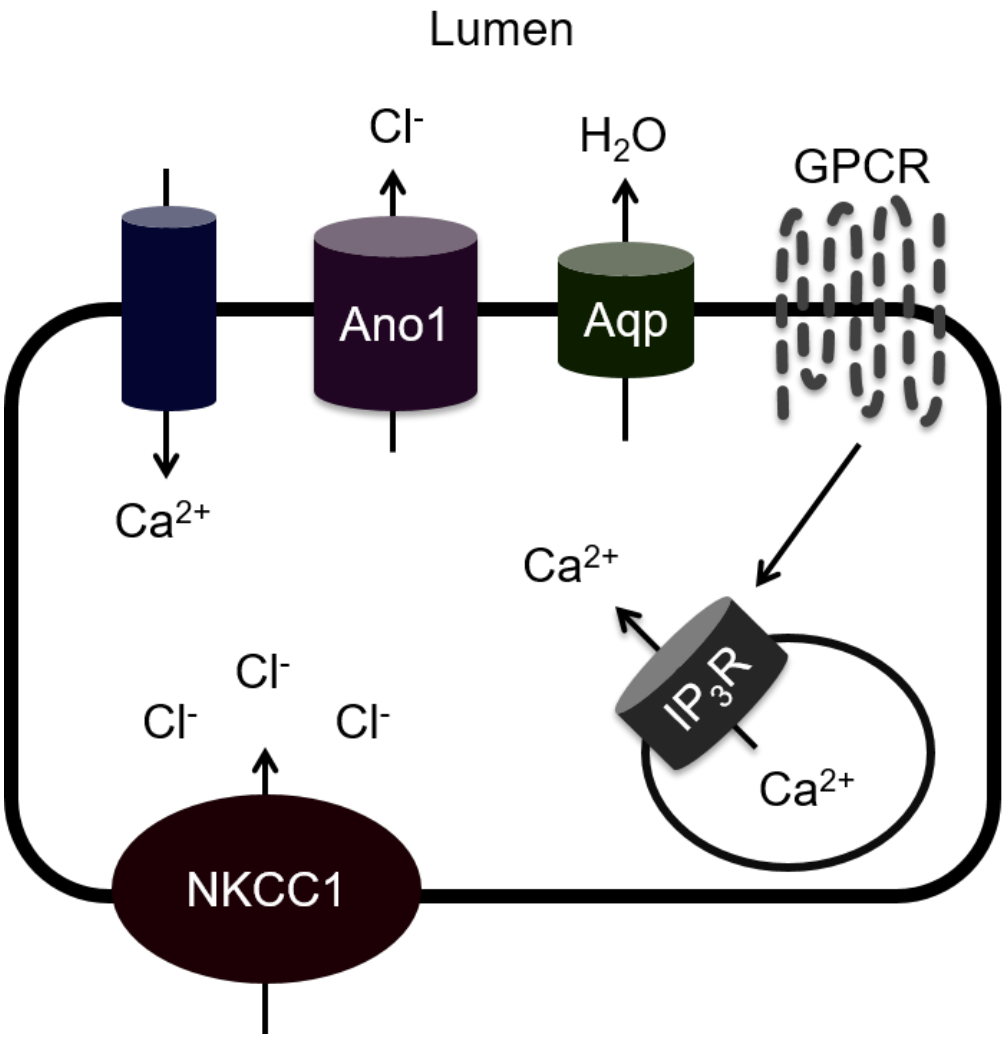
Lumen
Cl-
H2O
GPCR
Ano1
Aqp
Ca2+
Ca2+
IP3R
Cl-
Cl-
Cl-
Ca2+
NKCC1

Figure 1. ANO1 regulates secretion in secretory epithelium

ANO1 regulates fluid secretion in secretory tissues including salivary glands and the pancreas. In apical cells, basolaterally expressed NKCC1 cotransporter establishes an intracellular chloride concentration that is higher than outside. Increases in intracellular Ca2+ levels due to activation of voltage-gated Ca2+ channels or stimulation of GPCR-induced release of Ca2+ from internal stores leads to ANO1 channel opening. The subsequent efflux of Cl- ions through ANO1 generates an osmotic driving force for the secretion of water into the lumen via aquaporin channels.

Chapter 2: ANO1-mediated slow waves regulate gastrointestinal motility

2.1 Introduction

Interstitial cells of cajal (ICC) are specialized pacemaker cells within the gastrointestinal tract (GI) that organize and coordinate GI smooth muscle contractile behavior [1-3]. ICCs are classified according to their specific location within the tunica muscularis. Cells within the circular smooth muscle (CM) or longitudinal muscle (LM) layers are known as intramuscular ICCs (ICC-IM), while those found between the muscle layers are referred to as ICC-MY[4]. ICCs control smooth muscle contraction through active generation of spontaneous electrical currents called slow waves. These slow waves regulate GI smooth muscle excitability and peristalsis. Control of GI smooth muscle contraction by the enteric nervous system is also mediated by ICCs, which integrate both excitatory and inhibitory signals [5, 6].

Electrophysiology studies have suggested slow waves are generated by a $Ca2^{+}$-activated Cl^{-} conductance that can be blocked using membrane-permeable Ca^{2+} buffers or Cl^{-} channel blocking drugs [7-10]. More recently it was shown that calcium-activated chloride currents mediated by ANO1 are required for generation of slow waves in mouse GI smooth muscle [11]. Mice in which ANO1 has been genetically knocked out do not exhibit slow wave electrical activity in gastric antrum and small intestine muscle strips. Because ANO1 null mice die prematurely, the importance of ANO1 in the generation of slow waves and regulation of GI motility in adults is currently unknown. It is also unclear whether loss of slow waves due to disruption of ANO1 expression impairs intestinal transit or restricts gastric emptying in adult mice.

A recently developed mouse model carrying an inducible Cre-recombinase allele that expresses within ICCs (*c-Kit*^{CreERT2}) has enabled investigation of the effects of targeted deletion

of genes within the pacemaker population [6]. A previous study disrupted the ICC population by crossing the model with an inducible diphtheria toxin A (DTA) allele to demonstrate that specific loss of ICCs impairs GI motility, abrogates intestinal slow waves, increases transit time, and delays gastric emptying [6].

In the study we crossed animals carrying *c-Kit*^{CreERT2} allele to those expressing an ANO1 allele flanked by LoxP sites (*Ano1*^{f}) to determine the importance of ANO1 in ICC pacemaker activity and GI physiology. We first characterized recombination and ANO1 knockdown efficiency of the *c-Kit*^{CreERT2} allele within ICCs using immunohistochemistry. We next assessed electrical activity within gastric and small intestine muscles and the functional consequences on *in vivo* gastrointestinal motility. Our findings demonstrated that disrupting *Ano1* expression in the ICC population abolished slow waves in the gastric antrum, restricted gastric emptying and delayed total GI transit time.

2.2 Methods

Solutions and drugs

Tissues were constantly perfused with oxygenated KRB of the following composition (mM): NaCl 118.5; KCl 4.5; $MgCl_2$ 1.2; $NaHCO_3$ 23.8; KH_2PO_4 1.2; dextrose 11.0; $CaCl_2$ 2.4. The pH of the KRB was 7.3–7.4 when bubbled with 97% O_2–3% CO_2 at 37±0.5°C. Muscles were left to equilibrate for at least 1 hour before experiments were begun. Nifedipine was purchased from Sigma-Aldrich (St. Louis, MO), dissolved in ethanol to a concentration of 10 mM and added to the perfusion KRB solution at a final concentration of 1 μM.

Mouse generation

c-Kit$^{CreERT2/+}$ (Kit-Cre) mice were obtained from Dr Dieter Saur (Technical University Munich, Germany) [1] and crossed with previously described *Ano* $^{f/f}$ mice [2] to generate *c-Kit*$^{CreERT2/+}$*; Ano1*$^{f/f}$ and *c-Kit*$^{CreERT2/+}$*; Ano1*$^{f/+}$ animals. *c-Kit*$^{CreERT2/+}$ mice were also crossed with *Rosa*^{mtmg} reporter to produce *c-Kit*$^{CreERT2/+}$; *Ano1*$^{f/f}$; *Rosa*$^{mtmg/+}$ and *c-Kit*$^{CreERT2/+}$; *Ano1*$^{f/+}$; *Rosa* $^{mtmg/+}$ animals.

c-Kit$^{CreERT2/+}$*; Ano1*$^{f/f}$ and *c-Kit*$^{CreERT2/+}$*; Ano1*$^{f/+}$ mice (both sexes) between the ages of P60-P120 were used for the described experiments. To induce Cre recombinase mice were treated with Tamoxifen by oral gavage at 0.13mg/g body weight. Each animal received 4 consecutive doses of tamoxifen given every other day and experiments were performed 2-4 weeks following the last treatment. The Institutional Animal Use and Care Committees at the University of California, San Francisco and University of Nevada approved procedures used on mice.

Tamoxifen administration

400mg of Tamoxifen from Sigma-Aldrich (St. Louis, MO)was dissolved in 20 ml corn oil to create a solution with a final concentration of 2mg/ml. The tamoxifen solution was orally administered by gavage to mice 2-4 months of age at 0.13mg/gram of body weight. Each animal received 4 consecutive doses of tamoxifen given every other day and experiments were performed 1-2 weeks following the last treatment.

Morphological studies

Whole mount preparations were prepared after removing the mucosa from antral and intestinal tissues. The *tunica muscularis* were pinned to the base of a dish filled with Sylgard

elastomer (Dow Corning Corp., Midland, MI, USA) with the circular muscle layer facing upwards and fixed in either acetone at 4°C for 10 min or paraformaldehyde (4% w/v) for 20 min at 4°C. Following fixation, preparations were washed for 60 min in phosphate buffered saline (PBS). Tissues were incubated in Triton X-100 (0.3%) and bovine serum albumin BSA (1%) for 1 h at room temperature to reduce nonspecific antibody binding. For double labeling, tissues were incubated sequentially in a combination of primary antibodies (Kit/ANO1; eGFP/Kit combinations). The first incubation was carried out for 24 h at 4°C, tissues were subsequently washed in PBS before being incubated in a second antibody for an additional 24 h at 4°C. Following incubation in primary antibodies, tissues were washed and secondary antibodies were added independently (Alexa 488 and 594 diluted 1:1000 in PBS for 1 h at room temperature). Control tissues were prepared by either omitting primary or secondary antibodies from the incubation solutions. Tissues were examined with a Zeiss LSM 510 Meta confocal microscope (Zeiss, Germany) with appropriate excitation wavelengths. Confocal micrographs were digital composites of Z-series scans of 10–15 optical sections through a depth of 2-40 μm. Final images were constructed and montages were assembled using Zeiss LSM 5 Image Examiner and converted to Tiff files for final processing in Adobe Photoshop CS5 software (Adobe Co., Mountain View, CA, USA) and Photoshop 7.0 and Corel Draw X4 (Corel Corp. Ontario, Canada).

Total gastrointestinal transit time

To estimate total gastrointestinal transit time, mice were administered by oral gavage 100μl of a solution containing 60mg/ml carmine dye (Sigma C1022) suspended in 0.5% methylcellulose (Sigma M0262) in PBS. The elapsed time before excretion of the first red-

stained fecal pellet was recorded for each mouse at baseline and again following the tamoxifen treatment regimen. The change in transit time was calculated by subtracting the baseline transit time from the transit time after tamoxifen administration.

Ribonucleic acid isolation and qRT-PCR

Total ribonucleic acid (RNA) was isolated from antral and intestinal tissues using TRizol from ThermoFisher Scientific (Waltham, MA). Concentration and purity of RNA were measured using an ND-1000 Nanodrop Spectrophotometer (Thermo Scientific, Wilmington, DE, USA). Total RNA was reverse transcribed with qScript™ cDNA SuperMix (Quanta Biosciences, Gaithersburg, MD) in a 5X reaction buffer containing optimized concentrations of MgCl2, dNTPs (dATP, dCTP, dGTP, dTTP), recombinant RNase inhibitor protein, qScript reverse transcriptase, random primers, oligo(dT) primer and stabilizers, followed by heat inactivation. PCR was performed with specific primers to *Ano1*, *Kit* and *Gapdh* from Tamoxifen-treated *c-Kit*$^{CreERT/+2}$*; Ano1*$^{f/f}$ and *c-Kit*$^{CreERT2/+}$*; Ano1*$^{f/+}$ mice. qRT-PCR was performed with the same primers as PCR using Fast Sybr green chemistry on the 7900HT Real Time PCR System (Applied Biosystems, Foster City, CA, USA). Normalized values and standard deviations were calculated in differences of relative gene expression from 4 dilutions of technical duplicates of antrum and small intestine from each animal. The data are shown as averages and standard deviations of triplicate samples (n=3). Genes with a fold change *P*-value less than 0.05 between tissues represents a statistically significant difference. Unpaired students t-test was used to determine *P*-values in the parametric analysis.

Electrophysiological experiments

The gastrointestinal tracts were removed from animals and placed in Krebs Ringer Buffer (KRB) for further dissection. Stomachs were opened along the lesser curvature and gastric contents were washed away with KRB. The gastric corpus and antrum were pinned to the base of a Sylgard silicone elastomer (Dow Corning Corp., Midland, MI, USA) dish and the mucosa was removed by sharp dissection. Antrums were subsequently isolated by a surgical incision across the stomach at the level of the *incisura angularis.* Strips of gastric antrum (2 x 6 mm) were isolated from along the greater curvature and placed in a recording chamber with the serosal aspect of the muscle facing upward for intracellular microelectrode recordings. and isometric force measurements. A similar procedure was performed on jejunal tissues except the mucosal aspect of the muscle faced upwards.

Intracellular microelectrode recordings were performed as previously described[3]. Briefly, impalements of circular muscle cells along the greater curvature of the antrum and anti-mesenteric border of the small intestine were made with glass microelectrodes having resistances of 80-120 MΩ. Transmembrane potentials were recorded with a high impedance electrometer (Axon Instruments, Axon Instruments, Union City, CA, USA). Data were recorded on a PC running AxoScope 10 data acquisition software (Axon Instruments) and hard copies were made using Clampfit analysis software (Axon Instruments). Some experiments were performed in the presence of nifedipine (1 μM) to reduce contractions and facilitate impalements of cells for extended periods. It has been previously demonstrated that slow waves in the murine antrum and small intestine are not significantly affected by nifedipine.

Small intestine transit

To measure small intestine transit time, mice were administered by oral gavage 100µl of a 1:500 dilution of indocyanine green (MP Biomedicals) in 0.5% methylcellulose in PBS[12]. The animals were sacrificed by cervical dislocation either 1 hour or 20 minutes following gavage. The intact GI tracts were then dissected from the mice and imaged with an Odyssey imaging system. The distance travelled and GI tract area covered by the ICG fluorescent dye were analyzed using Fiji image analysis software[4].

Gastric emptying

To measure gastric emptying, mice were fasted overnight for 12 hours then orally administered 100µl of 25 mg/ml rhodamine-dextran tracer (R9379, Sigma, St. Louis, MO,) dissolved in 2% methylcellulose in PBS [13]. After 20 minutes, the animals were sacrificed by cervical dislocation. After removing the GI tracts, the stomachs were dissected and the small intestine was cut into 10 segments of equal length. The stomach and small intestine segments were opened and washed with 1ml PBS in microcentrifuge tubes. The luminal contents were then centrifuged at 2,500 rpm, the supernatants were collected and fluorescence was measured using a FLUOstar OPTIMA microplate reader (BMG LABTECH, Cary, NC). The fraction of rhodamine-dextran remaining in the stomach relative to the total amount recovered from the SI segments and stomach was used to calculate gastric emptying. Small intestine transit was analyzed by measuring the geometric center of the fluorescence (GCF) distribution within the small intestine. GCF = Σ [(fluorescence fraction in segment) X (segment number)] [13-16].

Video analysis of intact gastrointestinal tract contraction

Following sacrifice by CO_2 asphyxiation and cervical dislocation mouse gastrointestinal tracts were carefully removed and placed in pre-warmed PBS. Tissues were allowed to equilibrate for 15 minutes then videos were captured of spontaneous contractile behavior using a Samsung Galaxy Camera (Daegu, South Korea). Contractile behavior was recorded for 5 minutes per animal and contractile distance was analyzed using Tracker Video Analysis and Modeling Tool (Douglas Brown, http://physlets.org/tracker/). The total distance travelled by the jejunum in 1 minute was measured for each animal and the results are reported as means ± SEM.

Video analysis of jejunum segment contraction frequency

Following sacrifice mouse gastrointestinal tracts were carefully removed and placed in pre-warmed PBS. The entire jejunum was cut into 2cm segments and allowed to equilibrate for 15 minutes then videos were captured of spontaneous contractile behavior using Zeiss Lumar V12 Stereomicroscope (Oberkochen, Germany). Contractile behavior was recorded for 2 minutes per segment and the number of contractions per minute were counted. The average contractile frequency of the jejunum segments was determined for each animal. The results are reported as means ± SEM.

2.3 Results

Induction of *c-Kit*^{CreERT2} efficiently recombines reporter allele in ICCs

To determine the recombination efficiency of *c-Kit*^{CreERT2} allele in adult ICCs, *c-Kit*$^{CreERT2/+}$*;Ano1*$^{f/f}$ and *c-Kit*$^{CreERT2/+}$*;Ano1*$^{f/+}$animals were crossed with mice expressing a *Rosa*^{mtmg} reporter. Following tamoxifen administration, the small intestine and gastric antrum were collected from the animals. Confocal images of endogenous GFP expression within antrum

and small intestine smooth muscle strips showed robust GFP signal throughout the ICCs in both tissues (Figure 1 and 2).

Induction of *c-Kit*^{CreERT2} reduces ANO1 expression within gastric and small intestine ICCs

After confirming recombination competence of the *c-Kit*^{CreERT2} allele in antrum and small intestine ICCs, we then determined whether ANO1 expression was reduced following tamoxifen administration in *c-Kit*$^{CreERT2/+}$*;Ano1*$^{f/f}$ and *c-Kit*$^{CreERT2/+}$*;Ano1*$^{f/+}$ control animals. Gastric antrum and small intestine tissues were collected and immunohistochemistry experiments using antibodies against ANO1 and c-Kit were performed on whole mount preparations. Confocal images of the whole mounts showed comparable expression of c-Kit within the gastric antrum and small intestine ICC networks from both *c-Kit*$^{CreERT2/+}$*;Ano1*$^{f/f}$ (Figure 3B and 4B) and *c-Kit*$^{CreERT2/+}$*;Ano1*$^{f/+}$ controls (Figure 3A and 4A). However, ANO1 expression in the antrum and small intestine from *c-Kit*$^{CreERT2/+}$*;Ano1*$^{f/f}$ (Figure 3B and 4B) was diminished compared with *c-Kit*$^{CreERT2/+}$*;Ano1*$^{f/+}$ controls (Figures 3A and 4A).

To confirm and quantify the reduction in ANO1 expression following recombinase induction in *c-Kit*$^{CreERT2/+}$*;Ano1*$^{f/f}$ mice, qPCR analysis was performed using RNA isolated from gastric antrum and small intestine tissues. The qPCR analysis showed a significant decrease in ANO1 transcript level in both the antrum and small intestine from *c-Kit*$^{CreERT2/+}$*;Ano1*$^{f/f}$ animals compared to controls (Figure 5A). This reduction in *Ano1* transcript in *c-Kit*$^{CreERT2/+}$*;Ano1*$^{f/f}$ mice was calculated to be 4-fold (Figure 5B).

Reduced ANO1 expression in ICCs delays total and small intestine transit

To determine the effects of diminished ANO1 expression in adult ICCs on total GI transit *in vivo,* carmine red dye was administered via oral gavage and total GI transit times were measured for each mouse before and following administration of tamoxifen. *c-Kit*$^{CreERT2/+}$*; Ano1*$^{f/f}$ animals demonstrated increased total GI transit time after tamoxifen treatment, while *c-Kit*$^{CreERT2/+}$*;Ano1*$^{f/+}$controls showed no change in transit (Figure 6A). The transit time increase in *c-Kit*$^{CreERT2/+}$*;Ano1*$^{f/f}$ mice was approximately two hours (Figure 6B).

Indocyanine green (ICG) fluorescent dye was then used to assess *in vivo* small intestine transit in tamoxifen-treated mice. ICG was administered by oral gavage and fluorescence in the small intestine was imaged 15 minutes and 1 hour later. The percent of total small intestine area covered by fluorescence after 1 hour was smaller in *c-Kit*$^{CreERT2/+}$*;Ano1*$^{f/f}$ compared with *c-Kit*$^{CreERT2/+}$*;Ano1*$^{f/+}$controls (Figure 7A). The ICG dye also travelled shorter relative distance in the small intestine after 15 minutes in *c-Kit*$^{CreERT2/+}$*;Ano1*$^{f/f}$ mice (Figure 7B and C).

Diminished ANO1 expression abrogates slow waves in gastrointestinal smooth muscles

To determine whether the delayed gastrointestinal transit following tamoxifen treatment was a result of impaired slow wave activity, microelectrode recordings of gastric antrum and small intestine smooth muscles were performed. Spontaneous slow waves were detected in both small intestine (Figure 8A) and gastric antrum smooth muscles (Figure 8B) from all *c-Kit*$^{CreERT2/+}$*;Ano1*$^{f/+}$ mice analyzed (n=10). However, in the antrums collected from *c-Kit*$^{CreERT2/+}$*;Ano1*$^{f/f}$ mice, slow waves were absent (Figure 8B) (n=10). Additionally, the small intestine from one *c-Kit*$^{CreERT2/+}$*;Ano1*$^{f/f}$ animal failed to produce slow waves (Figure 8A).

Loss of slow waves in the antrum delays gastric emptying

Since loss of ANO1 expression in ICCs abrogated slow waves in the antrum, we then tested whether the animals had delayed gastric emptying using the indigestible rhodamine B-conjugated dextran tracer. Overnight-fasted mice were administered rhodamine-dextran by oral gavage and sacrificed after 20 minutes. The percent of total recovered fluorescence remaining in the stomach was higher in the *c-Kit*$^{CreERT2/+}$*; Ano1*$^{f/f}$ mice relative to controls (Figure 9A). Comparing the average fluorescence distribution among the small intestine segments showed a significant decrease within segment 6 of *c-Kit*$^{CreERT2/+}$*; Ano1*$^{f/f}$ mice while the others were similar (Figure 9B). As a result of the diminished fluorescence in the 6th segment, there was a shift in the geometric center of the fluorescence distribution toward the more proximal small intestine in *c-Kit*$^{CreERT2/+}$*; Ano1*$^{f/f}$ mice (Figure 9C).

Diminished ANO1 expression in gastrointestinal ICCs disrupts contractile behavior

To determine the effects of reduced ANO1 expression on smooth muscle contractile behavior, videos were recorded of intact gastrointestinal tracts from *c-Kit*^{CreERT2}*;Ano1*$^{f/f}$ mice and *c-Kit*^{CreERT2}*;Ano1*$^{f/+}$ control counterparts. The gastrointestinal tracts from *c-Kit*^{CreERT2}*;Ano1*$^{f/f}$ exhibited irregular spontaneous contractions, such that adjacent regions in the jejunum would contract simultaneously. In contrast, gastrointestinal tracts from *c-Kit*^{CreERT2}*;Ano1*$^{f/+}$ controls demonstrated rhythmical contractions that proceeded proximally to distally along the tract in a wave-like manner. To quantify the differences in the contractile pattern, the total distance moved by segments of jejunum in each animal were measured using video analysis software. The results showed that jejunum regions from *c-Kit*^{CreERT2}*; Ano1*$^{f/f}$ animals moved a greater total distance per minute than jejunum areas from *c-Kit*^{CreERT2}*; Ano1*$^{f/+}$ mice (Figure 10A).

To determine the contraction frequency of isolated jejunum segments, videos were recorded of the motor behavior of 1cm lengths of small intestine. The number of contractions per minute were counted for each segment to determine an average contraction frequency for the entire small intestine. Jejunum segments from *c-Kit*^{CreERT2}*;Ano1*$^{f/f}$ mice demonstrated a significant decrease in contractile frequency compared with controls (Figure 10B).

2.4 Discussion

The early postnatal lethality of ANO1 knockout mice has prevented investigation of the role of ANO1 in regulating GI slow waves and motility in adult mice. In this study, a *c-Kit*^{CreERT2} allele was used in combination with *Ano1*$^{f/f}$ to determine the consequences of disrupting ANO1 expression in ICC networks on electrical activity, motility and motor behavior. There was efficient recombination of a *Rosa*^{mtmg} reporter in gastric antrum and small intestine ICCs after *c-Kit*^{CreERT2} induction. Analysis of ANO1 expression through immunohistochemistry and qPCR experiments demonstrated a significant reduction in ANO1 expression in gastric antrum and small intestine of *c-Kit*$^{CreERT2/+}$*;Ano1*$^{f/f}$ animals compared to controls. This loss of ANO1 expression caused a delay in total gastrointestinal transit time, small intestine transit efficiency and gastric emptying in *c-Kit*$^{CreERT2/+}$*;Ano1*$^{f/f}$ mice. Gastric antrum tissues from all analyzed *c-Kit*$^{CreERT2/+}$*;Ano1*$^{f/f}$ mice lacked slow waves and one *c-Kit*$^{CreERT2/+}$*;Ano1*$^{f/f}$ mouse lacked slow waves in the small intestine. In contrast, all tested gastric antrum and small intestine muscle strips from *c-Kit*$^{CreERT2/+}$*;Ano1*$^{f/+}$ control animals displayed slow wave activity.

The results of this study confirm previous experiments utilizing ANO1 mice homozygous for the null allele, which demonstrated an absence of slow waves in the gastric antrum and small intestine. However, while all *c-Kit*$^{CreERT2/+}$*; Ano1*$^{f/f}$ mice lacked slow waves in the gastric antrum

following tamoxifen treatment, only one of the animals demonstrated a loss in slow wave activity in the small intestine. Both the small intestine and gastric antrum exhibited similar significant reductions in ANO1 expression, suggesting that slow wave activity in gastric antrum was more sensitive to decreased ANO1 expression. There could also be another ion channel in the small intestine that compensates for loss of ANO1.

Since ANO1 knockout mice die within the first week of life, experiments could not be performed to test the function of ANO1-mediated slow waves in gastrointestinal motility *in vivo*. In the present study, reducing ANO1 expression in adult antrum and small intestine ICCs delayed total gastrointestinal transit time. Loss of ANO1 in adult ICCs also delayed small intestine transit and restricted gastric emptying. The observation that most *c-Kit*$^{CreERT2/+}$*;Ano1*$^{f/f}$ mice analyzed had slow waves in the small intestine, despite reduced ANO1 expression, suggested that the defects in total transit and small intestine transit were a result of delayed gastric emptying. The assays used to test small intestine transit efficiency and total transit time could not differentiate between effects associated specifically with gastric emptying or small intestine peristalsis. Despite these complications, the experiments collectively demonstrate that ANO1-mediated slow waves regulate gastrointestinal motility *in vivo* and their loss impairs the transit of food during digestion.

Video analysis of intact gastrointestinal tracts demonstrated that small intestine contractions were uncoordinated in *c-Kit*^{CreERT2}*;Ano1*$^{f/f}$ mice following tamoxifen treatment. The occurrence of simultaneous contractions in adjacent regions of small intestine contributed to a significant increase in the total distance moved by the gastrointestinal tracts from *c-Kit*^{CreERT2}*; Ano1*$^{f/f}$ compared to *c-Kit*^{CreERT2}*;Ano1*$^{f/+}$ controls. When we analyzed the contraction frequency of 1cm length segments of small intestine, *c-Kit*^{CreERT2}*;Ano1*$^{f/f}$ mice demonstrated a significant

decrease in the number of contractions per minute. These experiments suggest that ANO1-mediated slow waves coordinate contractile events in the gastrointestinal tract.

In summary, the current study shows that the expression of ANO1 in ICCs is required for slow wave generation in the gastric antrum of adult mice. We also demonstrate for the first time that ANO1-mediated slow waves regulate GI transit time and gastric emptying *in vivo*. These findings advance our understanding of the physiological importance of ANO1 in adult animals.

References

1. Ward, S.M., et al., *Mutation of the proto-oncogene c-kit blocks development of interstitial cells and electrical rhythmicity in murine intestine.* J Physiol, 1994. **480 (Pt 1)**: p. 91-7.
2. Sanders, K.M., *A case for interstitial cells of Cajal as pacemakers and mediators of neurotransmission in the gastrointestinal tract.* Gastroenterology, 1996. **111**(2): p. 492-515.
3. Huizinga, J.D., et al., *W/kit gene required for interstitial cells of Cajal and for intestinal pacemaker activity.* Nature, 1995. **373**(6512): p. 347-9.
4. Sanders, K.M., S.M. Ward, and S.D. Koh, *Interstitial cells: regulators of smooth muscle function.* Physiol Rev, 2014. **94**(3): p. 859-907.
5. Ward, S.M., et al., *Interstitial cells of Cajal mediate cholinergic neurotransmission from enteric motor neurons.* J Neurosci, 2000. **20**(4): p. 1393-403.
6. Klein, S., et al., *Interstitial cells of Cajal integrate excitatory and inhibitory neurotransmission with intestinal slow-wave activity.* Nat Commun, 2013. **4**: p. 1630.
7. Kito, Y., H. Fukuta, and H. Suzuki, *Components of pacemaker potentials recorded from the guinea pig stomach antrum.* Pflugers Arch, 2002. **445**(2): p. 202-17.
8. Kito, Y. and H. Suzuki, *Properties of pacemaker potentials recorded from myenteric interstitial cells of Cajal distributed in the mouse small intestine.* J Physiol, 2003. **553**(Pt 3): p. 803-18.
9. Hirst, G.D., et al., *Regenerative component of slow waves in the guinea-pig gastric antrum involves a delayed increase in [Ca(2+)](i) and Cl(-) channels.* J Physiol, 2002. **540**(Pt 3): p. 907-19.

10. Edwards, F.R., G.D. Hirst, and H. Suzuki, *Unitary nature of regenerative potentials recorded from circular smooth muscle of guinea-pig antrum.* J Physiol, 1999. **519 Pt 1**: p. 235-50.

11. Hwang, S.J., et al., *Expression of anoctamin 1/TMEM16A by interstitial cells of Cajal is fundamental for slow wave activity in gastrointestinal muscles.* J Physiol, 2009. **587**(Pt 20): p. 4887-904.

12. Schindelin, J., et al., *Fiji: an open-source platform for biological-image analysis.* Nat Methods, 2012. **9**(7): p. 676-82.

13. De Lisle, R.C., *Altered transit and bacterial overgrowth in the cystic fibrosis mouse small intestine.* Am J Physiol Gastrointest Liver Physiol, 2007. **293**(1): p. G104-11.

14. Kondo, J., et al., *LRIG1 Regulates Ontogeny of Smooth Muscle-Derived Subsets of Interstitial Cells of Cajal in Mice.* Gastroenterology, 2015. **149**(2): p. 407-19 e8.

15. Capasso, R., et al., *Fatty acid amide hydrolase controls mouse intestinal motility in vivo.* Gastroenterology, 2005. **129**(3): p. 941-51.

16. Miller, M.S., J.J. Galligan, and T.F. Burks, *Accurate measurement of intestinal transit in the rat.* J Pharmacol Methods, 1981. **6**(3): p. 211-7.

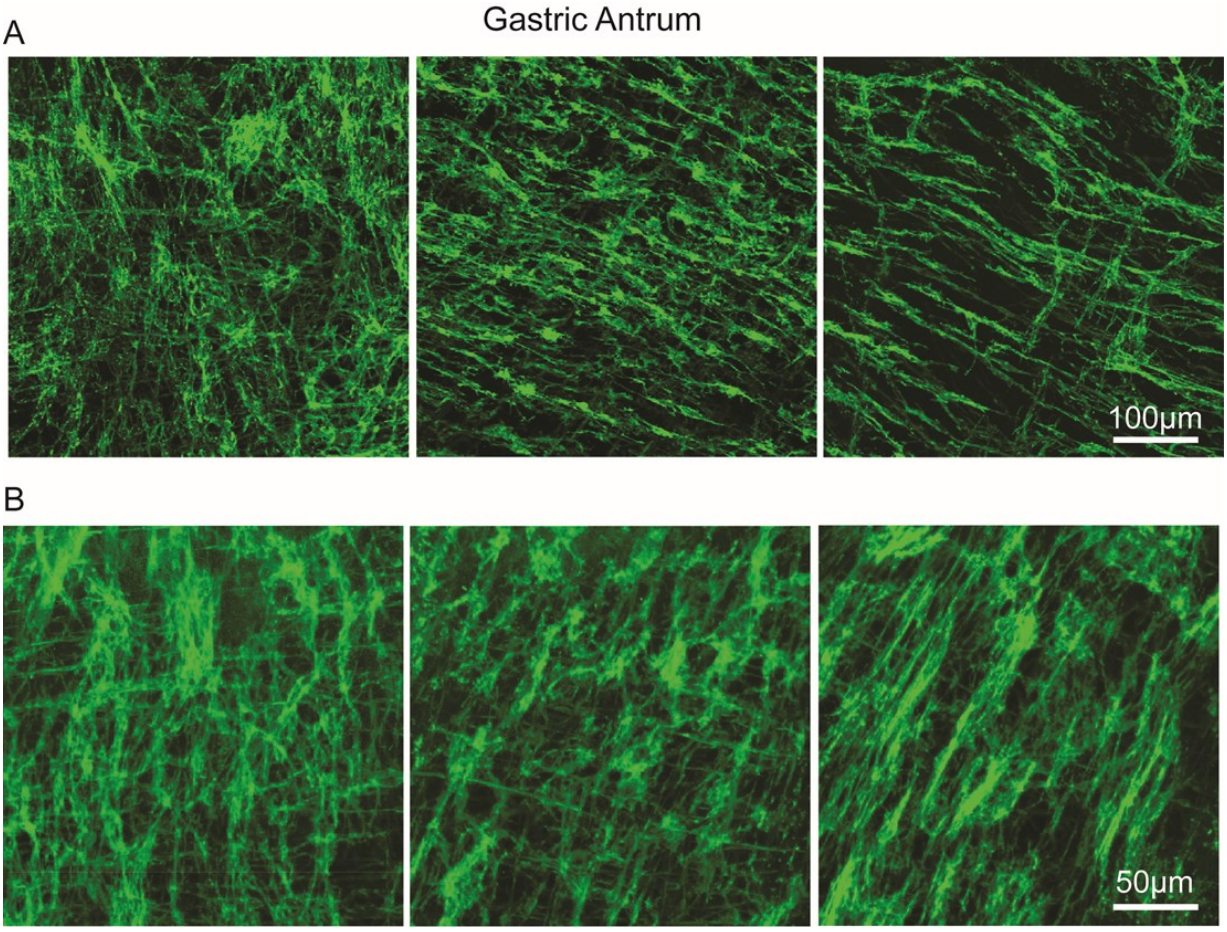
Gastric Antrum
A
100μm
B
50μm

Figure 1. c-Kit^{CreERT2} induction leads to reporter expression in gastric antrum

Whole mounts of smooth muscle from gastric antrum were prepared immediately after sacrifice of the mice and imaged with a confocal microscope. Green fluorescence indicates endogenous green fluorescent protein expression (GFP) from the *Rosa*^{mtmg} reporter. (A-B) Representative images demonstrate GFP expression of throughout the ICC networks.

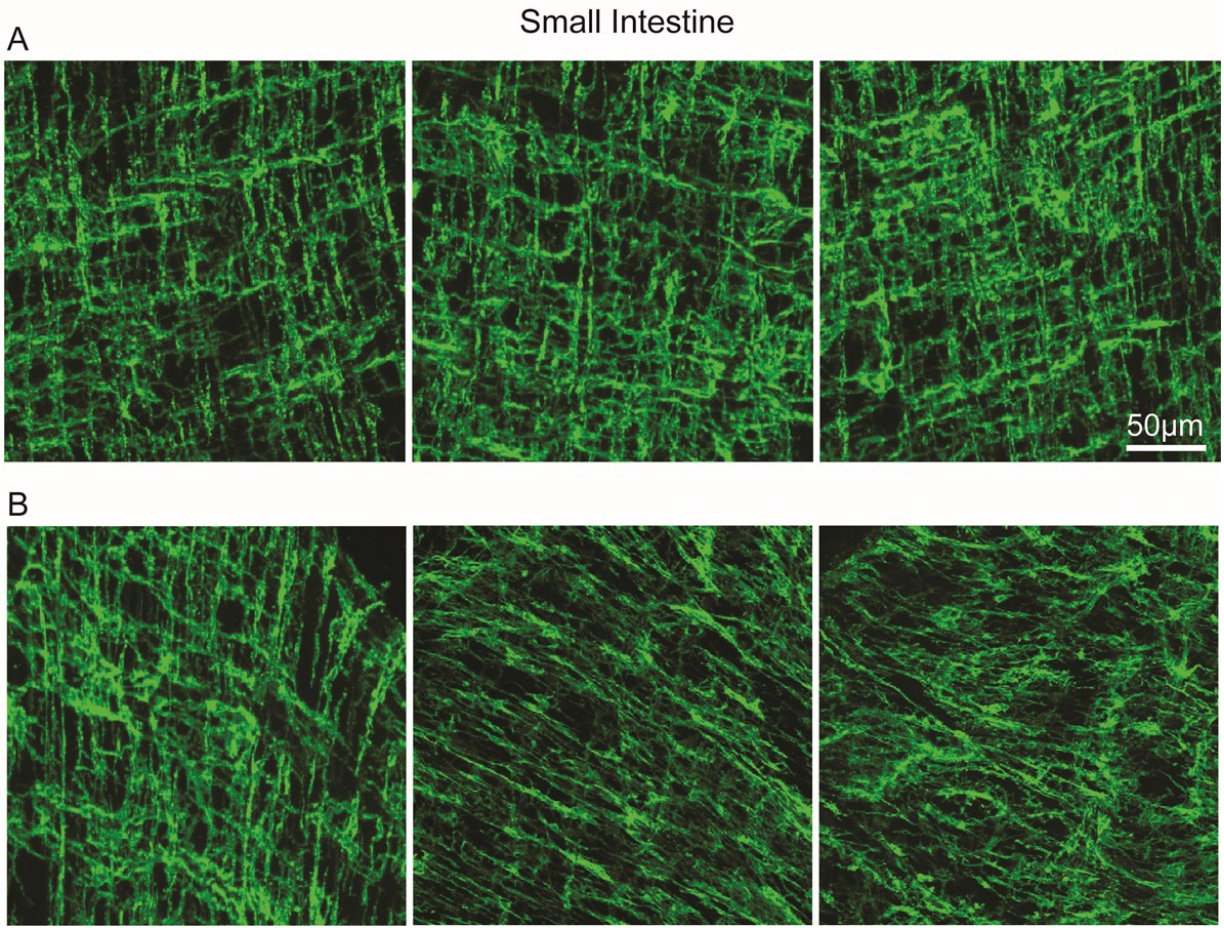
Small Intestine
A
50μm
B

Figure 2. c-Kit^{CreERT2} induction leads to reporter expression in small intestine

Whole mounts of smooth muscle from the small intestine were prepared immediately following sacrifice of the mice. Confocal microscopy was performed to visualize green fluorescence protein (GFP) expression. (A-B) Representative images demonstrate endogenous GFP expression throughout the ICC networks in small intestine.

A

c-Kit$^{CreERT2/+}$; *Ano1*$^{f/+}$

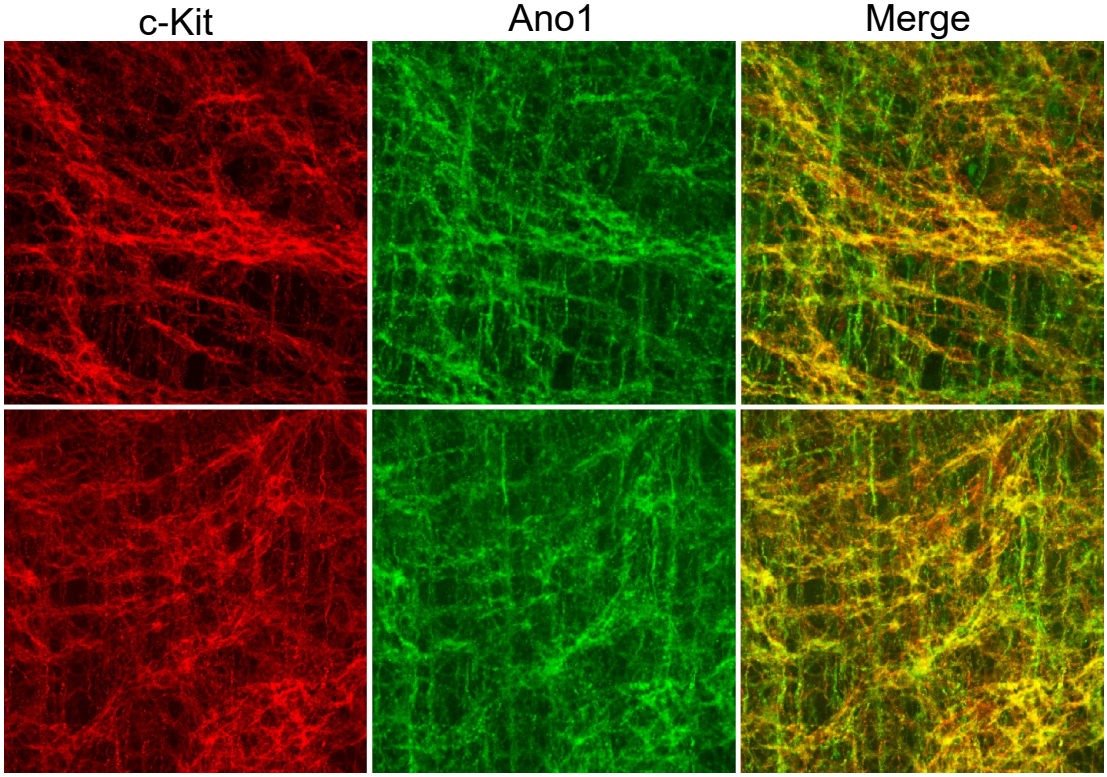

B

c-Kit$^{CreERT2/+}$; *Ano1*$^{f/f}$

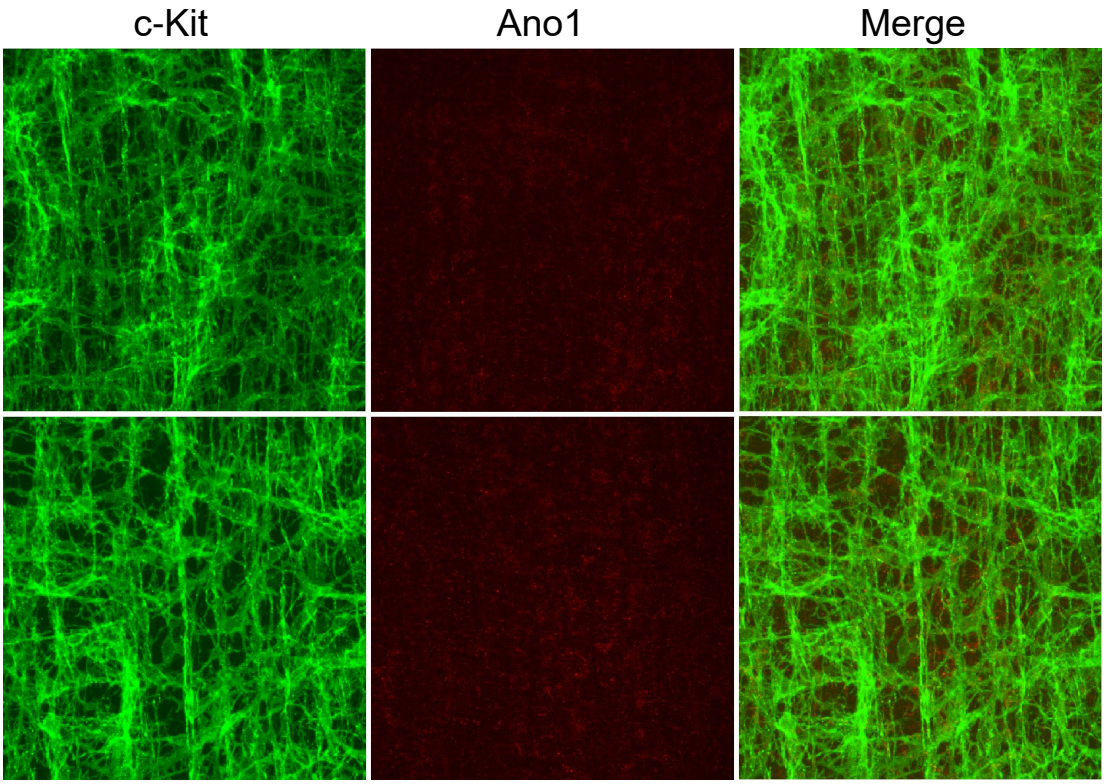

Figure 3. ANO1 expression in the antrum is reduced after c-Kit^{CreERT2} induction

Immunohistochemistry experiments were performed on whole mount preparations of gastrointestinal smooth muscle. The tissues were co-labeled with c-Kit and ANO1 antibodies. (A) Images captured by confocal microscopy of gastric antrums from *c-Kit*$^{CreERT2/+}$; *Ano1*$^{f/+}$ mice showed co-localized ANO1 (green) and c-Kit (red) expression throughout ICC networks. (B) Images from *c-Kit*$^{CreERT2/+}$; *Ano1*$^{f/f}$ mice showed a reduction in ANO1 expression (red), while c-Kit (green) was still observed throughout the ICCs.

A

c-Kit$^{CreERT2/+}$; *Ano1*$^{f/+}$

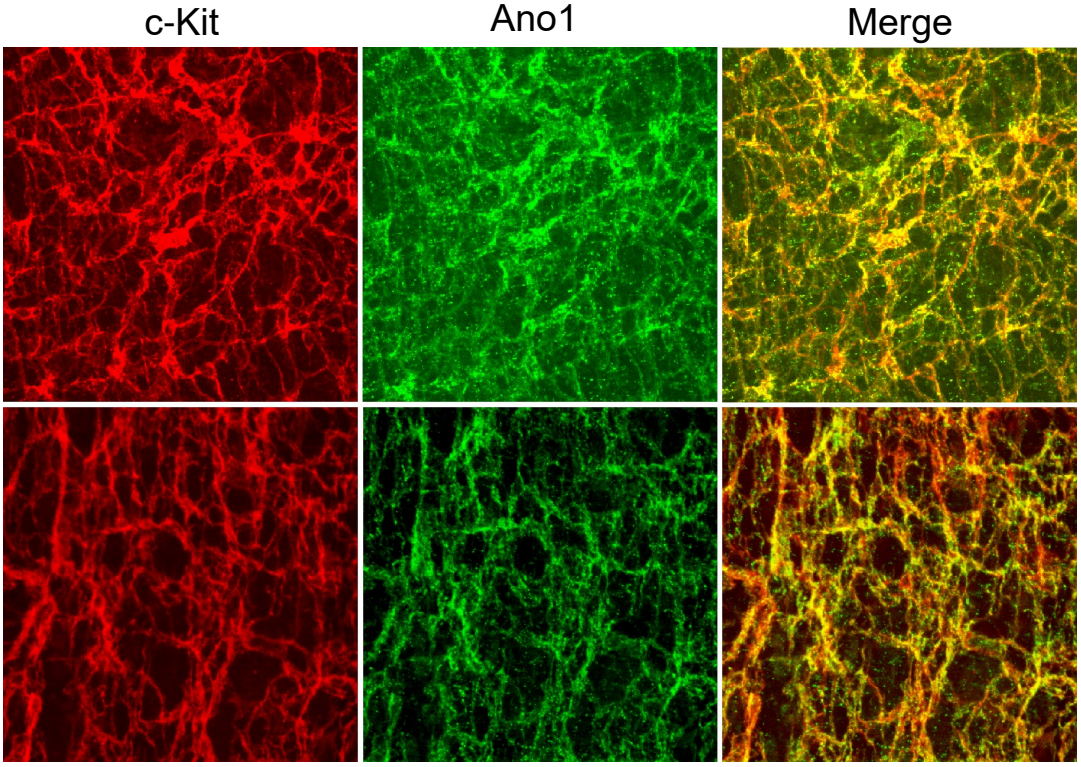

B

c-Kit$^{CreERT2/+}$; *Ano1*$^{f/f}$

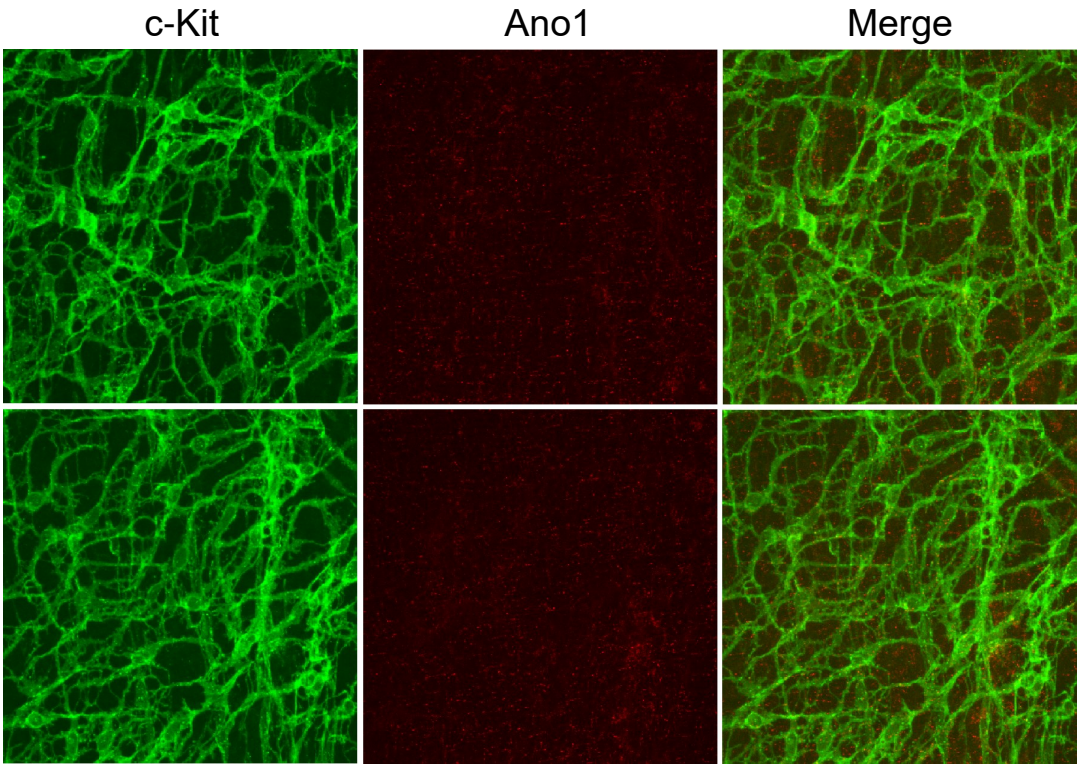

Figure 4. ANO1 expression in the small intestine is reduced after c-Kit^{CreERT2} induction

Immunohistochemistry experiments using c-Kit and ANO1 antibodies were performed on whole mount preparations of small intestine smooth muscle. (A) Images acquired by confocal microscopy showed overlapping expression of c-Kit (red) and ANO1 (green) in ICCs from *c-Kit$^{CreERT2/+}$*; *Ano1$^{f/+}$* mice. (B) *c-Kit$^{CreERT2/+}$*; *Ano1$^{f/f}$* mice showed reduced expression of ANO1 (red), while c-Kit (green) was still observed throughout the ICC networks.

A

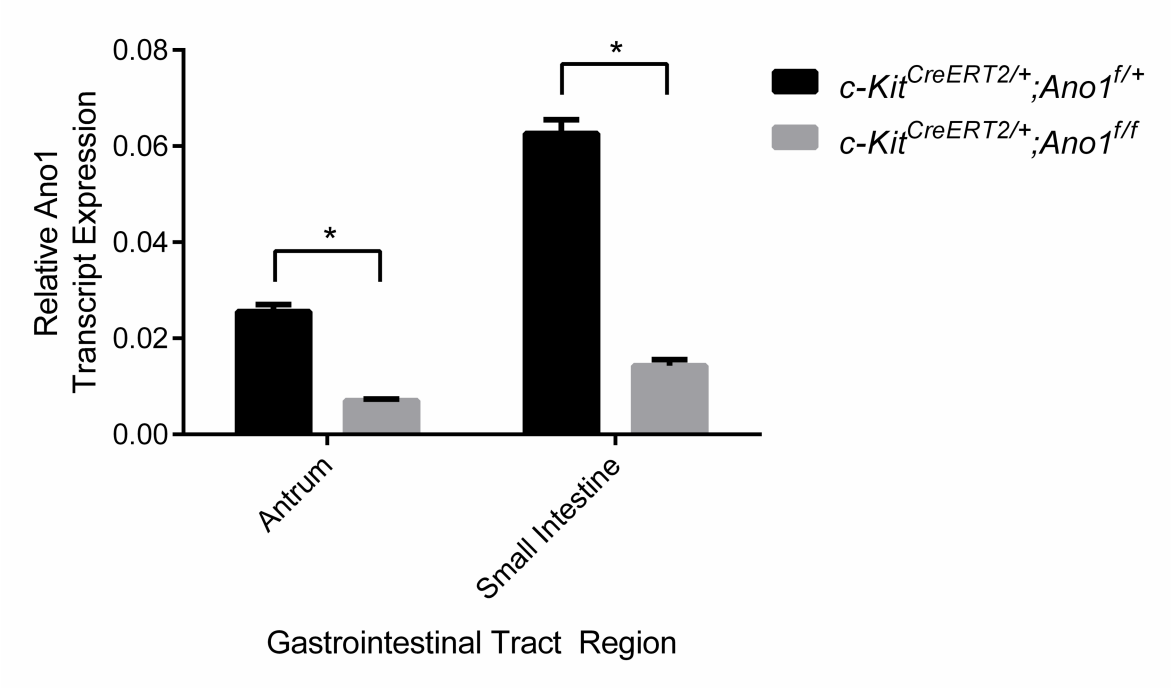
0.08
0.06
0.04
0.02
0.00
Relative Ano1 Transcript Expression
*
*
c-Kit^CreERT2/+;Ano1^f/+
c-Kit^CreERT2/+;Ano1^f/f
Antrum
Small Intestine
Gastrointestinal Tract Region

B

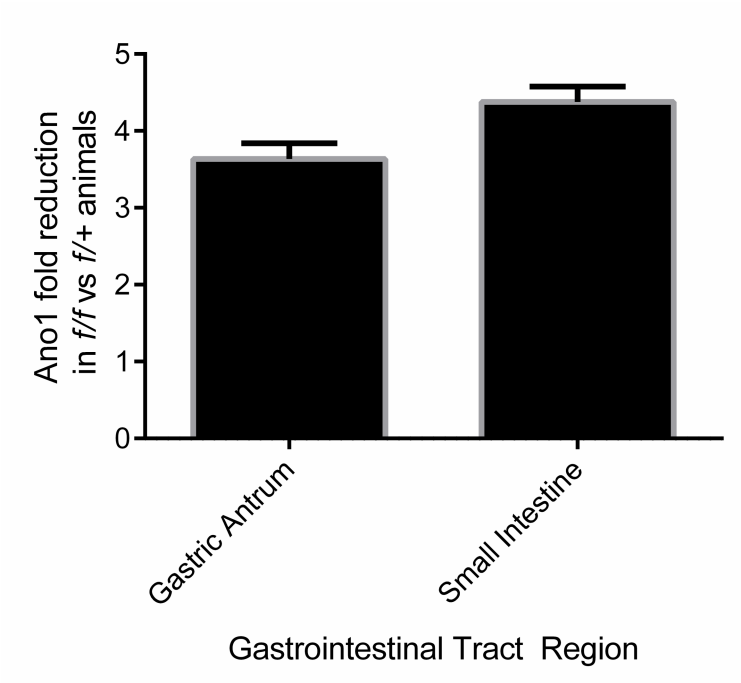
5
4
3
2
1
0
Ano1 fold reduction in f/f vs f/+ animals
Gastric Antrum
Small Intestine
Gastrointestinal Tract Region

Figure 5. ANO1 transcript is reduced in antrum and small intestine after c-Kit^{CreERT2} induction

RNA was isolated from gastric antrum and small intestine smooth muscle tissues following tamoxifen treatment. (A) qPCR experiments were performed and the ANO1 transcript level was normalized to GAPDH internal control for each animal. The results showed a significant reduction in the relative ANO1 transcript level in both gastric antrum and small intestine from *c-Kit$^{CreERT2/+}$*; *Ano1$^{f/f}$* mice. (B) The reduction in relative ANO1 transcript level was approximately 4-fold for both antrum and small intestine.

A

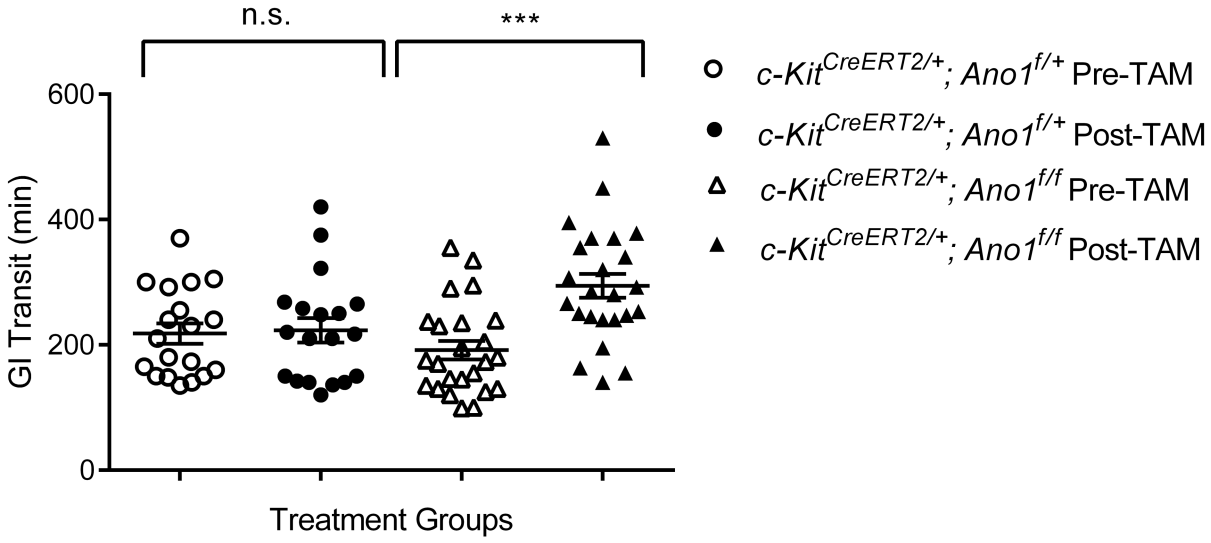
n.s.
***
600
400
200
0
GI Transit (min)
Treatment Groups
c-Kit^CreERT2/+; Ano1^f/+ Pre-TAM
c-Kit^CreERT2/+; Ano1^f/+ Post-TAM
c-Kit^CreERT2/+; Ano1^f/f Pre-TAM
c-Kit^CreERT2/+; Ano1^f/f Post-TAM

B

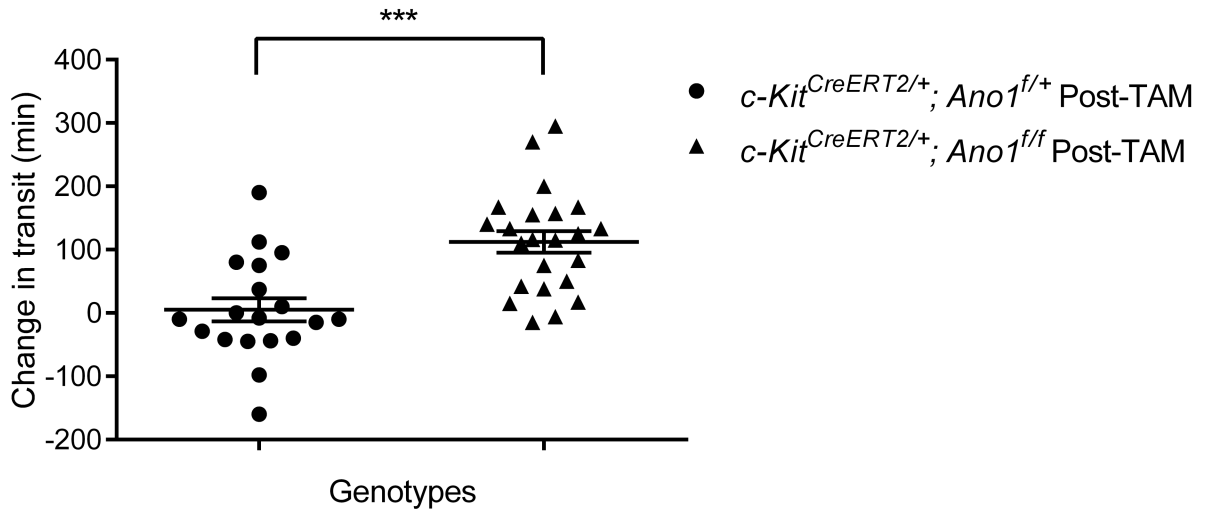
***
400
300
200
100
0
-100
-200
Change in transit (min)
Genotypes
c-Kit^CreERT2/+; Ano1^f/+ Post-TAM
c-Kit^CreERT2/+; Ano1^f/f Post-TAM

Figure 6. Reducing ANO1 expression increases total gastrointestinal transit time *in vivo*

Mice were administered by oral gavage 100µl of carmine red dye in methylcellulose and the time required for excretion of the first red-stained fecal pellet was recorded as total transit time. Transit times were determined at baseline and after tamoxifen treatment for each animal. *c-Kit$^{CreERT2/+}$; Ano1$^{f/f}$* mice showed an increase in transit time after tamoxifen treatment, while the *c-Kit$^{CreERT2/+}$; Ano1$^{f/+}$* control animals did not change. (B) The change in transit time was measured by subtracting the baseline transit from the post-tamoxifen transit. The transit time increase in *c-Kit^{CreERT2}; Ano1$^{f/f}$* mice was around 120 minutes. All graphs show mean ± SEM. n = 19,24. *** = $p < 0.0001$

A

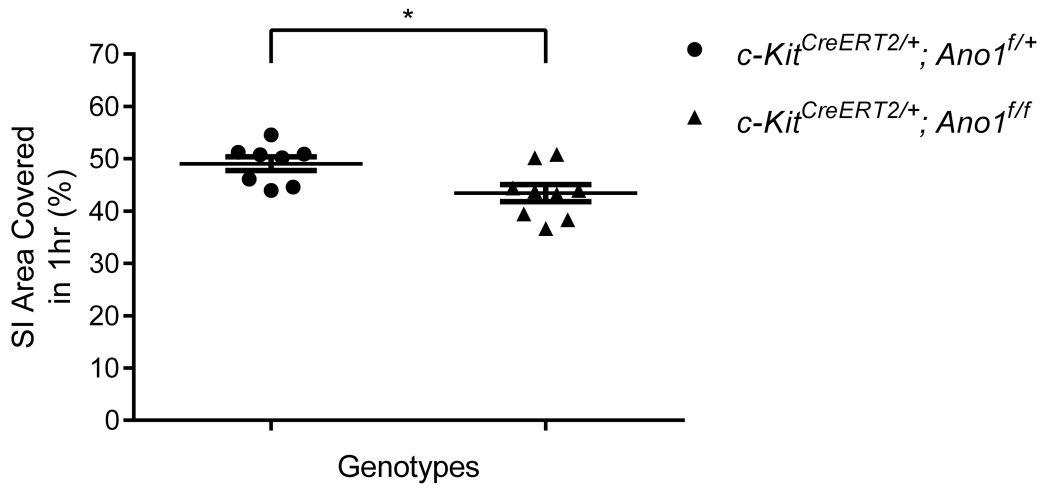
*
70
60
50
40
30
20
10
0
SI Area Covered in 1hr (%)
Genotypes
c-Kit^CreERT2/+; Ano1^f/+
c-Kit^CreERT2/+; Ano1^f/f

B

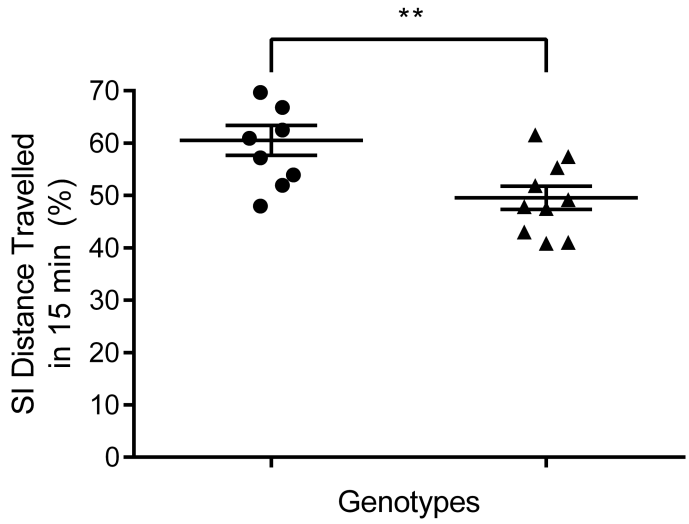
**
70
60
50
40
30
20
10
0
SI Distance Travelled in 15 min (%)
Genotypes

C

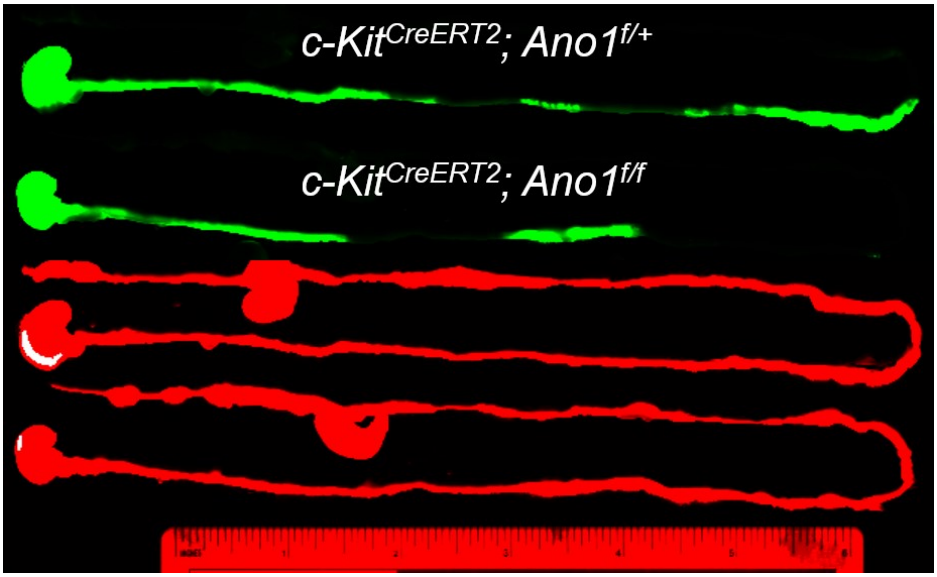
c-Kit^CreERT2; Ano1^f/+
c-Kit^CreERT2; Ano1^f/f

Figure 7. Reducing ANO1 expression delays small intestine transit *in vivo*

Mice were administered by oral gavage 100µl of indocyanine green fluorescent dye and sacrificed after 15 minutes or 1 hour. The digestive tracts were dissected and imaged using an Odyssey near infrared scanner. (A) Small intestine % area covered by green fluorescence in 1 hour was measured using Fiji. *c-Kit*^{CreERT2}*; Ano1*$^{f/f}$ mice showed a decreased area covered by the fluorescent dye compared to controls. (n=8,9). (B) The % distance travelled by fluorescent dye after 15 minutes was calculated using Fiji. *c-Kit*^{CreERT2}*; Ano1*$^{f/f}$ animals displayed a reduction in the fraction of total length reached by the dye after 15 minutes compared to controls. (n= 8, 10). (C) Representative scans of dissected murine digestive tracts show the decreased distance travelled by the fluorescent dye (green) after 15 minutes relative to total GI tract length (red). All graphs show mean ± SEM. * = $p < 0.05$, ** = $p < 0.01$

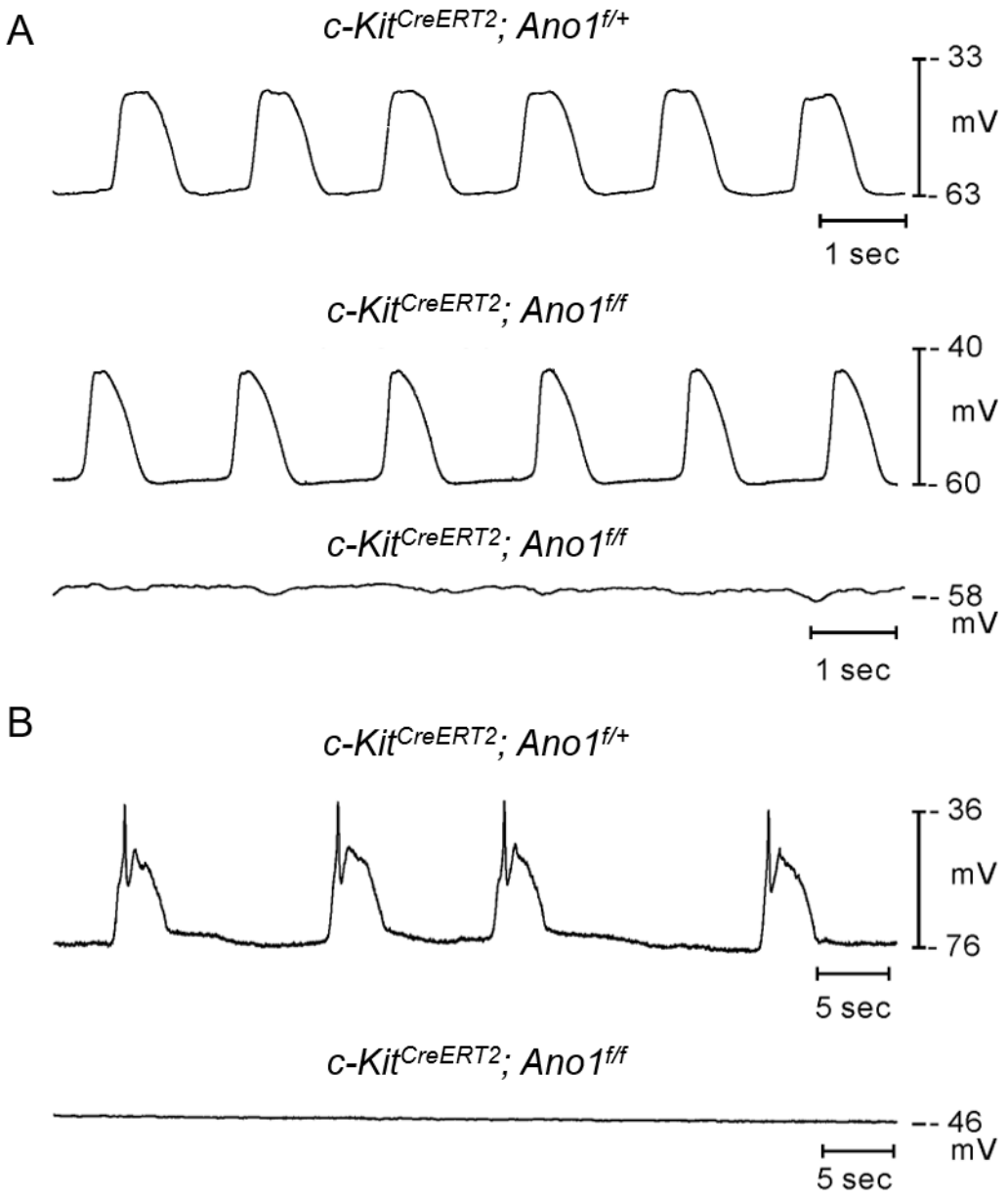
A
c-Kit^CreERT2; Ano1^f/+
33
mV
63
1 sec
c-Kit^CreERT2; Ano1^f/f
40
mV
60
c-Kit^CreERT2; Ano1^f/f
58
mV
1 sec
B
c-Kit^CreERT2; Ano1^f/+
36
mV
76
5 sec
c-Kit^CreERT2; Ano1^f/f
46
mV
5 sec

Figure 8. Reducing ANO1 expression abrogates slow waves in the gastric antrum

Microelectrode recordings were performed on isolated smooth muscle strips from antrum and small intestine. (A) Slow waves were detected in small intestines from *c-Kit*$^{CreERT2/+}$; *Ano1*$^{f/+}$ controls and all *c-Kit*$^{CreERT2/+}$; *Ano1*$^{f/f}$ mice tested except for one animal (lower trace in A). (B) In Slow waves were absent in gastric antrum from *c-Kit*$^{CreERT2/+}$; *Ano1*$^{f/f}$ mice. *c-Kit*$^{CreERT2/+}$; *Ano1*$^{f/+}$ controls exhibited slow waves in antrum.

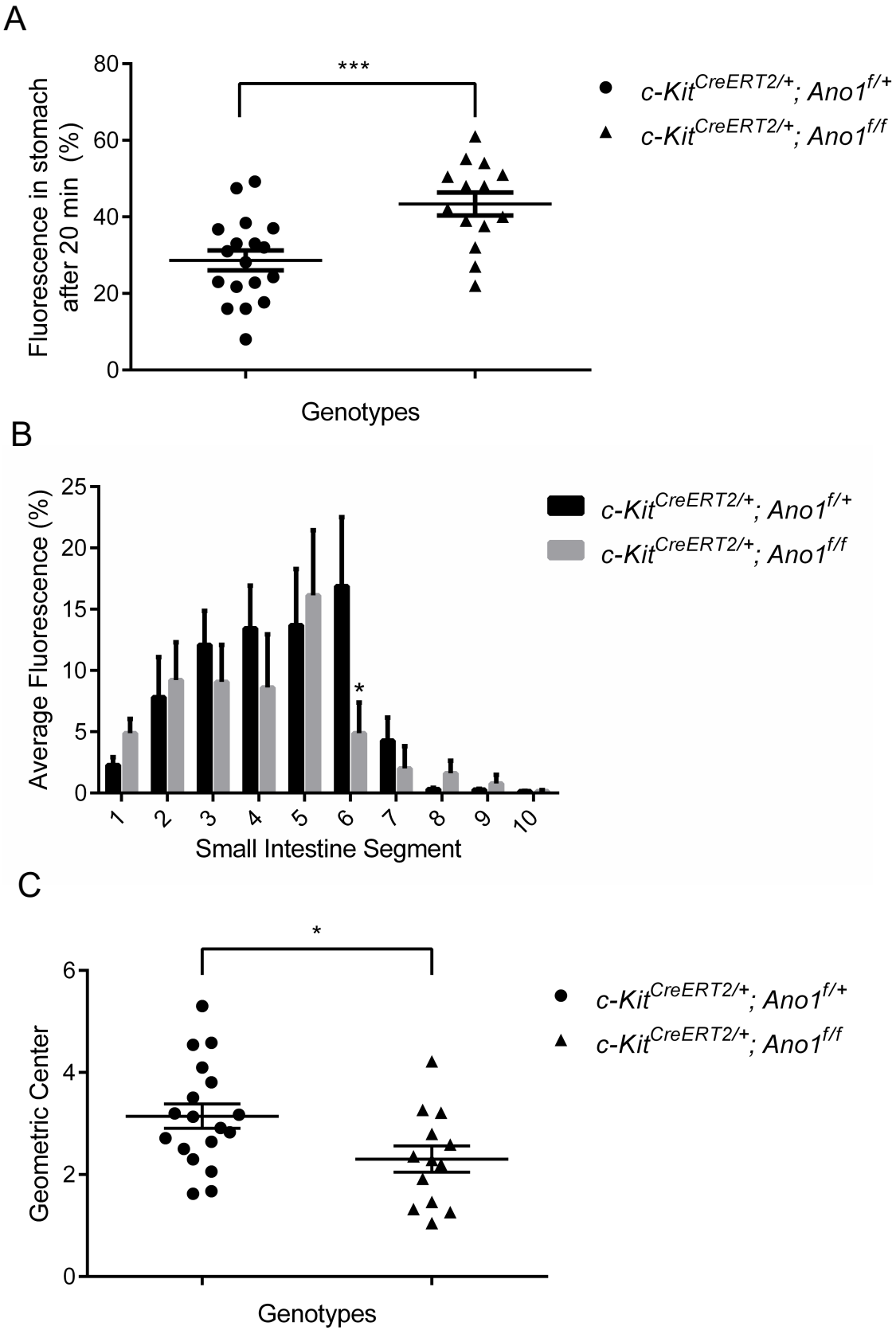
A
***
Fluorescence in stomach after 20 min (%)
80
60
40
20
0
Genotypes
c-Kit^CreERT2/+; Ano1^f/+
c-Kit^CreERT2/+; Ano1^f/f
B
Average Fluorescence (%)
25
20
15
10
5
0
*
1
2
3
4
5
6
7
8
9
10
Small Intestine Segment
c-Kit^CreERT2/+; Ano1^f/+
c-Kit^CreERT2/+; Ano1^f/f
C
*
Geometric Center
6
4
2
0
Genotypes
c-Kit^CreERT2/+; Ano1^f/+
c-Kit^CreERT2/+; Ano1^f/f

Figure 9. Loss of slow waves restricts gastric emptying *in vivo*

Mice were administered by oral gavage 100μl of rhodamine-dextran fluorescent tracer and sacrificed after 20 minutes. The luminal contents from the stomach and 10 equal-length segments of small intestine were recovered and the fluorescence was measured with a microplate reader. (A) The fraction of fluorescence remaining in the stomach relative to the total fluorescence recovered from the stomach and small intestine is shown. *c-Kit*^{CreERT2}*; Ano1*$^{f/f}$ mice showed an increased % of fluorescence remaining in the stomach relative to controls. (B) The average % fluorescence remaining in each small intestine segment is plotted to show the distribution of tracer throughout the small intestine. (C) The geometric center of the fluorescence distribution among the small intestine segments was calculated and demonstrates a shift towards more proximal small intestine. All graphs show mean ± SEM (n=14-18). *** = $p < 0.001$, * = $p < 0.05$

A

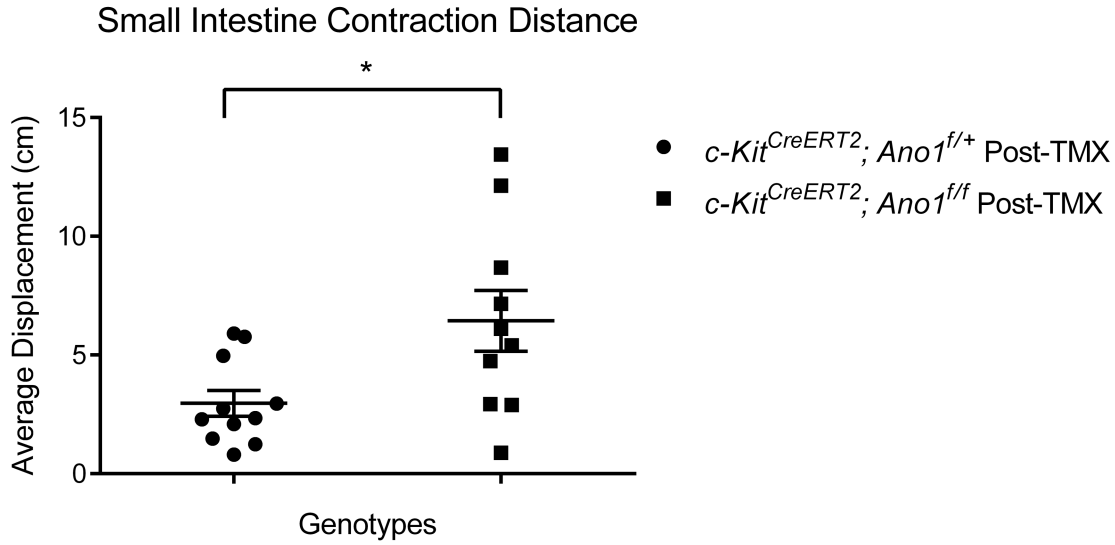
Small Intestine Contraction Distance
*
Average Displacement (cm)
15
10
5
0
Genotypes
c-Kit CreERT2; Ano1 f/+ Post-TMX
c-Kit CreERT2; Ano1 f/f Post-TMX

B

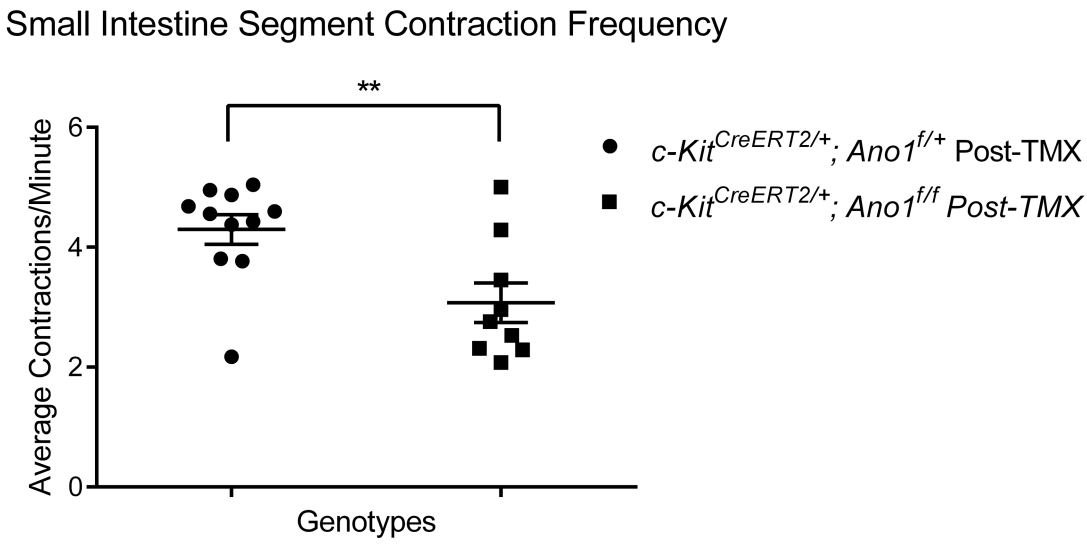
Small Intestine Segment Contraction Frequency
**
Average Contractions/Minute
6
4
2
0
Genotypes
c-Kit CreERT2/+; Ano1 f/+ Post-TMX
c-Kit CreERT2/+; Ano1 f/f Post-TMX

Figure 10. Reducing ANO1 expression impairs contractile behavior

(A) Gastrointestinal tracts were carefully dissected from the mice and placed in pre-warmed PBS. Videos were captured of spontaneous contractile behavior. Total distance travelled by jejunum in 1 minute was analyzed using Tracker video analysis software. *c-Kit*^{CreERT2}*; Ano1*$^{f/f}$ mice showed a significant increase in jejunum movement. (B) Jejunum was dissected into 1cm segments and placed in pre-warmed PBS. Videos were captured of the spontaneous contractions of each segment comprising the entire jejunum length. The mean number of contractions per minute was calculated for each mouse. Graph shows mean ± SEM. * = $p < 0.05$, ** = $p < 0.005$

Chapter 3: Loss of Ano1 delays pubertal mammary gland development

3.1 Introduction

While calcium-induced chloride currents have been recognized for some time, with an established role in regulating fluid and electrolyte secretion in secretory tissues including salivary gland and mammary gland, their molecular identity was only recently identified to be ANO1[1–3]. Activation of G-protein-coupled receptors (GPCRs) by various ligands including ATP, acetylcholine and histamine triggers ANO1-mediated calcium-induced chloride currents by stimulating the release of intracellular Ca^{2+} from internal stores[4–7]. ANO1 is expressed in many secretory epithelia including the pancreas, salivary glands, mammary glands and lung airways[2,8]. Mice carrying null mutations die within one month of life as a result of tracheal malformations[9], which has precluded characterization of its role in the development and function of adult secretory tissues.

Murine mammary gland (MG) development begins during embryogenesis when the ectoderm gives rise to bilateral mammary/milk lines that resolve into five pairs of placodes and form a rudimentary mammary ductal tree by parturition[10,11]. Extensive MG development occurs during puberty when hormones and growth factors initiate formation of terminal end buds (TEBs), which are multilayered epithelial swellings at the tips of the rudimentary ducts[10,12]. TEBs are comprised of a single layer of cap cells surrounding multiple layers of body cells, which will differentiate into myoepithelial cells and luminal cells in a mature duct[10]. Pubertal MG expansion is driven by the proliferation of cap and body cells leading to ductal elongation, bifurcation and lateral branching until the majority of the fat pad is occupied[10–12].

ANO1 is expressed in luminal epithelial cells in pubertal and adult MG and regulates mammary epithelial cell proliferation *in vitro*[13], but its role in MG development is unknown. Chloride transport has been shown to regulate mammary branching morphogenesis. Disruption of the Na^+-K^+-$2Cl^-$ cotransporter NKCC1 impaired MG development following transplantation, such that there was increased secondary branching, incomplete filling of the fat pad and persistence of TEBs[14]. NKCC1 is expressed in the basolateral membrane of secretory epithelial cells where it maintains a high intracellular chloride concentration to facilitate chloride efflux into the lumen following the opening of apical chloride channels such as ANO1[15,16]. It is currently unknown whether ANO1-mediated chloride secretion also regulates branching morphogenesis.

To determine the localization of ANO1 expression within murine mammary epithelial cells, immunohistochemistry (IHC) analysis using an ANO1 antibody was performed and demonstrated strong expression of ANO1 in the luminal-facing membrane of mammary ducts. Animals carrying *MMTV-Cre* (*M-Cre*) allele were then crossed with *Ano1*$^{f/f}$ mice to reduce ANO1 expression in pubertal developing MGs. Analysis of mammary gland whole mounts from these mice demonstrated a delay in branching morphogenesis and ductal elongation that subsided by the end of puberty. A role for ANO1 in mammary ductal elongation was supported by analysis of *Ano1*$^{n/n}$ animals, which demonstrated reduced MG ductal length on postnatal day 4. The results of the study suggest that ANO1 may play an important role in MG branching morphogenesis during puberty but its expression is not required for development of normal MGs.

3.2 Methods

Mammary gland whole mounts

For the mammary gland whole-mount experiments, 6, 8 and 10 week old female mice of the indicated genotypes were sacrificed by CO_2 asphyxiation followed by cervical dislocation. The inguinal mammary glands were carefully dissected, spread onto microscope slides, allowed to adhere to the slide for 5 minutes then immersed in Carnoy's fixative (6:3:1; 100% EtOH, chloroform and glacial acetic acid) overnight at 4 ^{O}C. Then the slides were washed in 70% and 50% ethanol for 15 minutes each. Distilled water was then gradually added to the slides to replace the 50% ethanol with pure water. The slides were left in the distilled water wash for 5 minutes and stained in carmine alum solution overnight at 4 ^{O}C. The next day, the carmine stain was removed and replaced with 50%, 70%, 95% and 100% ethanol and incubated for 15 minutes each then cleared in xylenes overnight. After the tissue was fully dehydrated, images of the mammary gland whole-mount slides were taken using a Zeiss Lumar V12 Stereomicroscope.

To measure the extent of mammary gland development, ductal length and the number of secondary and tertiary branches were calculated. Ductal penetration into the fat pad was determined by measuring the length past the lymph node of the three longest primary ducts in each gland and finding the average. Secondary branch frequency was quantified by dividing the number of ramifications extending from 10 portions of primary duct divided by the lengths of the duct portions. Similarly, tertiary branch frequency was determined by dividing the number of ramifications extending from 10 lengths of secondary ducts divided by their measured lengths. The 10 counts of branches per

millimeter were used to find an average secondary and tertiary branch frequency for each animal. The results for the 6, 8 and 10 week experiments are reported as means of the average branches per millimeter values that were assessed for each animal.

Statistics

The results are presented as means +/- standard error of the mean (SEM). T-tests were used to calculate statistical significance with cutoff of $p<0.05$.

Immunohistochemistry

Mammary glands were fixed in 4% PFA in PBS for 1 hour then washed in PBS three times. Cryosections were blocked with 10% donkey serum and 10% goat serum in 0.1% Triton X-100. ANO1 antibody from Abcam(53212, Cambridge, UK) and Keratin 8 antibody from DSHB (Iowa) were used at 1:500 dilutions in blocking buffer. Alexa Fluor secondary dyes from ThermoFisher Scientific (Waltham, MA) were used at 1:500 dilutions in blocking buffer. In proliferation studies, mice were injected with 5mg/ml EdU (ThermoFisher Scientific) at a dose of 10μl/gram of body weight 2 hours before sacrifice. EdU incorporation was assessed using the Click-iT EdU kit from ThermoFisher Scientific.

To calculate the fluorescence intensities within the mammary gland ducts, Fiji image analysis software was used. The total measured amount of ANO1 fluorescent signal was divided by the total measured amount of Keratin 8 signal for a selected mammary duct to determine the relative luminal cell intensity of ANO1 expression. The

average of measurements from ten ducts per animal were found and reported as means for each genotype.

Laboratory Animals

Mice carrying the *MMTV-Cre* allele (*M-Cre*) were generously provided by the Werb lab at UCSF and bred with previously generated mice carrying floxxed versions of *Ano1* (*Ano1*$^{f/f}$). The mice were then backcrossed to create *M-Cre*; *Ano1*$^{f/f}$ animals, which were used for experiments. *M-Cre*; *Ano1*$^{f/+}$ and *Ano1*$^{f/f}$ animals served as controls. All mouse experiments were approved by the UCSF institutional animal care and use committee.

3.3 Results

Adult mice express ANO1 in the luminal membrane of mammary duct epithelial cells

To determine the localization of ANO1 within adult murine mammary gland, immunohistochemistry analysis was performed using antibodies against ANO1 and Keratin 8. The results showed colocalization of ANO1 and Keratin 8. There was also concentrated expression of ANO1 along the luminal-facing membrane of apical cells within mammary ducts of 6 and 10-week old mice (Figure 1A and B).

ANO1 expression in the mammary glands of *M-Cre*; *Ano1*$^{f/f}$ is reduced

After observing robust expression of ANO1 in the luminal-facing membrane of mammary ductal cells, *Ano1*$^{f/f}$ mice were crossed with *MMTV-Cre* expressing animals

(*M-Cre*) to determine the importance of ANO1 in mammary gland development. M-Cre expression within the mammary gland begins around 3 weeks and can be detected throughout the developing gland by 6 weeks of age[17]. Immunohistochemistry analysis using ANO1 antibody showed that mammary glands from 6 and 10-week old *M-Cre*; *Ano1*$^{f/f}$ animals have reduced expression of ANO1 compared with *MMTV-Cre*; *Ano1*$^{f/+}$ controls (Figure 1A and 1B). Comparing the ratios of total ANO1 fluorescence relative to total K8 fluorescence in 10-week MG ducts showed a 50% reduction in ANO1 signal in *M-Cre; Ano1*$^{f/f}$ animals compared with controls (Figure 1C).

Reducing ANO1 expression impairs ductal growth and branching

To determine the effects of reduced ANO1 expression within mammary gland on branching morphogenesis and ductal growth, MG whole-mounts were stained with carmine red dye. MG whole-mounts were prepared from 6 and 10 week old mice (Figure 2A and 2B). Measurement of ductal penetration into the fat pad of 6 and 10-week old *M-Cre; Ano1*$^{f/f}$ animals compared with controls did not show differences (Figure 3C). Analysis of the frequency of secondary branching also failed to show a difference between *M-Cre; Ano1*$^{f/f}$ animals and controls (Figure 2C). However, there was a trending reduction in secondary branches when comparing 10 week old MGs from *M-Cre; Ano1*$^{f/f}$ mice with controls.

To determine whether loss of ANO1 expression delayed MG development midway through puberty, MG whole-mounts were prepared from 8-week old *M-Cre; Ano1*$^{f/f}$ *mice* and control littermates (Figure 3A). Analysis of branching frequency revealed significant decreases in secondary and tertiary branching in *M-Cre; Ano1*$^{f/f}$ mice

compared with control littermates (Figure 3B). *M-Cre; Ano1$^{f/f}$* animals also demonstrated reduced ductal extension into the fat pad compared with controls (Figure 3C).

To determine whether the impaired ductal growth within MGs from 8-week old *M-Cre; Ano1$^{f/f}$* mice was a result of impaired luminal cell proliferation, Edu incorporation was assessed with immunohistochemistry. There was a trending increase in the percent of Keratin 8-expressing luminal cells that also incorporated Edu within MGs from *M-Cre; Ano1$^{f/f}$* mice compared with control littermates (Figure 5). Two out of the three *M-Cre; Ano1$^{f/f}$* mice assessed had a greater percentage of luminal cells harboring Edu than their control littermates.

Global loss of ANO1 expression during embryogenesis reduced ductal growth

Since reducing MG ANO1 expression during postnatal MG development impaired branching morphogenesis and ductal extension midway through puberty, to determine whether ANO1 also plays a role in embryonic and early postnatal MG development whole-mounts were prepared from *Ano1$^{n/n}$* mice at postnatal day 3 (Figure 4A). *Ano1$^{null/null}$* mice showed a decrease in ductal length compared with littermate controls (Figure 4B).

3.4 Discussion

There have been few previous studies investigating the role of ion channels during mammary gland development. In one study, loss of Na-K-Cl cotransporter (NKCC1) expression in mice increased ductal side branching and delayed ductal outgrowth[18]. While it has been previously shown that ANO1 is expressed in lactating mouse mammary

epithelial cells where it contributes to CaCC activity[19], its role in mammary gland development and branching morphogenesis is unknown. To characterize ANO1 expression within pubertal and adult mouse mammary duct epithelium, immunohistochemistry analysis was performed utilizing antibodies against ANO1 and a marker of luminal cells (Keratin 8), which demonstrated localized ANO1 expression on the luminal-facing membrane of K8-expressing ductal epithelial cells.

To determine the importance of ANO1 for MG branching and ductal outgrowth, *Ano1*$^{f/f}$ mice were crossed with mice expressing Cre-Recombinase under control of the mouse mammary tumor virus (MMTV) promoter, which expresses throughout the mammary epithelium during puberty[17]. Reduced ANO1 expression in *M-Cre; Ano1*$^{f/f}$ mice did not cause defects in mammary growth during early or late puberty. However, assessment of MGs from animals at 8 weeks of age demonstrated that loss of ANO1 expression caused a significant delay in mammary branching and ductal extension midway through puberty that recovered by 10 weeks of age. This delay in mammary branching morphogenesis and ductal elongation may be associated with increased luminal cell proliferation, but future studies will need to clarify this finding with more animals.

The importance of ANO1 in mammary growth was also supported by the observation that *Ano1*$^{nl/n}$ mice have reduced ductal elongation at postnatal day 3. Since *Ano1*$^{n/n}$ mice do not survive beyond the first week of life, this model could not be used to corroborate the role of ANO1 during pubertal MG development. Future experiments should use additional Cre-recombinase models to interrogate and clarify the specific requirements for ANO1 expression within luminal cells during branching morphogenesis.

The mechanism for how ANO1 regulates mammary branching and ductal extension could be through activation of EGFR-dependent and MAPK signaling. ANO1 has been shown to promote breast cancer growth through activation of EGFR and CAMKII and subsequent stimulation of AKT and mitogen-activated protein kinase 1 (MAPK) pathways[20]. It was also shown that ANO1 facilitates secretion of EGF and TGF-β to activate these signaling pathways and support tumor growth and proliferation. Since it has been shown that EGF promotes TEB formation[21] and MG expression of EGFR within the stroma is required for ductal outgrowth and branching morphogenesis[22,23], it is possible that ANO1 regulates MG branching and ductal extension by stimulating the secretion of EGF.

One challenge with characterizing the specific effects of ANO1 depletion on MG growth during puberty using the described models was the unavailability of *Ano1*^{f} alleles in mice on a pure background at the time of investigation. It is well established that different mouse background strains display variations in pubertal mammary branching, terminal end bud and ductal growth kinetics [24–27] and the mice used in this study were on a C57BL/6J and FVB/NJ mixed background. As a result, there was considerable variation among the *M-Cre; Ano1*$^{f/f}$ mice and their littermate controls used in the studies. For example, as shown in Figure 2C within the cohort of mice used for the 6-week MG analysis, there were outliers demonstrating branching frequencies much higher than the rest of the group. This is also consistent with a previous study, which characterized the intrinsic variation within adult mammary glands from mice on a pure background[24]. The group discovered that among 29 adult C57BL/6J mice, the MG branching morphology patterns could be classified into three different groups based on the frequency of primary,

secondary, and tertiary branches, alveolar buds and alveoli[24]. This intrinsic variation in higher-order branching that is observed among age-matched animals of identical background together with strain influence on MG ductal growth kinetics complicated assessment of the phenotype resulting from the genetic perturbation of ANO1 expression. Both sources of variation were observed in the present study where considerable differences were encountered within and among the mouse cohorts assessed at the different time points.

To reduce the influence of mixed strain background that was observed in the present study, *Ano1*$^{f/f}$ animals on a pure C57BL/6J background were acquired and bred with an *M-Cre* allele in the same strain. These mice could be used in future experiments to clarify the importance of ANO1 in MG branching morphogenesis during various stages of pubertal development.

Previous studies have focused on characterizing the role of ion channels in mammary ductal secretion[28,29]. The observation that normal mouse mammary ducts express ANO1 on the luminal-facing membrane together and its role in promoting proliferation of breast cancer cells suggested that ANO1 may influence the formation and growth of developing mammary gland ducts. It is important to determine whether perturbing ANO1 function and expression interferes with normal mammary tissue, since preclinical experiments in mice have supported the potential for using ANO1 inhibitors therapeutically in the treatment of cancer. In the current study, we show that reducing ANO1 expression during pubertal MG growth delays branching morphogenesis and ductal extension but this impairment subsides later in puberty. Future experiments should

use this model to determine the importance of ANO1 in lactation *in vivo* and the consequent ability of the dams to nurse their young.

References

1. Yang, Y. D. *et al.* TMEM16A confers receptor-activated calcium-dependent chloride conductance. *Nature* **455,** 1210–1215 (2008).
2. Schroeder, B. C., Cheng, T., Jan, Y. N. & Jan, L. Y. Expression cloning of TMEM16A as a calcium-activated chloride channel subunit. *Cell* **134,** 1019–1029 (2008).
3. Caputo, A. *et al.* TMEM16A, a membrane protein associated with calcium-dependent chloride channel activity. *Science* **322,** 590–4 (2008).
4. Large, W. A. & Wang, Q. Characteristics and physiological role of the Ca(2+)-activated Cl- conductance in smooth muscle. *Am J Physiol* **271,** C435-54 (1996).
5. Lee, M. G., Zeng, W. & Muallem, S. Characterization and localization of P2 receptors in rat submandibular gland acinar and duct cells. *J Biol Chem* **272,** 32951–32955 (1997).
6. Zholos, A. *et al.* Ca(2+)- and volume-sensitive chloride currents are differentially regulated by agonists and store-operated Ca2+ entry. *J Gen Physiol* **125,** 197–211 (2005).
7. Lee, M. G., Ohana, E., Park, H. W., Yang, D. & Muallem, S. Molecular mechanism of pancreatic and salivary gland fluid and HCO3 secretion. *Physiol Rev* **92,** 39–74 (2012).
8. Huang, F. *et al.* Studies on expression and function of the TMEM16A calcium-activated chloride channel. (2009).
9. Rock, J. R., Futtner, C. R. & Harfe, B. D. The transmembrane protein TMEM16A is required for normal development of the murine trachea. *Dev Biol* **321,** 141–149

(2008).

10. Macias, H. & Hinck, L. Mammary gland development. *Wiley Interdiscip Rev Dev Biol* **1,** 533–557 (2012).
11. Cowin, P. & Wysolmerski, J. Molecular mechanisms guiding embryonic mammary gland development. *Cold Spring Harb Perspect Biol* **2,** a003251 (2010).
12. Gjorevski, N. & Nelson, C. M. Integrated morphodynamic signalling of the mammary gland. *Nat Rev Mol Cell Biol* **12,** 581–593 (2011).
13. Britschgi, A. *et al.* Calcium-activated chloride channel ANO1 promotes breast cancer progression by activating EGFR and CAMK signaling. **110,** (2013).
14. Shillingford, J. M. *et al.* Mouse Mammary Epithelial Cells Express the Na-K-Development and Morphogenesis. **16,** 1309–1321 (2014).
15. Jang, Y. & Oh, U. Anoctamin 1 in secretory epithelia. *Cell Calcium* **55,** 355–61 (2014).
16. McManaman, J. L., Reyland, M. E. & Thrower, E. C. Secretion and fluid transport mechanisms in the mammary gland: comparisons with the exocrine pancreas and the salivary gland. *J. Mammary Gland Biol. Neoplasia* **11,** 249–68 (2006).
17. Wagner, K. U. *et al.* Spatial and temporal expression of the Cre gene under the control of the MMTV-LTR in different lines of transgenic mice. *Transgenic Res* **10,** 545–553 (2001).
18. Shillingford, J. M., Miyoshi, K., Flagella, M., Shull, G. E. & Hennighausen, L. Mouse mammary epithelial cells express the Na-K-Cl cotransporter, NKCC1: characterization, localization, and involvement in ductal development and morphogenesis. *Mol Endocrinol* **16,** 1309–1321 (2002).

19. Kamikawa, A., Ichii, O., Sakazaki, J. & Ishikawa, T. Ca^{2+} -activated Cl^{-} channel currents in mammary secretory cells from lactating mouse. *Am. J. Physiol. - Cell Physiol.* ajpcell.00050.2016 (2016). doi:10.1152/ajpcell.00050.2016

20. Britschgi, A. *et al.* Calcium-activated chloride channel ANO1 promotes breast cancer progression by activating EGFR and CAMK signaling. *Proc Natl Acad Sci U S A* **110,** E1026-34 (2013).

21. Coleman, S., Silberstein, G. B. & Daniel, C. W. Ductal morphogenesis in the mouse mammary gland: evidence supporting a role for epidermal growth factor. *Dev Biol* **127,** 304–315 (1988).

22. Robinson, G. W. Cooperation of signalling pathways in embryonic mammary gland development. *Nat. Rev. Genet.* **8,** 963–72 (2007).

23. Wiesen, J. F., Young, P., Werb, Z. & Cunha, G. R. Signaling through the stromal epidermal growth factor receptor is necessary for mammary ductal development. *Development* **126,** 335–344 (1999).

24. Fata, J. E., Chaudhary, V. & Khokha, R. Cellular turnover in the mammary gland is correlated with systemic levels of progesterone and not 17beta-estradiol during the estrous cycle. *Biol. Reprod.* **65,** 680–688 (2001).

25. Maclennan, M. B., Anderson, B. M. & Ma, D. W. L. Differential mammary gland development in FVB and C57Bl/6 mice: Implications for breast cancer research. *Nutrients* **3,** 929–936 (2011).

26. Olson, L., Tan, Y., Zhao, Y., Aupperlee, M. & Haslam, S. Pubertal exposure to high fat diet causes mouse strain-dependent alterations in mammary gland development and estrogen responsiveness LK Olson. *Int. J. Obes.* **1734,** 1415–

1426 (2010).

27. Aupperlee, M. D. *et al.* Strain-specific differences in the mechanisms of progesterone regulation of murine mammary gland development. *Endocrinology* **150,** 1485–1494 (2009).

28. Mobasheri, A. & Barrett-Jolley, R. Aquaporin water channels in the mammary gland: From physiology to pathophysiology and neoplasia. *J. Mammary Gland Biol. Neoplasia* **19,** 91–102 (2014).

29. Blaug, S. *et al.* ENaC- and CFTR-dependent ion and fluid transport in mammary epithelia. *Am. J. Physiol. Cell Physiol.* **281,** C633–C648 (2001).

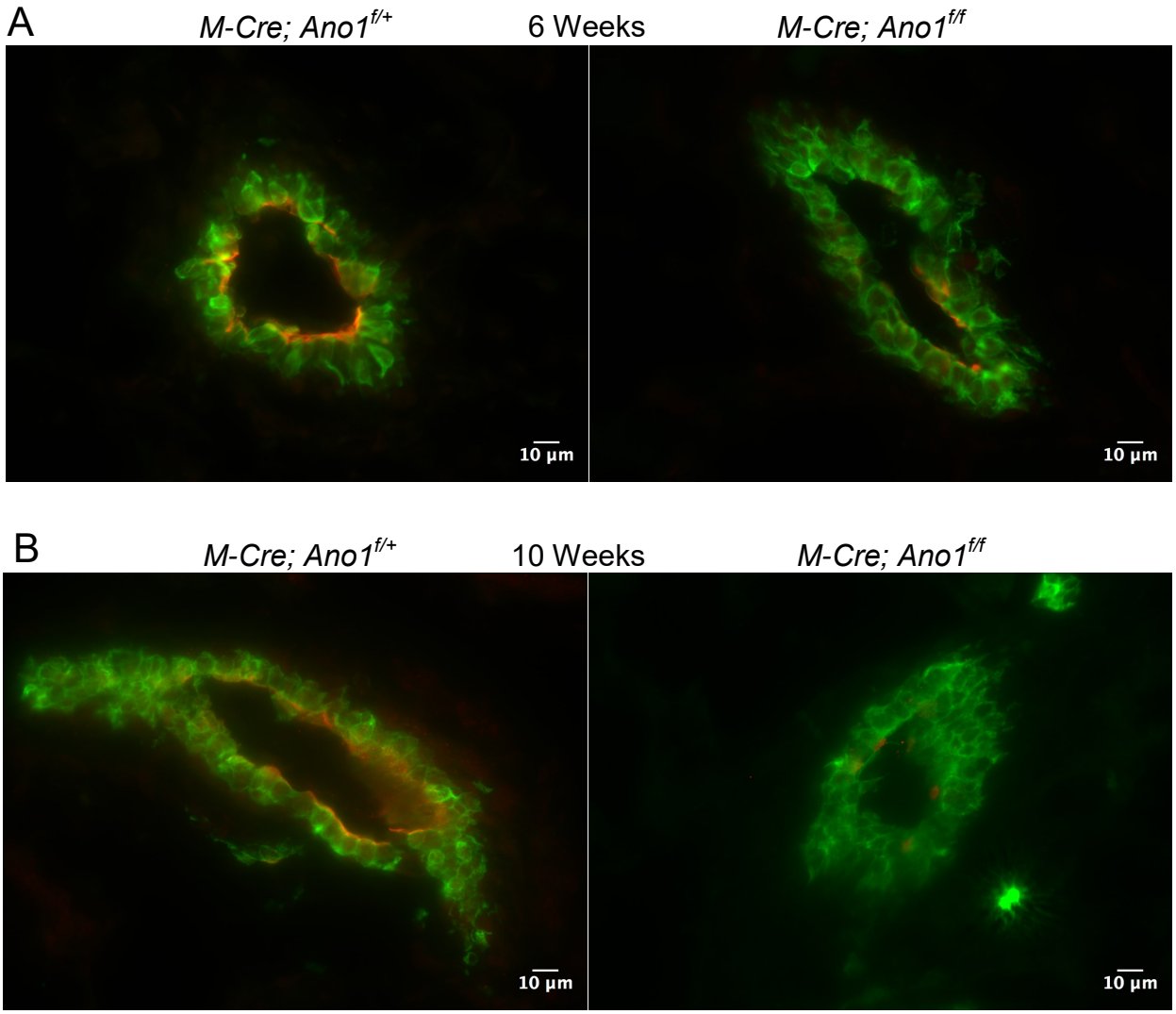
A
M-Cre; Ano1f/+
6 Weeks
M-Cre; Ano1f/f
10 µm
10 µm
B
M-Cre; Ano1f/+
10 Weeks
M-Cre; Ano1f/f
10 µm
10 µm
C
Ano1/K8 Flouorescence Intensity
1.5
1.0
0.5
0.0
**
M-Cre; Ano1f/+
M-Cre; Ano1f/f

Figure 1. MMTV-Cre reduces ANO1 expression in mouse mammary gland ducts

(A-B) Mammary glands were collected from 6 and 10 week old mice and cryosections were labelled with antibodies against ANO1 (red) and Keratin 8 (green). Fluorescence microscopy showed localization of ANO1 in the luminal-facing membrane of mammary ducts in *M-Cre*; *Ano1*$^{f/+}$ control mice (left), which was reduced in *M-Cre*; *Ano1*$^{f/f}$ animals (right). (C) Quantification of fluorescence intensity showed a significant reduction in the total Ano1 signal relative to total Keratin 8 in *M-Cre*; *Ano1*$^{f/f}$ mice compared to *M-Cre*; *Ano1*$^{f/+}$ controls. Graph shows mean ± SEM. ** = $p < 0.005$.

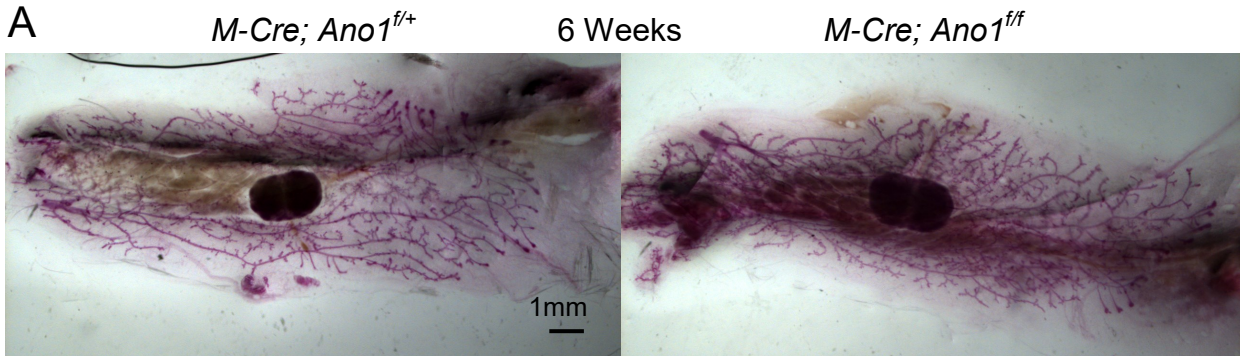
A
M-Cre; Ano1f/+
6 Weeks
M-Cre; Ano1f/f
1mm

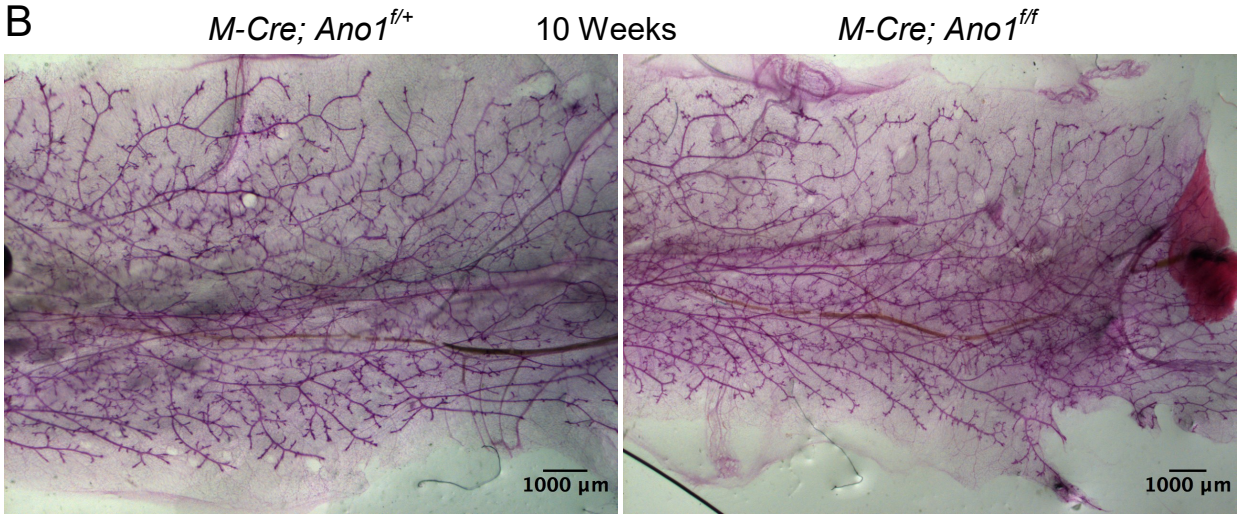
B
M-Cre; Ano1f/+
10 Weeks
M-Cre; Ano1f/f
1000 µm
1000 µm

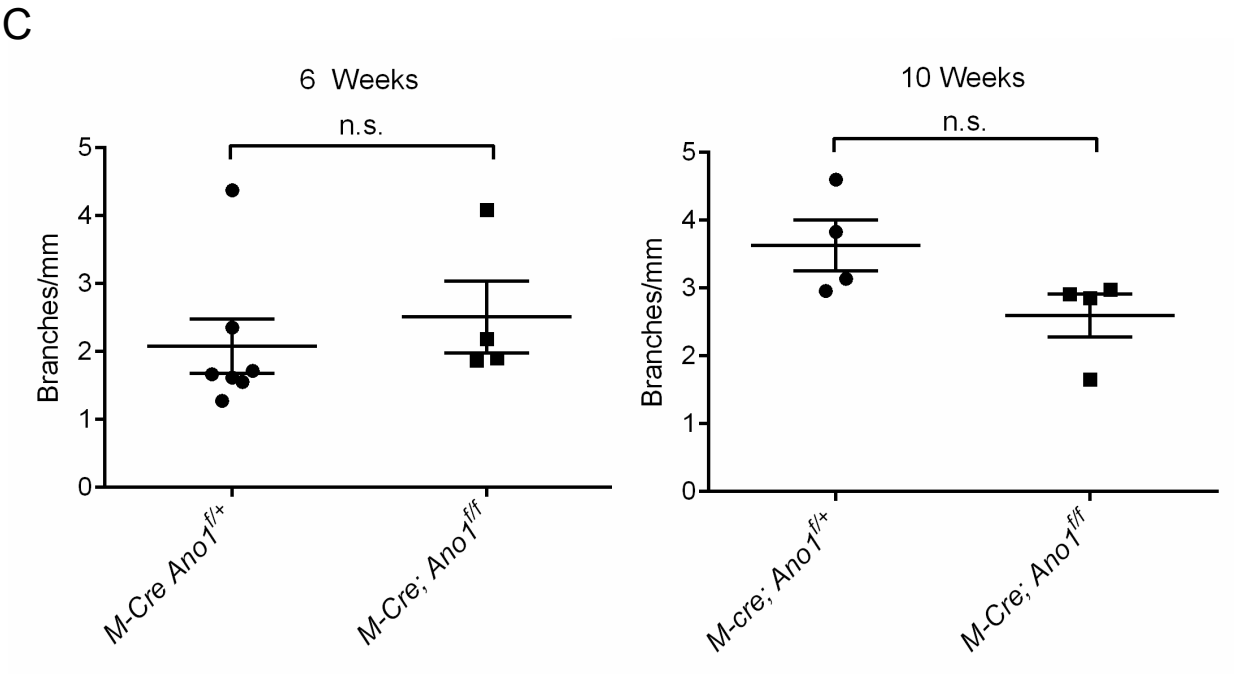
C
6 Weeks
n.s.
Branches/mm
0
1
2
3
4
5
M-Cre Ano1f/+
M-Cre; Ano1f/f
10 Weeks
n.s.
Branches/mm
0
1
2
3
4
5
M-cre; Ano1f/+
M-Cre; Ano1f/f

Figure 2. Reducing ANO1 expression does not affect 6 and 10-week old mammary growth

(A and B) Inguinal mammary glands were collected from 6 and 10-week old mice, whole mounts were prepared and stained with carmine red to show ductal outgrowth and branching. The slides were imaged with a Zeiss Lumar V12 Stereomicroscope. (C) The number of secondary branches per millimeter was quantified in the 6 week old (C) and 10 week old mammary glands (D). The results did not show a difference in the number of secondary branches in *M-Cre*; *Ano1*$^{f/f}$ animals compared to *M-Cre*; *Ano1*$^{f/+}$ controls. n.s. = not significant

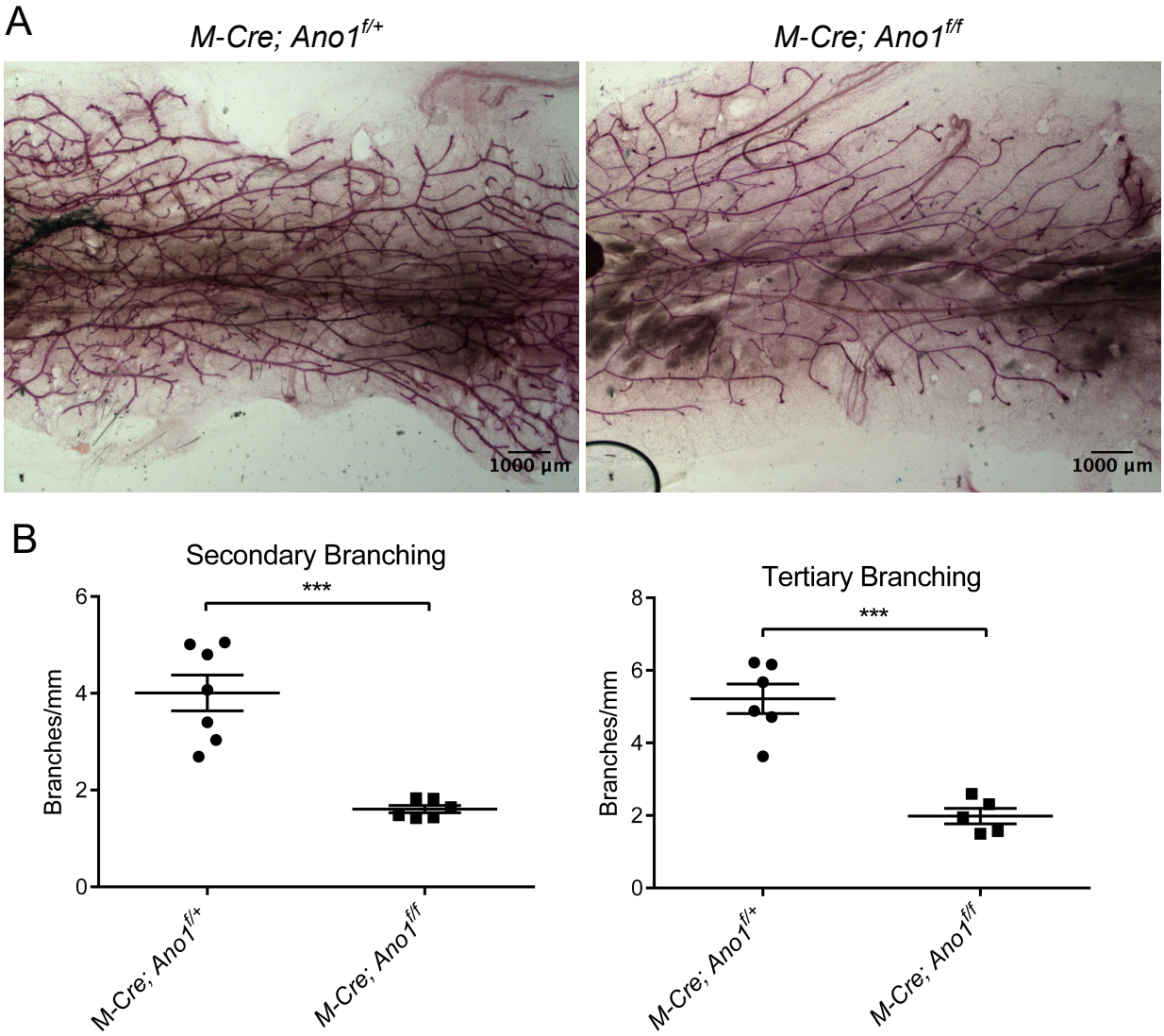
A
M-Cre; Ano1f/+
M-Cre; Ano1f/f
1000 µm
1000 µm
B
Secondary Branching
***
Branches/mm
0
2
4
6
M-Cre; Ano1f/+
M-Cre; Ano1f/f
Tertiary Branching
***
Branches/mm
0
2
4
6
8
M-Cre; Ano1f/+
M-Cre; Ano1f/f
C
*
Duct Length (mm)
0
5
10
15
20
6
8
10
Age (weeks)
M-Cre; Ano1f/+
M-Cre; Ano1f/f

Figure 3. Reducing ANO1 expression delays pubertal mammary gland development

(A) Inguinal mammary glands were collected from 8-week old mice, whole mounts were prepared and stained with carmine red to show ductal outgrowth and branching. The slides were imaged with a Zeiss Lumar V12 Stereomicroscope. (B) The numbers of secondary and tertiary branches per millimeter were quantified. (D) There was a significant decrease in the frequency of secondary and tertiary branches in M-*Cre*; *Ano1*$^{f/f}$ animals compared to *M-Cre*; *Ano1*$^{f/+}$ controls. (C) Ductal length past the lymph node was measured. The results showed a significant decrease in the ductal length of 8-week old *Cre*; *Ano1*$^{f/f}$ mice compared with controls. Graphs show mean ± SEM. *** = $p < 0.0001$; * = $p<0.05$.

A

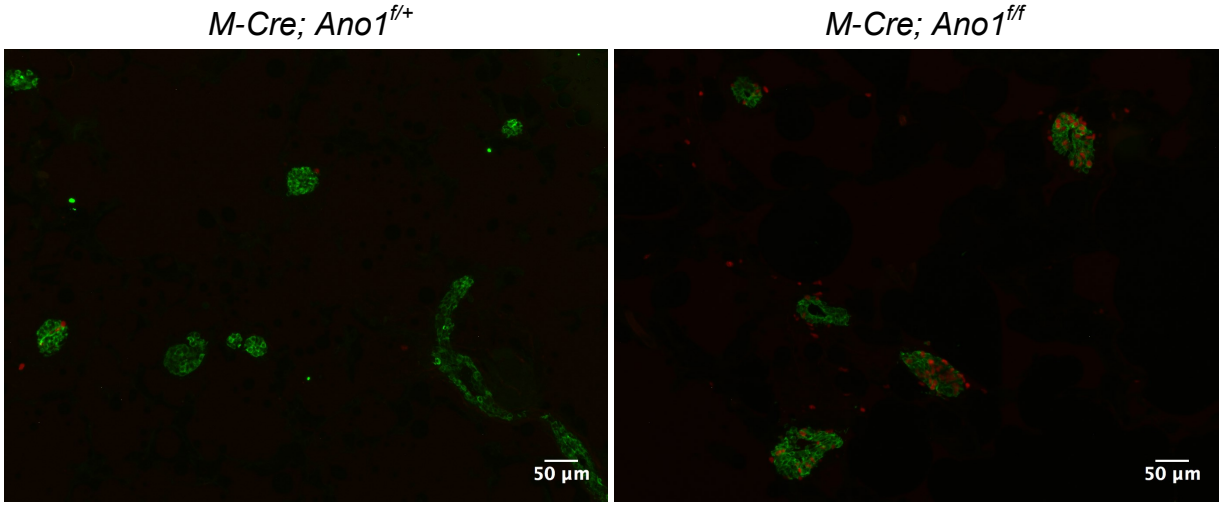
M-Cre; Ano1f/+
M-Cre; Ano1f/f
50 µm
50 µm

B

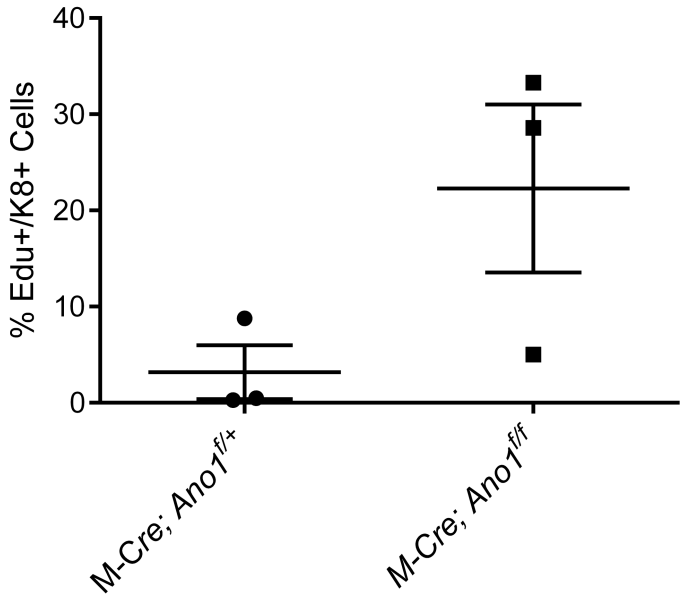
% Edu+/K8+ Cells
40
30
20
10
0
M-Cre; Ano1f/+
M-Cre; Ano1f/f

Figure 4. Delayed mammary growth shows increased luminal cell proliferation

(A and B) 8-week old mice were injected with Edu prior to sacrifice. Cryosections were stained with Keratin 8 (Green) and Edu was labelled using Click-iT® EdU Alexa Fluor (Red). Representative images from *Cre*; *Ano1*$^{f/f}$ mammary gland (A) and *M-Cre*; *Ano1*$^{f/+}$ mammary gland (B) are shown. (C) The percent of Keratin 8-expressing cells that also incorporated Edu was determined for at least 10 mammary ducts per mouse and used to calculate an average. The results showed an increase in the percent of Keratin 8+ luminal cells that incorporated Edu in 2/3 *Cre*; *Ano1*$^{f/f}$ mice compared to controls. Graph shows mean ± SEM.

A

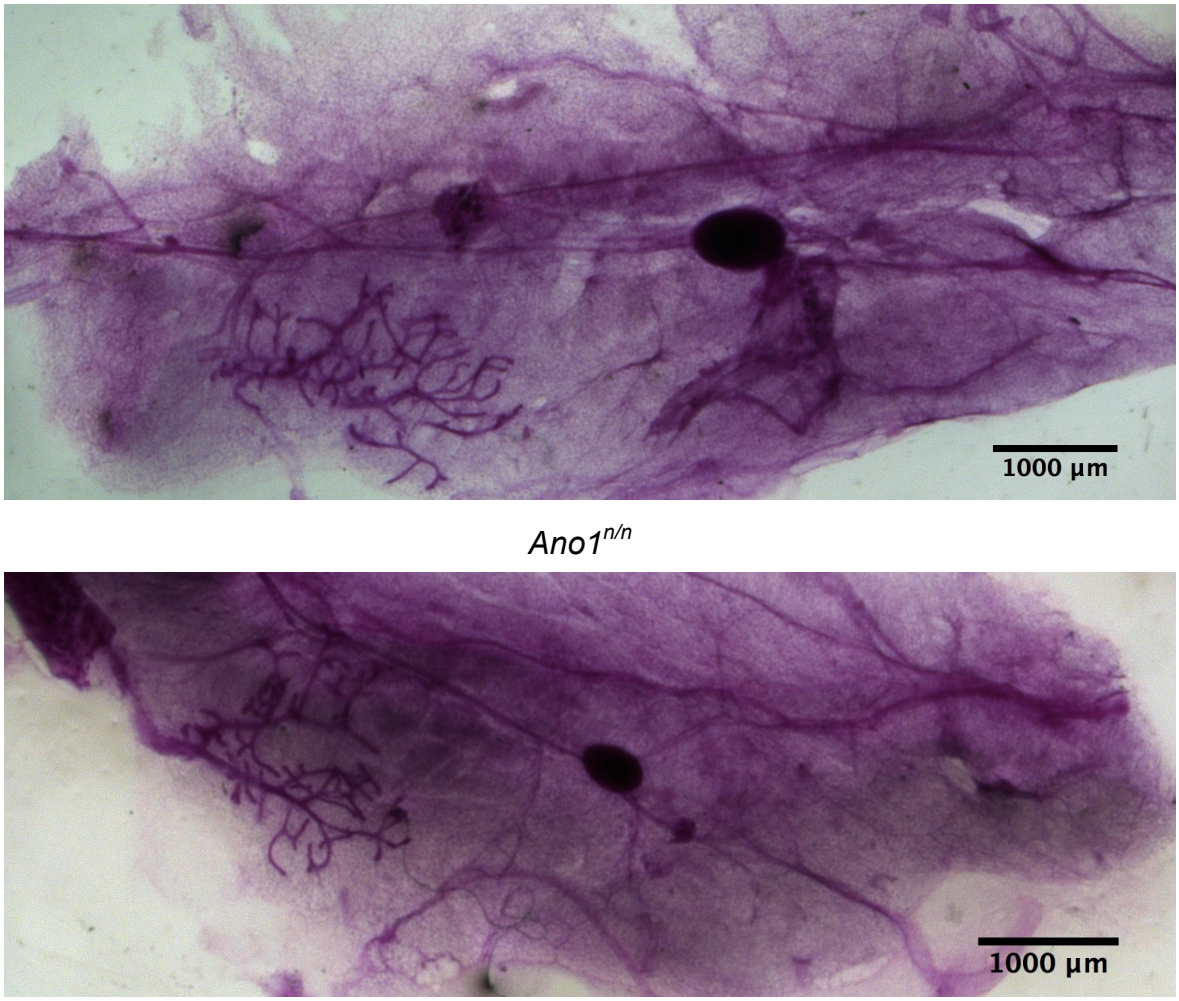

B

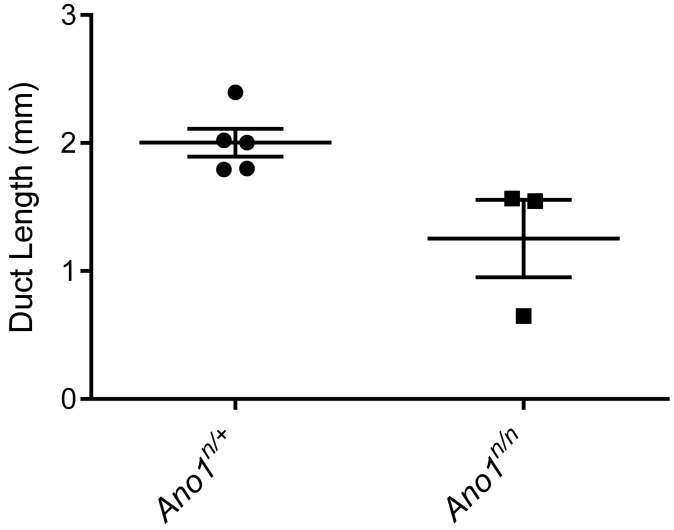

Figure 5. Loss of ANO1 during embryogenesis reduces pre-pubertal ductal elongation

(A and B) Mammary glands were dissected from 3 day old *Ano1*$^{n/n}$ and *Ano1*$^{+/+}$ mice, mounted on slides and stained with carmine red dye. Representative images of *Ano1*$^{n/n}$ (A) and *Ano1*$^{+/+}$ (B) mammary glands are shown. (C) Average ductal length was determined for each mouse and *Ano1*$^{n/n}$ animals showed a significant reduction compared to controls. Graph shows mean ± SEM. * = $p<0.05$.

Chapter 4: ANO1 promotes growth of *MMTV-PyMT* tumors

4.1 Introduction

Even before *Ano1* was demonstrated to be a calcium-activated chloride channel, its upregulation had been observed in several cancers leading to its classification under various names including tumor-amplified and overexpressed sequence 2 (*TAOS2*), discovered on gastrointestinal stromal tumors protein 1 (*DOG1*), and oral cancer overexpressed 2 (*ORAOV2*)[1–3]. *Ano1* is encoded by the 11q13 chromosomal region, which is frequently amplified in human cancers and correlates with poor prognosis[4,5]. Recent studies have demonstrated that increased expression of ANO1, as a result of 11q13 amplification, correlates with worse survival and prognosis in breast cancer, head and neck squamous cell carcinoma (HNSCC) and prostate cancer[6–9]. Experiments utilizing patient-derived cell lines carrying 11q13 amplification have revealed that ANO1 promotes cell growth *in vitro* and in xenograft models through activation of EGFR, MAPK and AKT signaling pathways[7,10]. However, the requirement for ANO1 expression during various stages of cancer progression is currently unknown

Genetically engineered mouse models of breast cancer have been invaluable tools for studying the roles of different oncogenes and signaling pathways in tumor initiation, progression, invasion and metastasis[11,12]. They also enable investigation of the pathogenesis of spontaneously growing breast cancers in the context of an intact immune system, which is known to influence tumor initiation, growth and metastasis[12]. While ANO1 amplification occurs in several breast cancer subtypes, it is more frequently observed in luminal subtypes[13,14]. The *MMTV-PyMT* transgenic mouse has been extensively used as a model for luminal breast cancers because progression to

malignancy in the system is morphologically and molecularly similar to what is observed in human breast cancers[15]. ANO1 is expressed in cells in both the primary tumors and lung metastases in this model but its functional role in tumor initiation and progression has not been studied.

The goal of this study was to establish whether the *MMTV-PyMT* mouse model of luminal breast cancer can be used to study the role of ANO1 in tumorigenesis *in vivo*. To first determine whether ANO1 was expressed in tumors from this breast cancer model, immunohistochemistry (IHC) analysis was performed using antibody against ANO1. The results showed that ANO1 is expressed in primary breast tumors and lung metastasis in this model. shRNA-mediated knockdown of ANO1 in a *MMTV-PyMT* cell line decreased colony formation capacity *in vitro* and delayed tumor growth *in vivo*. These results support that ANO1 promotes breast cancer growth and establishes the *MMTV-PyMT* mouse model as a useful tool for studying the specific contributions of ANO1 to tumor growth, invasion and metastasis *in vivo* in animals with intact immune systems.

4.2 Methods

Cell Culture

MMTV-PyMT cells were previously derived from a *MMTV-PyMT* mouse tumor on FVB/NJ background and were obtained as a gift from Jay Debnath at UCSF. The cells were cultured and propagated in DMEM/F12 supplemented with 10% fetal bovine serum (FBS) and penicillin/streptomycin at 37 ^{o}C in 5% CO_2.

qPCR Analysis of Transcript Levels

MMTV-PyMT cells were resuspended in TRizol from ThermoFisher (Waltham, MA) to extract RNA. cDNA was prepared from the RNA using SuperScript VILO cDNA Synthesis Master Mix from ThermoFisher. qPCR was performed on a Applied Biosystems ViiA 7 Real-Time PCR System (Foster City, CA). GAPDH was used as an internal control. The following primer sequences were used for ANO1 and GAPDH:

shRNA Infections

An ANO1-targetting shRNA (TRCN0000193) and Non-Target shRNA control (SHC016) from the RNAi consortium library were purchased through Sigma (St. Louis, MO). The puromycin marker carried in the pLKO.1 backbone was substituted for turboRFP from a pTRIPZ empty vector. The UCSF ViraCore was used for production of the lentivirus particles. 5×10^5 *MMTV-PyMT* cells were plated per well in a 6 well tissue culture dish and allowed to adhere overnight. Then the cells were transduced with 5×10^6 infectious units overnight and washed with PBS the next day. The cells were grown to confluency then fluorescence activated cell sorting (FACS) was used to select RFP-expressing *MMTV-PyMT* cells. The RFP+ cells were cultured, passaged and used for colony growth assays and transplantation. The maintenance of RFP expression was periodically verified using a fluorescence microscope.

Colony Formation Assay

For the colony formation assay, growth factor reduced Matrigel was first spread on the bottom of a 24-well tissue culture plate. Then *MMTV-PyMT* cells were harvested from a confluent 10cm plate using 0.05% trypsin, subjected to centrifugation and

washing with PBS. After counting, the cells were resuspended in growth factor reduced Matrigel such that 5 x 10^3 cells were plated per well in a 20μl volume of Matrigel. Growth media containing the different chemical inhibitors was added to the wells as indicated. Colony formation efficiency was determined after 1 week in culture by dividing the number of multicellular spheres in each well by 5 x 10^3. The relative colony formation efficiency was then calculated by normalizing the colony formation efficiency associated with each treatment condition by the negative control condition.

Compounds

T16Ainh-A01 (Calbiochem #613551) was dissolved in DMSO to generate a 24mM stock. Benzbromarone from Sigma (St. Louis, MO) was dissolved in DMSO at 500mg/ml then diluted in DMSO to make a 10mM stock. Erlotinib from LC Laboratories #E-4007 (Woburn, MA) and Gefitinib from Selleckchem #S1025 (Houston, TX) were dissolved in DMSO to make solutions with a final concentration of 10mM. The *MMTV-PyMT* cells were treated with the designated concentrations of chemical inhibitors and equal volumes of DMSO as a negative control.

***In vivo* mouse experiments**

For the *in vivo MMTV-PyMT* orthotopic transplant experiments, shRNA-transduced *MMTV-PyMT* cells were cultured to 70% confluency on 15cm plates. The cells were then harvested with 0.05% trypsin, counted and resuspended in 20% Matrigel (v/v) in PBS at a concentration of 2 x 10^4 cells/μl. 6-8 week old FVB/NJ mice were then subcutaneously injected with 50μl of the 20% Matrigel solution so that each mouse was

inoculated with 1 x 10^6 *MMTV-PyMT* cells. All experiments using laboratory mice were conducted in accordance with US law and institutional guidelines.

Immunohistochemistry

Animals were sacrificed by CO_2 asphyxiation followed by cervical dislocation. Engrafted tumors were then dissected and fixed in 4% paraformaldehyde (w/v) in PBS for 1 hour. The tissues were then washed 3 times with PBS and incubated overnight in 30% (w/v) sucrose in PBS. The next day equal volume of O.C.T compound was added and mixed with the tissues for 2 hours then the tissues were frozen. Cryosections with a thickness of 12 μm were mounted onto slides and permeabilized with 0.3% Triton X-100 for 5 minutes, followed by washing with PBS 3 times. The tissues were blocked in PBS containing 3% BSA, 10% donkey serum and 0.1% Triton X-100 for 1 hour then incubated overnight in blocking solution containing primary antibody. For ANO1 staining a 1:500 dilution of the Abcam (Cambridge, U.K.) rabbit anti-Tmem16a polyclonal antibody (ab53212) was used. E-cadherin antibody. Alexa Fluor from ThermoFisher (Waltham, MA) secondary antibodies were used at concentrations of 1:500 in blocking buffer and incubated on the slides for 1-3 hours. Images were collected using a Zeiss Axio Imager M2 (Oberkochen, Germany).

Statistical Analysis

GraphPad Prism was used for figure construction and statistical analysis. Data is expressed as means +/- standard error of the mean (SEM) as indicated.

4.3 Results

MMTV-PyMT tumors express ANO1

To determine whether *MMTV-PyMT* tumors express ANO1 during tumorigenesis and metastasis, immunohistochemistry (IHC) using an ANO1 antibody was performed. An invasive adenocarcinoma from the mammary gland demonstrated robust expression of ANO1 around luminal-facing cells (Figure 1A). A similar ANO1 expression pattern was observed in a lung metastasis from this model (Figure 1B).

Cell lines derived from *MMTV-PyMT* tumors have been useful tools to study the role of particular oncogenes or tumor suppressors in the growth of *PyMT*-driven cancer of the mouse mammary gland *in vitro* and *in vivo*. To determine whether a cell line derived from a *MMTV-PyMT* metastasis expressed ANO1, qPCR analysis was performed comparing expression of ANO1 in the *MMTV-PyMT* line with expression in the Eph4.9 non-tumorigenic mammary epithelial cell line. To confirm that the *MMTV-PyMT* cells expressed functional ANO1, patch-clamp recordings were performed and demonstrated the presence of a calcium-induced chloride current with similar kinetics to previously established ANO1-mediated activity patterns (Chris Peters, Jan Lab).

Blocking ANO1 activity decreases colony formation efficiency *in vitro*

Previous studies using human breast cancer cell lines have shown that blocking ANO1 chloride channel activity with chemical inhibitors reduces growth *in vitro* and in xenograft models[10]. To determine whether ANO1 also promotes growth of *MMTV-PyMT* tumor cells, a colony formation assay was conducted by culturing single *MMTV-PyMT* cells in Matrigel in the presence of two previously described ANO1 inhibitors,

Benzbromarone and T16a01. While T16a01 caused a significant reduction in colony formation efficiency compared with DMSO-treated controls, Benzbromarone treatment had no effect (Figure 2A).

In previous studies it has been demonstrated that ANO1 promotes tumor growth by stimulating EGFR-dependent signaling through MAPK and Akt pathways. To determine whether a similar mechanism of ANO1-mediated growth is present in *MMTV-PyMT* cells, colony formation was assessed in the presence of the EGFR inhibitors Erlotinib and Gefitinib alone and in combination with ANO1 inhibitors. The results showed that Erlotinib treatment alone and in combination with T16a01 reduced colony formation efficiency of *MMTV-PyMT* cells, while Gefitinib treatment and in combination with T16a01 had no effect (Figure 2A). Furthermore, treatment of the cells with T16a01 inhibitor in combination with EGF resulted in growth efficiency that was not significantly different from DMSO-treated cells.

shRNA-mediated knockdown of ANO1 reduces colony formation *in vitro*

To determine whether reducing ANO1 expression also decreased growth, *MMTV-PyMT* cells were infected with lentivirus expressing shRNA that targets ANO1 ($PyMT^{Ano1shRNA}$) or with lentivirus expressing a non-targeting control shRNA ($PyMT^{CtlshRNA}$). To confirm that the ANO1-shRNA reduced ANO1 RNA transcript levels, qPCR was used to compare ANO1 transcript levels between $PyMT^{Ano1shRNA}$ cells and $PyMT^{CtlshRNA}$ cells. The results show a greater than 50% reduction in ANO1 mRNA level in $PyMT^{Ano1shRNA}$ cells compared with $PyMT^{ctlshRNA}$ controls (Figure 3A).

An Edu incorporation assay was performed first to compare proliferative capacities of the cells when cultured in monolayer. FACS analysis of Edu incorporation did not show a significant decrease in proliferation in *PyMT*^{Ano1shRNA} cells compared with *PyMT*^{ctlshRNA} controls (data not shown).

To determine the effects of reduced ANO1 expression on colony formation efficiency, *PyMT*^{Ano1shRNA} and *PyM*^{ctlshRNA} cells were cultured in Matrigel and colony formation was assessed 1 week later. The results showed that *PyMT*^{Ano1shRNA} cells had significantly reduced colony formation ability compared with *PyMT*^{ctlshRNA} cells (Figure 3B and 3C). Furthermore, *PyMT*^{Ano1shRNA} cells treated with EGF displayed reduced colony formation compared with EGF-treated *PyMT*^{ctlshRNA} *cells* (Figure 3B).

shRNA-mediated knockdown of ANO1 reduces growth *in vivo*

To determine whether reducing ANO1 expression in *MMTV-PyMT* cells also reduces their growth *in vivo*, *PyMT*^{Ano1shRNA} and *PyMT*^{CtlshRNA} cells were transplanted orthotopically into the mammary glands of syngeneic FVB/NJ mice. Tumor volume was measured for 4 weeks and the results showed a significant reduction in the sizes of tumors derived from *PyMT*^{Ano1shRNA} cells versus *PyMT*^{ctlshRNA} controls at 2, 3 and 4 weeks following transplantation (Figure 4A).

To confirm whether the shRNA-mediated reduction in ANO1 expression is maintained after growing the tumors *in vivo*, IHC analysis using antibody against ANO1 was performed on *PyMT*^{Ano1shRNA} and *PyMT*^{ctlshRNA}- derived tumor grafts (Figure 4B). The results showed a reduction in ANO1 antibody staining in the *PyMT*^{Ano1shRNA} grafts with residual ANO1 expression in some areas of the tumor (Figure 4B).

4.4 Discussion

Previous studies have established a role for ANO1 in supporting the growth of a variety of cancer types including breast cancer, squamous cell carcinoma of the head and neck (HNSCC), pancreatic cancers, glioblastomas and hepatocellular carcinomas. The results have demonstrated that ANO1 promotes tumor growth in breast cancer and HNSCC through activation of EGFR-dependent MAPK and Akt signaling pathways[10] but the requirement for expression of ANO1 during various stages of cancer progression has not been characterized.

This study demonstrated the utility of a genetically engineered mouse model of luminal breast cancer, *MMTV-PyMT*, for studying the importance of ANO1 in various stages of spontaneous tumor initiation, growth and metastasis *in vivo*. ANO1 is expressed in luminal-facing areas within both primary tumors and lung metastasis in this model. Blocking ANO1-mediated currents with an inhibitor and transcript reduction with shRNA both reduced colony formation efficiency of the cells. Furthermore, ANO1-shRNA reduced tumor growth *in vivo* at 2, 3 and 4 weeks following transplantation. The $PyMT^{Ano1shRNA}$-derived tumors grown *in vivo* also displayed a general reduction in ANO1 antibody staining, although patches with residual ANO1 signal were observed.

To determine whether the mechanism of ANO1-mediated tumor growth in the *MMTV-PyMT* mouse model is consistent with studies from human breast cancer cells, *MMTV-PyMT* cells were treated with chemical inhibitors targeting EGFR alone and in combination with ANO1 inhibitors. The results demonstrated that the EGFR inhibitor, Erlotinib, and ANO1 inhibitor, T16a01, both reduced colony formation efficiency when

used alone. A similar reduction in colony growth was also observed when cells were treated with T16a01 and Erlotinib together, suggesting that combinatorial treatment with the two inhibitors was not synergistic. The result also showed that the reduction in growth observed following inhibition of ANO1, involved decreased signaling through EGFR, since there was no additional growth impairment when both treatments were used simultaneously. Furthermore, the observation that the addition of EGF along with the T16a01 inhibitor did not result in a significant decrease in colony growth, corroborated that the diminished growth following ANO1 inhibition was a result of reduced EGFR signaling.

While ANO1 channel inhibition with T16a01 appeared to reduce colony growth as a result of diminished EGFR signaling, impaired growth resulting from shRNA-induced knockdown of ANO1 may involve other signaling pathways as well. This is suggested by the observation that treatment of $PyMT^{Ano1shRNA}$ cells with EGF did not rescue colony growth. However, when EGF was added along with a pharmacological inhibitor of ANO1 (T16a01) growth was rescued. This is consistent with previous studies demonstrating that ANO1 promotes growth in human breast cancer cells through both EGFR and CAMKII-dependent signaling[10], such that stimulation of either pathway alone does completely rescue the growth impairments resulting from ANO1 knockdown.

These experiments suggest that the *MMTV-PyMT* mouse model of luminal breast cancer could be used to study the specific contributions of ANO1 during various stages of tumor progression *in vivo* in spontaneously growing cancers. This model also enables experiments in which ANO1 expression is reduced through genetic disruption as opposed to RNA interference. Future studies should use the extant $Ano1^{fx}$ allele to study the

effects of ANO1 ablation on different stages of cancer progression in the *MMTV-PyMT* model. One approach could be to cross *Ano1*^{f} mice with those carrying *MMTV-Cre* and *MMTV-PyMT* to reduce ANO1 expression in mammary epithelium *in vivo*. This experiment would also enable investigation of the effects of ANO1 loss during the pathogenesis of spontaneously growing breast cancers within the context of an intact immune system, which has a profound influence on tumor initiation, growth and metastasis[12].

This study provides evidence supporting a role for ANO1 in promoting tumor growth through stimulating EGFR-dependent signaling pathways in an additional form of breast cancer. The results establish the *MMTV-PyMT* model for use in future studies interrogating the mechanism of ANO1-mediated cancer growth in various stages of tumor progression. Further studies are warranted to test whether ANO1 inhibitors could be used clinically in the treatment of cancers harboring 11q13 amplification. However, given the widespread expression of ANO1 across secretory organs, the reproductive system and the gastrointestinal tract, it will be important to consider the potential systemic consequences and associated side-effects resulting from perturbing ANO1 activity as a treatment strategy.

References

1. Huang, X., Gollin, S. M., Raja, S. & Godfrey, T. E. High-resolution mapping of the 11q13 amplicon and identification of a gene, TAOS1, that is amplified and overexpressed in oral cancer cells. *Proc. Natl. Acad. Sci. U. S. A.* **99,** 11369–11374 (2002).
2. West, R. B. *et al.* The novel marker, DOG1, is expressed ubiquitously in gastrointestinal stromal tumors irrespective of KIT or PDGFRA mutation status. *Am. J. Pathol.* **165,** 107–13 (2004).
3. Kashyap, M. K. *et al.* Genomewide mRNA profiling of esophageal squamous cell carcinoma for identification of cancer biomarkers. *Cancer Biol. Ther.* **8,** 34–46 (2009).
4. Jönsson, G. *et al.* Genomic subtypes of breast cancer identified by array-comparative genomic hybridization display distinct molecular and clinical characteristics. *Breast Cancer Res.* **12,** R42 (2010).
5. Wilkerson, P. & Reis-Filho, J. The 11q13-q14 Amplicon: Clinicopathological Correlations and Potential Drivers. *Genes, Chromosom. Cancer* **52,** 333–355 (2013).
6. Liu, W., Lu, M., Liu, B., Huang, Y. & Wang, K. Inhibition of Ca(2+)-activated Cl(-) channel ANO1/TMEM16A expression suppresses tumor growth and invasiveness in human prostate carcinoma. *Cancer Lett* **326,** 41–51 (2012).
7. Duvvuri, U. *et al.* TMEM16A induces MAPK and contributes directly to tumorigenesis and cancer progression. *Cancer Res.* **72,** 3270–81 (2012).
8. Ayoub, C., Wasylyk, C., Li, Y. & Thomas, E. ANO1 amplification and expression

in HNSCC with a high propensity for future distant metastasis and its functions in HNSCC cell lines. *Br. J. …* **103,** 715–726 (2010).

9. Ruiz, C. *et al.* Enhanced expression of ANO1 in head and neck squamous cell carcinoma causes cell migration and correlates with poor prognosis. *PLoS One* **7,** e43265 (2012).
10. Britschgi, A. & Bill, A. Calcium-activated chloride channel ANO1 promotes breast cancer progression by activating EGFR and CAMK signaling. *Proc. …* **110,** E1026-34 (2013).
11. Nash, C. & Speirs, V. Pre-Clinical Modeling of Breast Cancer: Which Model to Choose? 161–175 (2013). doi:10.1007/978-1-4614-5647-6_9
12. Vargo-Gogola, T. & Rosen, J. M. Modelling breast cancer: one size does not fit all. *Nat. Rev. Cancer* **7,** 659–72 (2007).
13. Cerami, E. *et al.* The cBio Cancer Genomics Portal: An open platform for exploring multidimensional cancer genomics data. *Cancer Discov.* **2,** 401–404 (2012).
14. Gao, J. *et al.* Integrative analysis of complex cancer genomics and clinical profiles using the cBioPortal. *Sci. Signal.* **6,** pl1 (2013).
15. Lin, E. Y. *et al.* Progression to malignancy in the polyoma middle T oncoprotein mouse breast cancer model provides a reliable model for human diseases. *Am. J. Pathol.* **163,** 2113–26 (2003).

A

Primary Tumor

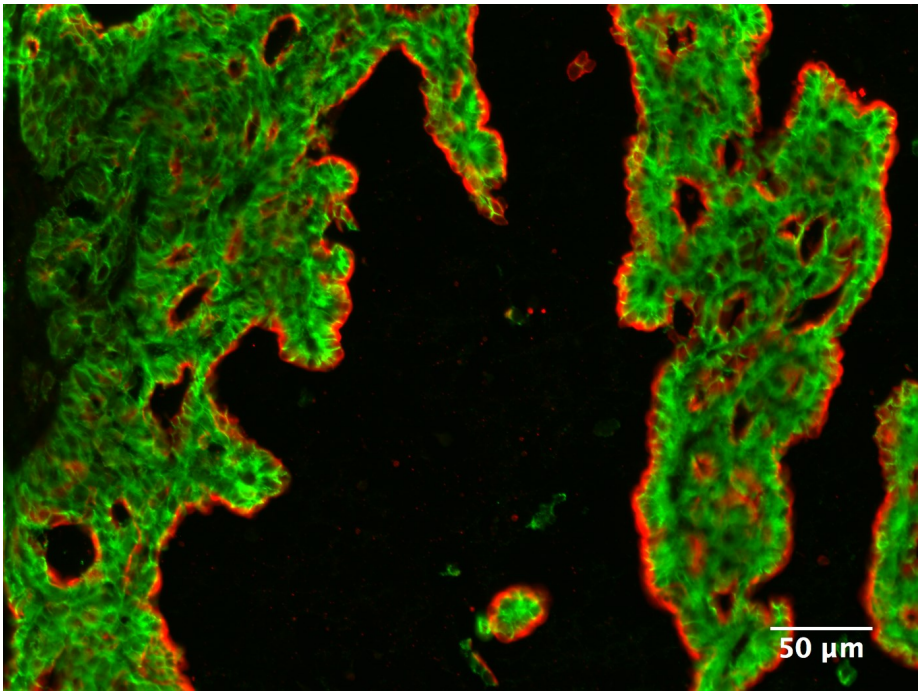

B

Lung Metastasis

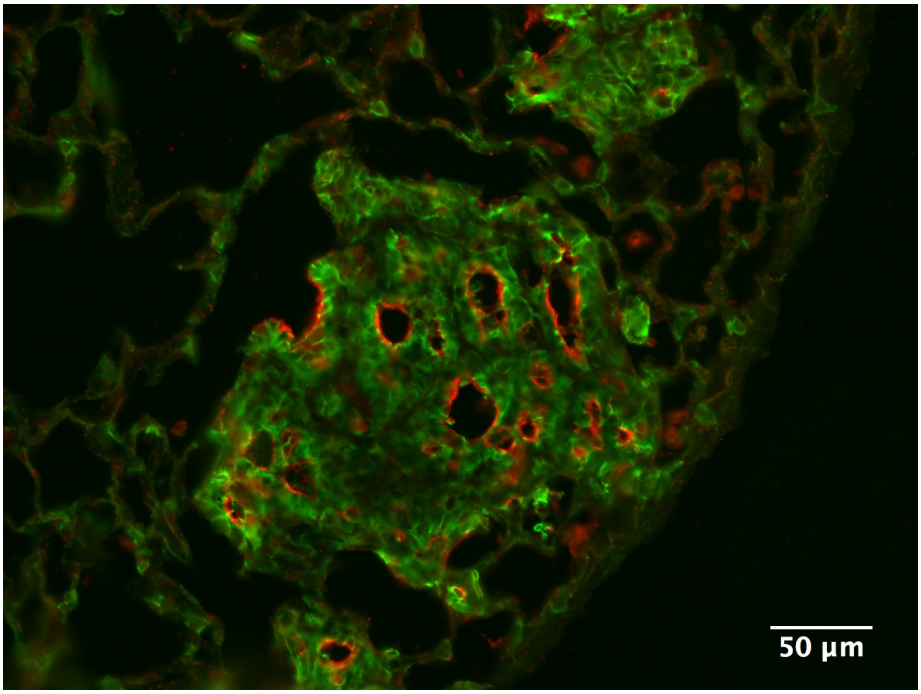

Figure 1: ANO1 was expressed by *MMTV-PyMT* primary tumors and metastasis

Late-stage *MMTV-PyMT* primary mammary tumor (A) and lung metastasis (B) were dissected, sectioned and stained with antibodies against E-cadherin (green) and ANO1 (red). Representative images show ANO1 expression in luminal-facing regions of the tumors, while E-cadherin was expression was broad.

A

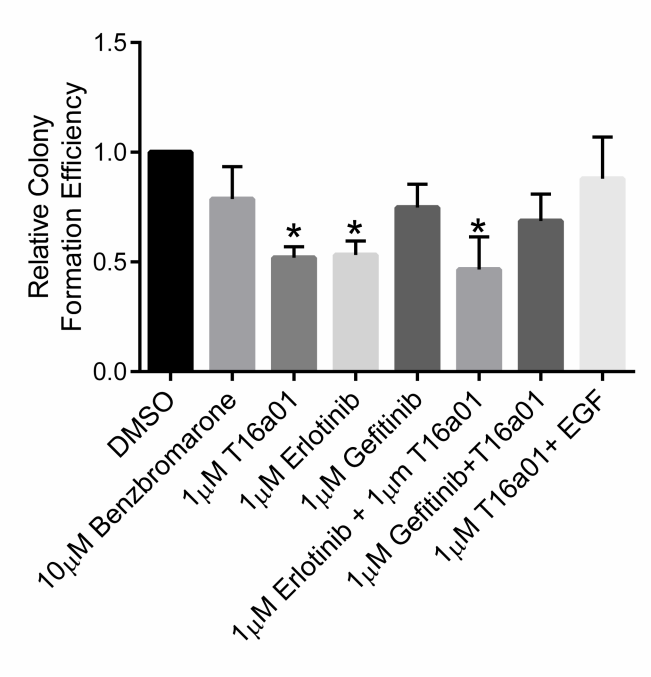
Relative Colony Formation Efficiency
1.5
1.0
0.5
0.0
*
*
*
DMSO
10μM Benzbromarone
1μM T16a01
1μM Erlotinib
1μM Gefitinib
1μM Erlotinib + 1μm T16a01
1μM Gefitinib+T16a01
1μM T16a01+ EGF

B

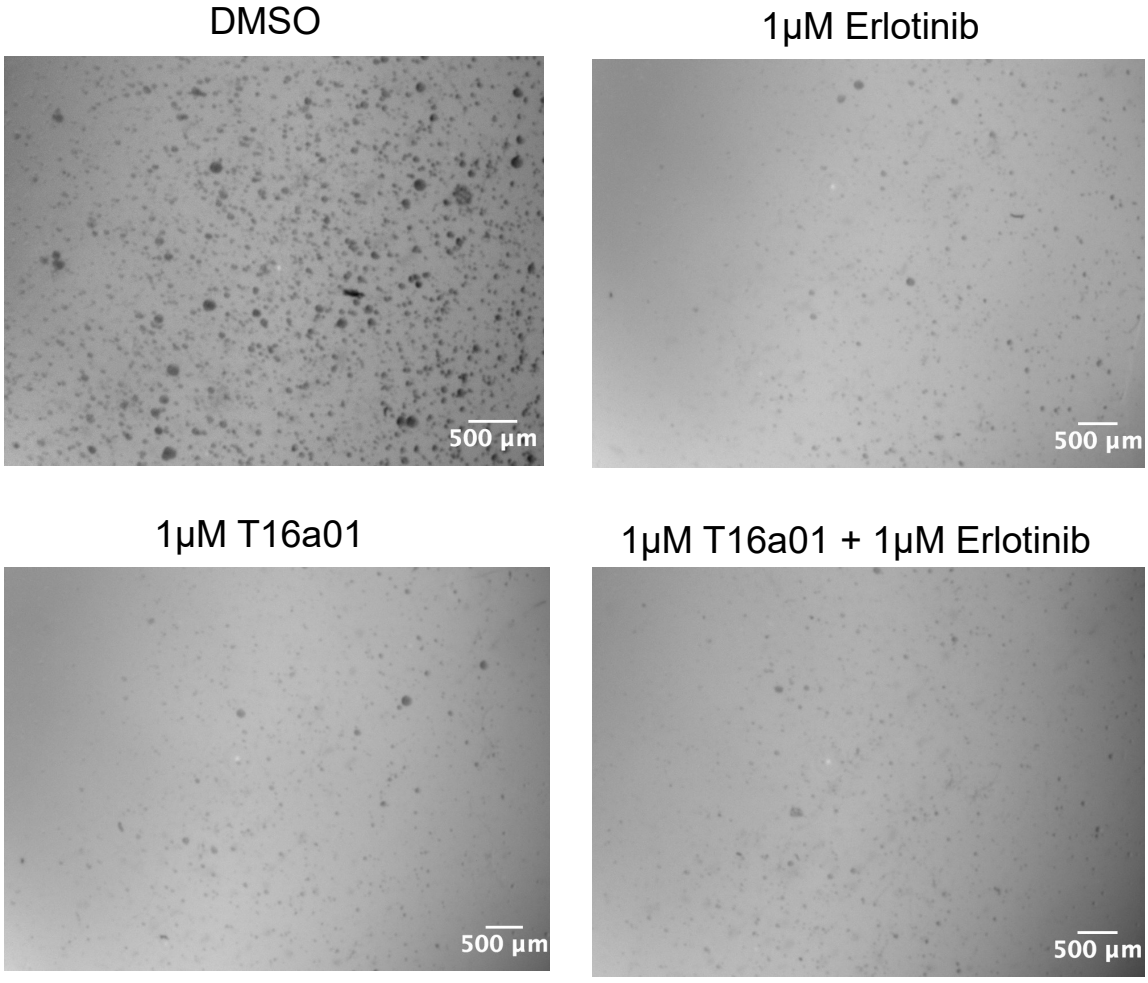
DMSO
500 μm
1μM Erlotinib
500 μm
1μM T16a01
500 μm
1μM T16a01 + 1μM Erlotinib
500 μm

Figure 2: Inhibiting ANO1 in *MMTV-PyMT* cells reduces colony growth *in vitro*

MMTV-PyMT cells were cultured in Matrigel in the presence of 1μM T16a01, 1μM Erlotinib, 1μM Gefitinib or a combination. (A) Quantification of colony formation efficiency among the different inhibitor treatments showed that T16a01 and Erlotinib alone and together blocked colony growth. (B) Representative images after 1 week in culture. Graph shows mean ± SEM. * = $p < 0.05$.

A

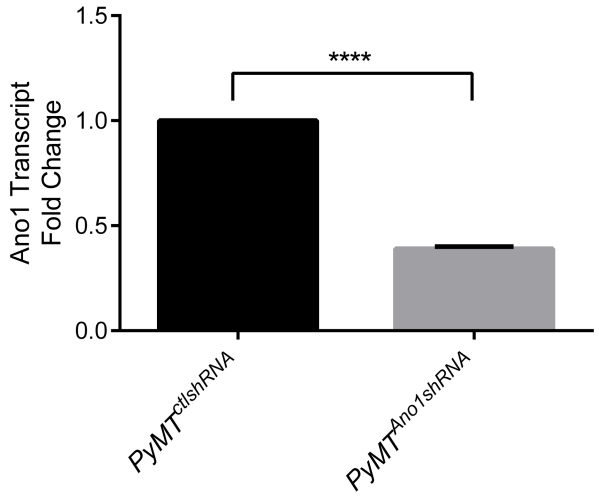
Ano1 Transcript
Fold Change
1.5
1.0
0.5
0.0
****
PyMTctlshRNA
PyMTAno1shRNA

B

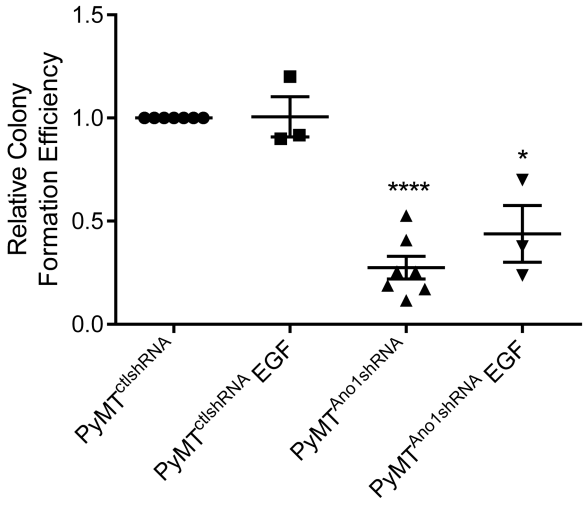
Relative Colony
Formation Efficiency
1.5
1.0
0.5
0.0
****
*
PyMTctlshRNA
PyMTctlshRNA EGF
PyMTAno1shRNA
PyMTAno1shRNA EGF

C

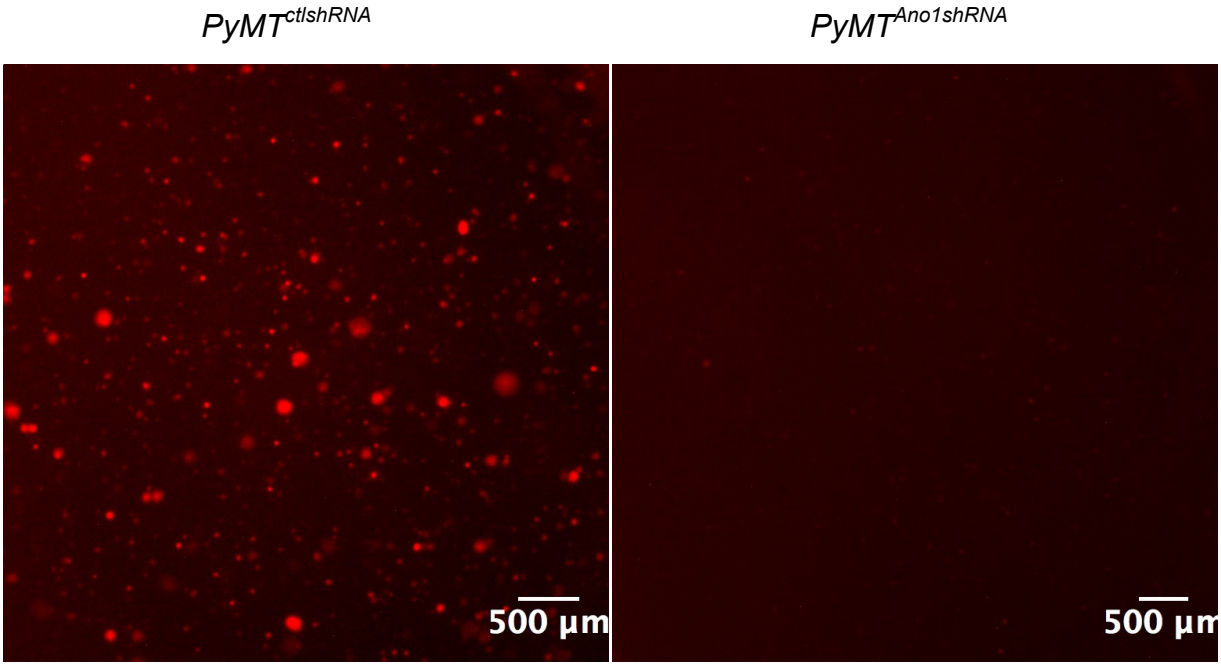
PyMTctlshRNA
PyMTAno1shRNA
500 µm
500 µm

Figure 3: shRNA-mediated knockdown of ANO1 reduces colony growth *in vitro*.

MMTV-PyMT cells were transduced with lentivirus expressing RFP and a control non-targeting shRNA or an shRNA against ANO1. (A) The ANO1 shRNA significantly reduced the ANO1 transcript level. (B) Quantification of colony formation efficiency showed a significant reduction in colony growth of ANO1-shRNA expressing cells after 1 week in culture. (C) Representative images of RFP fluorescence in $PyMT^{ctlshRNA}$ and $PyMT^{Ano1shRNA}$ cultures after 1 week. Graphs show mean ± SEM. **** = $p < 0.0001$

A

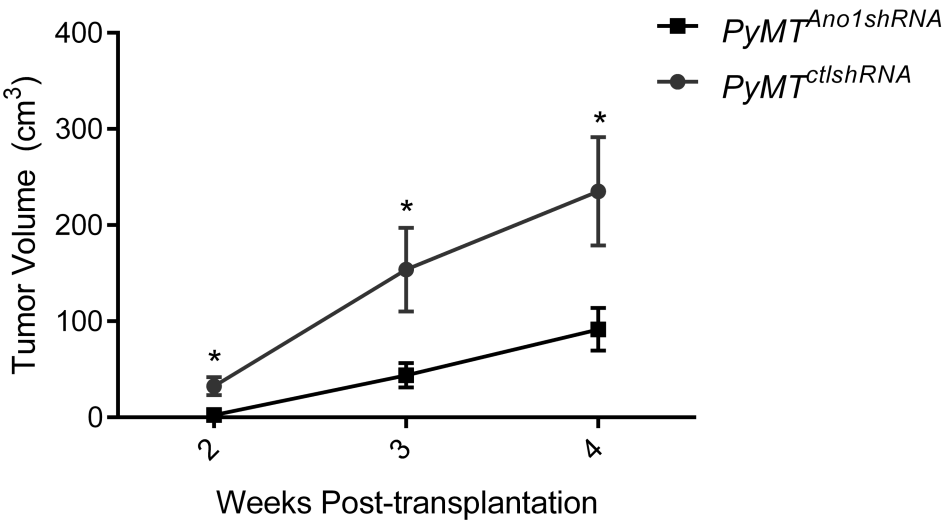
PyMT^Ano1shRNA
PyMT^ctlshRNA
Tumor Volume (cm3)
400
300
200
100
0
*
*
*
2
3
4
Weeks Post-transplantation

B

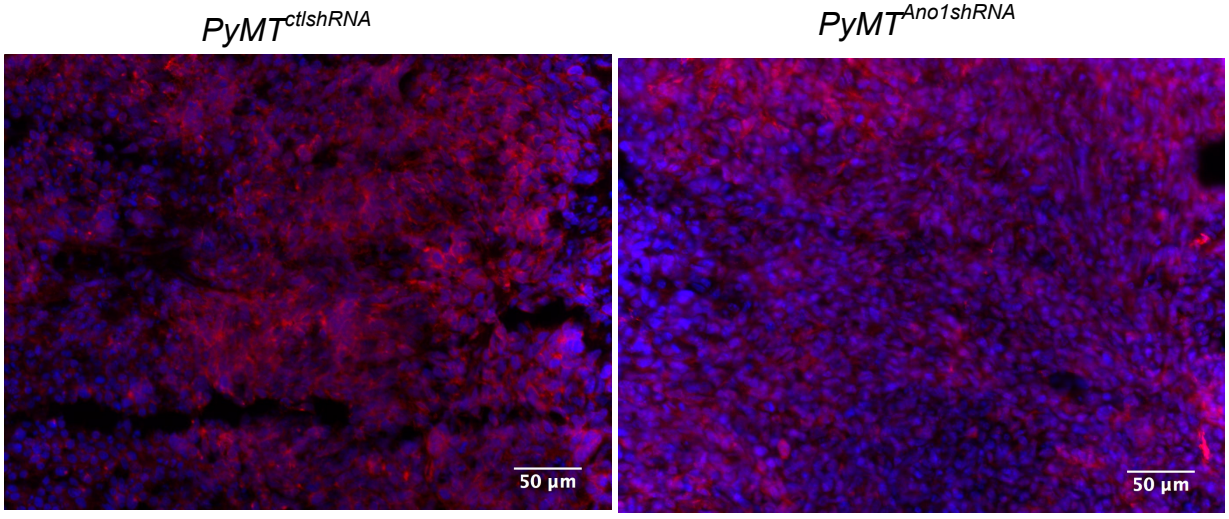
PyMT^ctlshRNA
PyMT^Ano1shRNA
50 µm
50 µm

Figure 4: shRNA-mediated knockdown of ANO1 delays growth *in vivo*

MMTV-PyMT cells were transduced with lentivirus expressing a control shRNA or an ANO1 shRNA then injected orthotopically into the mammary glands of FVB mice. (A) Tumor volume was measured in the weeks following transplantation. *MMTV-PyMT*^{Ano1shRNA} tumors demonstrated a significant decrease in tumor volume at 2, 3 and 4 weeks following transplantation. (B) The tumors were labelled with ANO1 antibody (red) and DAPI (blue).

Chapter 5: ANO1 modulates capacitation and fertility of mouse sperm

5.1 Introduction

The successful fertilization of mammalian oocytes requires coordinated molecular, structural and physiological changes of spermatozoa following ejaculation as they journey through the female reproductive tract. Upon exiting the vas deferens, sperm cells encounter higher concentrations of Na^+, Cl^- and $HCO3^-$ and elevated pH in the seminal and, later on, in the female reproductive fluids, which orchestrate the process of capacitation [1]. During capacitation, sperm undergo many biochemical changes including increased intracellular cAMP and Protein Kinase A (PKA) activation and hyperpolarization of the membrane potential[2,3]. Collectively, these changes induce a hyperactivated motility pattern and enable sperm to undergo the acrosome reaction (AR) that is critical for fertilization [4]. The acrosome is a secretory vesicle found in the head of sperm and, during AR, it fuses with the plasma membrane via exocytosis [5]. The secreted proteins facilitate sperm binding to and penetrating the zona pellucida and subsequent fusion with the oocyte plasma membrane [5]. The AR is regulated by increased intracellular Ca^{2+}[6].

Cl^- ions regulate tyrosine phosphorylation and hyperpolarization during capacitation and the acrosome reaction [7]. It was shown that that capacitation-associated tyrosine phosphorylation and *in vitro* fertilization ability are abolished when sperm are incubated in media lacking Cl^- ions but the required Cl^- transporters have not been fully characterized [8]. Several lines of evidence suggest that calcium-activated chloride channels (CaCC) might be important for AR and fertilization. For example, CaCC inhibitors such as niflumic acid (NFA) block Cl^- currents and *in vitro*-induced acrosome

reaction in mouse and human sperm[9]. Moreover, after ANO1 was shown to contribute a major component of the calcium-induced chloride current [10–12], patch-clamp experiments were performed in human sperm and showed that the calcium-induced chloride current could be blocked with an ANO1-specific inhibitor[13]. The inhibitor also blocked induction of the AR by addition of recombinant zona pellucida protein (ZP3) in the human sperm samples, which is a commonly used physiological trigger of the AR *in vitro* [13].

While there is evidence that Ano1-mediated currents are present in mammalian sperm and regulate the acrosome reaction, the localization and physiological functions of ANO1 in sperm have not been fully characterized. Since mice homozygous for the null allele of ANO1 (*Ano1*$^{n/n}$) die prematurely 1-2 weeks following parturition, it has not been possible to determine whether genetic loss of ANO1 leads to infertility[14]. Notably, *Ano1*$^{n/+}$ heterozygous animals are fertile, but carefully controlled breeding experiments have not been performed to assess whether they exhibit any subfertility.

The goal of the present study was to determine the expression and localization of ANO1 in mouse sperm and its role during capacitation, the acrosome reaction and fertilization. To first assess ANO1 localization and expression within mouse sperm, we performed immunohistochemistry and western blot analysis. Wild-type sperm express ANO1 in their heads and proximal tail regions and ANO1 expression was reduced in sperm isolated from mice heterozygous for a null allele of ANO1 (*Ano1*$^{n/+}$*)*. To test the functional consequences of reduced ANO1 expression in sperm during capacitation, chlortetracycline (CTC) staining and western blot for tyrosine phosphorylated proteins were performed on sperm isolated from *Ano1*$^{n/+}$ mice and *Ano1*$^{+/+}$ control littermates. The results demonstrated that decreased ANO1 expression in *Ano1*$^{n/+}$ sperm facilitated

capacitation and increased the incidence of spontaneous acrosome exocytosis, which was confirmed with PNA-FITC labelling. *Ano1*$^{n/+}$ sperm subsequently displayed a reduction in the ability to fertilize eggs *in vitro* and *Ano1*$^{n/+}$ males produced less offspring when bred conventionally. The study demonstrates a novel and critical role for ANO1 in regulating capacitation-associated processes that are necessary for fertilization.

5.2 Methods

Statistics

The results are presented as means +/- standard deviation (SD). T-tests were used to calculate statistical significance with cutoff of $p<0.05$.

Sperm collection

Sperm collection for experiments was performed as previously described[15] with some modifications. First, EmbryoMax Human Tubal Fluid (HTF) media (MR-070-D; EMD Millipore) was preincubated at 37^{O}C, 5% CO_2, and 20% O_2 in a tissue culture plate with mineral oil (M5310; Sigma-Aldrich) overlay. Following sacrifice of the animals, the cauda epididymis and vas deferens were carefully dissected from the mice and placed in the pre-warmed HTF media. The vas deferens was gently pressed to extrude the sperm and the cauda epididymis was perforated with a needle. The sperm were allowed to swim out from the cauda epididymis and vas deferens elution in the 37^{O}C, 5% CO_2, and 20% O_2 incubator for 5-15 minutes depending on the experiment. After 15 minutes, the cauda epididymis and vas deferens tissue were removed and the plate was returned to the incubator for additional incubations as described.

Chlortetracycline staining

Chlortetracycline (CTC) staining for capacitation was performed as previously described[16] with some modifications. CTC solution was prepared fresh and contained 30mg of chlortetracycline hydrochloride (Sigma-Aldrich) dissolved in a 20mM Tris and 130mM NaCl solution with a pH of 7.8. After extraction from vas deferens and cauda epididymis into HTF media, the mouse sperm were returned to the incubator for 5 minutes. Then 10µl of sperm was spotted on two slides and spread with a pipette tip. 10µl of a chlortetracycline solution containing was then added and mixed with the sperm solution. 30 seconds later, 2µl of 4% PFA was added. A coverslip was applied and the frequencies of the three different CTC stain patterns were counted using a Zeiss Axio Imager M2 fluorescence microscope (Oberkochen, Germany). A minimum of 300 sperm were counted per animal.

Assessment of acrosome reaction

To induce the acrosome reaction 10µm Ionomycin (Sigma-Aldrich) or equal volume of DMSO were added to the sperm in HTF media. The plates were returned to the incubator for 60 minutes. For acrosome labeling, 10µl of sperm were spread onto duplicate slides, allowed to air-dry then immersed in methanol for 15 minutes. After fixation, the sperm were washed three times with PBS, placed in 15µg/ml PNA-FITC (Sigma-Aldrich) in PBS for 45 minutes then washed three times with PBS. Next the slides were placed in PBS containing DAPI nuclear stain for 5 minutes and coverslips were mounted with FluorSave (EMD Millipore).

The slides with acrosome and nuclear-stained sperm were then visualized with the Zeiss Axio Imager M2 fluorescence microscope. The numbers of sperm with intact and reacted acrosomes were counted for the DMSO and Ionomycin treatment groups (Intact: bright PNA-FITC fluorescence; Reacted: weak or absent PNA-FITC fluorescence). Average counts were found for at least 200 sperm per animal. To determine the acrosome reaction induction by Ionomycin, the percentage of acrosome-reacted sperm in the DMSO control condition was then subtracted from the percentage of acrosome-reacted sperm found in the Ionomycin-treated group. The results are expressed as means from all of the mice tested.

In vitro Fertilization

In vitro fertilization (IVF) experiments were performed as previously described[17] with the following modifications. Wild-type 4-8 week old C57BL/6J females were first superovulated by intraperitoneal injection of 5 IU of pregnant mare serum gonadotropin (PMSG) (EMD Millipore) and 5 IU of human chorionic gonadotropin (HCG) (Sigma-Aldrich) 48 hours later. IVF was performed 14 hours after the HCG injection. The afternoon before IVF, plates were prepared for the oocytes, sperm, and IVF and placed in a humidified $37^{O}C$ incubator with 5% CO_2, and 20% O_2. Dishes with drops of HTF media (EMD Millipore; MR-070-D) covered by mineral oil were used for oocyte, sperm collection and IVF. Potassium simplex optimization medium (KSOM) with amino acids (EMD Millipore; MR-106-D) under mineral oil was used for embryo culture and washing. 12 hours after the HCG injection, the male was sacrificed and sperm extracted from the vas deferens and cauda epididymis into HTF media. The sperm were allowed to

swim out for 15 minutes at 37^{O}C, 5% CO_2, and 20% O_2. Then the tissues were removed, and motility and concentration were assessed. The sperm were incubated for an additional 45 minutes. The female mice were then sacrificed and ampullas were carefully dissected and placed in HTF media. Cumulous oocyte complexes (COCs) were extracted by gentle tearing of the ampulla wall and coincubated with sperm at density of 2 X 10^6 sperm/mL for 4 hours in the 37^{O}C 5% CO_2, and 20% O_2 incubator. The embryos were washed and cultured in KSOM media in the same incubator. The fertilization rate was determined by counting the number of unfertilized oocytes and 2-cell embryos 18 hours after fertilization and the number of blastocysts 96 hours after fertilization. The blastocyst rate was the percent of 2-cell embryos that developed into blastocysts.

Immunohistochemistry

Animals were sacrificed by CO_2 asphyxiation followed by cervical dislocation. The testes were dissected and fixed in 4% paraformaldehyde (w/v) in PBS for 30 minutes. The tissues were then washed 3 times with PBS and incubated overnight in 30% (w/v) sucrose in PBS. The next day equal volume of O.C.T compound was added and mixed with the tissues for 2 hours then the tissues were frozen. Cryosections with a thickness of 15 μm were mounted onto slides and permeabilized with 0.3% Triton X-100 for 5 minutes, followed by washing with PBS 3 times. The tissues were blocked in PBS containing 3% BSA, 10% donkey serum and 0.1% Triton X-100 for 1 hour then incubated overnight in blocking solution containing primary antibody. 1:500 dilutions of ANO1 antibody (Abcam; ab53212) and GFP antibody (Aves Labs) were used. Alexafluor secondary antibodies (ThermoFisher Scientific) were used at concentrations of 1:500 in

blocking buffer and incubated on the slides for 1-3 hours. PNA-FITC was added to the slides for 1 hour at a concentration of 15μg/ml in PBS then DAPI was added at 5μg/ml in PBS and coverslips were mounted with FluorSave. Images were collected using a Zeiss Axio Imager M2 (Oberkochen, Germany) or Leica Sp5 laser-scanning confocal microscope (Buffalo Grove, IL). For confocal analysis Z stacks of optical sections were captured.

Western Blot

The corpus and caput regions of the epididymis were carefully dissected from the mice and placed in cold RIPA buffer supplemented with cOmplete mini protease inhibitor (Sigma-Aldrich) and PhosSTOP phosphatase inhibitor (Sigma-Aldrich). The tissues were minced and homogenized then centrifuged. The supernatants were collected and frozen until needed. For isolation of sperm proteins, the sperm samples were transferred from their culture dishes to Eppendorf tubes, centrifuged, washed and resuspended in RIPA buffer (10mM Tris-Cl, 1mM EDTA, 0.5mM EGTA, 1%Triton X-100, 0.1% sodium deoxycholate, 0.1% SDS, 140mM NaCl) at a density of 1 X 10^6 sperm/75μl. The lysate was centrifuged again and the supernatant was kept frozen until used for an experiment.

For western blot analysis protein samples were separated using precast Protean TGX gels (Bio-Rad) using 25mM Tris, 190mM glycine and 0.1% SDS. Proteins were transferred to nitrocellulose membranes at 75V for 2 hours, then blocked with 5% BSA for 1 hour. Primary antibodies were diluted in blocking buffer and incubated with the nitrocellulose membrane overnight at 4^{o}C. Anti-Phosphotyrosine (4G10; EMD Millipore)

was used at 1:1000, anti-acetyl-alpha tubulin antibody (6-11B-1; EMD Millipore) at 1:250, Anti-GFP (Aves Labs) at 1:500, and Anti-ANO1 (53212; Abcam) at 1:100. The nitrocellulose was then washed three times with TBST (20mM Tris, 150mM NaCl, 0.1% Tween 20). 1:5000 dilutions of HRP-conjugated secondary antibodies were added and mixed with gentle agitation for two hours (Goat anti-chicken HRP antibody; ThermoFisher Scientific), (Sheep Amersham ECL AntiMouse IgG HRP-linked Antibody; GE Healthcare), (NA931 Donkey Anti-Rabbit IgG HRP-linked Antibody; GE Healthcare). The membrane was washed three times with TBST, Clarity ECL substrate (Bio-Rad) was added then the membrane was imaged using a Fuji LAS-3000 Imaging System. Fiji image analysis software[18] was used for quantification of western blot band intensity. Band intensity of tyrosine phosphorylated proteins was normalized to acetylated tubulin.

Animals

All animal procedures were approved by the Institutional Animal Care and Use Committee of the University of California, San Francisco. C57BL/6J female mice were from The Jackson Laboratory. The *Ano1*$^{n/+}$ [14] and *Ano1*$^{GFP/GFP}$ [19] mice were also on a C57BL/6 background and have been previously described. The *Ano1*$^{n/+}$, *Ano1*$^{+/+}$, and *Ano1*$^{GFP/GFP}$ male mice used in experiments were 2-4 months old.

5.3 Results

Ano1 is expressed in normal mouse sperm

To determine whether mouse sperm express ANO1, we performed immunohistochemistry on murine testis using an ANO1 antibody and PNA-FITC probe for the acrosome. ANO1 was strongly expressed by elongated spermatids and spermatozoa in the seminiferous tubules of mouse testis (Figure 1A), while round immature spermatids did not express detectable levels of ANO1 (Figure 1B). ANO1 and PNA-FITC fluorescence overlapped in the head region of elongated spermatids and spermatazoa within seminiferous tubules (Figure 1A). To confirm antibody specificity and ANO1 expression by mature mouse sperm, whole sperm protein was extracted from mice homozygous for an ANO1-GFP fusion protein (*Ano1*$^{GFP/GFP}$) and analyzed by western blot (Figure 1C). GFP and ANO1 antibodies detected a faint band of a similar size around 115 kDa (Figure 1C).

To clarify the localization of ANO1, mature mouse sperm were isolated from vas deferens and cauda epididymis, spread on slides and co-stained with an antibody against ANO1 and PNA-FITC (Figure 1D). ANO1 was detected in the acrosome region of sperm heads in a region that overlapped with PNA-FITC fluorescence (Figure 1D). Sperm that had undergone the acrosome reaction (AR), indicated by loss of PNA-FITC acrosome marker, showed diminished expression of ANO1 (Figure 1D). Mature sperm also demonstrated expression of ANO1 in the midpiece (Figure 1E). Labeling *Ano1*$^{GFP/GFP}$ sperm with a GFP antibody showed a similar localization of ANO1 to the sperm head and midpiece (Figure 1E).

Ano1 expression is decreased in *Ano1*$^{n/+}$ sperm

We analyzed *Ano1*$^{n/+}$mice to determine the importance of ANO1 in capacitation-associated processes, acrosome reaction and fertilization. We performed immunohistochemistry on testes from *Ano1*$^{n/+}$ mice using an antibody against ANO1 and PNA-FITC to assess ANO1 expression and spermatogenesis (Figure 2A). The seminiferous tubules of *Ano1*$^{n/+}$mice did not appear different from those of control littermates (Figure 1A) and ANO1 expression overlapped with PNA-FITC in the heads of mature sperm within seminiferous tubule lumens (Figure 2A).

ANO1 expression in mature sperm was assessed by spreading sperm isolated from the vas deferens and epididymis on slides and performing immunohistochemistry with an antibody against ANO1 and PNA-FITC label (Figure 2B). A reduction in ANO1 signal intensity was detected in the heads of sperm from *Ano1*$^{n/+}$ mice (Figure 2B). To confirm the reduction of ANO1 in mature mouse sperm, we performed western blot analysis on whole protein extract from caput and corpus epididymis and sperm isolated from vas deferens and cauda epididymis (Figure 2C). The results showed a reduction in ANO1 expression in caput/corpus epididymis and extracted sperm from *Ano1*$^{n/+}$ mice compared to *Ano1*$^{+/+}$ control littermates. There was no difference in the number of sperm extracted from the vas deferens and epididymis of *Ano1*$^{n/+}$ mice ($3.691 \times 10^6 \pm 1.066$; n=7) compared to control littermates ($3.744 \times 10^6 \pm 1.074$; n=7).

Ano1$^{n/+}$ sperm demonstrate increased capacitation

We performed chlortetracycline (CTC) staining to determine whether the observed reduction in ANO1 expression in mature sperm from *Ano1*$^{n/+}$ mice impaired capacitation (Figure 3A). After staining with CTC, uncapacitated sperm displayed

uniform fluorescence in the entire head region with a brighter band along the equatorial segment (F Pattern), while capacitated sperm showed bright fluorescence in the anterior portion of the head with a darker area in the post-equatorial region (Pattern B) (Figure 3A). Acrosome reacted sperm lacked fluorescence throughout the head (Pattern R) (Figure 3A).

We isolated and stained sperm from *Ano1*$^{n/+}$ mice and *Ano1*$^{+/+}$ control littermates with CTC after timed incubations in HTF media. The frequency of each CTC fluorescence pattern was counted using fluorescence microscopy. Surprisingly, after incubation for 5 minutes in HTF media, *Ano1*$^{n/+}$ mice showed a significant decrease ($p=0.0001$) in the number of sperm with the F pattern (48.8% ± 9.7; n=7) compared to *Ano1*$^{+/+}$control littermates (71.5% ± 6.1; n=8) (Figure 3B). This was accompanied by a significant increase in the number of sperm with the B pattern ($p<0.0001$) in *Ano1*$^{n/+}$ sperm (46.6% ± 6.7; n=7) compared to *Ano1*$^{+/+}$ control littermates (27.2% ± 6.2; n=8). The frequency of pattern R was also significantly increased ($p=0.03$) in *Ano1*$^{n/+}$ sperm (4.8% ± 3.9; n=7) compared to *Ano1*$^{+/+}$ mice (1.4 ± 0.7; n=8). (Figure 3B). Representative images of CTC-stained sperm from *Ano1*$^{+/+}$ and *Ano1*$^{n/+}$animals show examples of the common patterns observed in both groups (Figure 3C). F was the most common pattern observed in *Ano1*$^{+/+}$ sperm, while significantly more *Ano1*$^{n/+}$ sperm showed the B pattern (Figure 3C).

To confirm that *Ano1*$^{n/+}$ mice had increased capacitation after 5 min in HTF medium, we performed western blot analysis using an antibody against tyrosine phosphorylated proteins. Quantification of phosphotyrosine band intensity relative to acetylated tubulin loading control showed a significant increase ($p=0.019$) in the level of

tyrosine phosphorylated proteins in *Ano1*$^{n/+}$ (1.365 ± 0.09; n=4) animals compared to *Ano1*$^{+/+}$ controls (1.123 ± 0.124; n=4) (Figure 3D). The average increase was around 25%. There was not a significant difference in the percent of motile sperm between *Ano1*$^{n/+}$ (61.8% ± 5.3; n=6) and *Ano1*$^{+/+}$ animals (60.2% ± 6.6; n=6).

Ano1$^{n/+}$ sperm show increased spontaneous acrosome reaction

To determine whether the increased capacitation in *Ano1*$^{n/+}$ sperm affected AR progression, we assessed AR status using PNA-FITC label following 5 and 60-minute incubations in capacitation media. After the 5-minute incubation in HTF media, *Ano1*$^{n/+}$ and *Ano1*$^{+/+}$ sperm were spread on slides and labeled with PNA-FITC. *Ano1*$^{n/+}$ animals showed a significant increase (p=0.0065) in the number of acrosome reacted sperm (10.2% ± 2.1; n=5) compared to *Ano1*$^{+/+}$ control littermates (5.1% ± 1.8; n=4) (Figure 4A). *Ano1*$^{n/+}$ also showed a significant increase (p=0.0018) in spontaneous AR following the 60-minute incubation in HTF media (17.7% ± 2.9; n=5) compared to *Ano1*$^{+/+}$ siblings (9.4% ± 2.0; n=4) (Figure 4A). Representative images of sperm labeled with PNA-FITC following the 60-minute incubation show the increased frequency of spontaneous AR in *Ano1*$^{n/+}$sperm (Figure 4B). The increased spontaneous AR in *Ano1*$^{n/+}$sperm also resulted in a significant decrease (p=0.0002) in AR induction by treatment with 10µm of ionomycin for 1 hour (7.4% ± 5.5; n=5) compared to *Ano1*$^{+/+}$ controls (39.8% ± 12.1; n=7) (Figure 4C).

Decreased fertility of *Ano1*$^{n/+}$ sperm *in vitro* and *in vivo*

We performed in vitro fertilization to determine whether the increased incidence of spontaneous acrosome reaction in *Ano1*$^{n/+}$ impaired fertilization. Sperm were isolated from *Ano1*$^{n/+}$ males and *Ano1*$^{+/+}$ control littermates and incubated with oocytes extracted from superovulated C57/Bl6J mice. The fertilization efficiency was assessed by counting the number of 2-cell embryos and blastocysts. Oocytes incubated with *Ano1*$^{n/+}$ sperm had a significantly reduced (p=0.0021) 2-cell embryo frequency following IVF (35.3% ±13.1; n=5) compared to *Ano1*$^{+/+}$ control littermates (77.5% ± 13.5; n=4) (Figure 5A). Oocytes incubated with *Ano1*$^{n/+}$ sperm also demonstrated a significant reduction (p=0.0018) in the frequency of blastocysts formed (29.2 ± 10.7; n=5) compared with *Ano1*$^{+/+}$ siblings (62.4% ± 9.2; n=4) (Figure 5A). Representative images of blastocysts show the reduced blastocyst frequency of oocytes incubated with *Ano1*$^{n/+}$ sperm compared to *Ano1*$^{+/+}$ controls (Figure 5B). There was no difference in the percent of 2-cell embryos that developed to blastocyst stage between oocytes fertilized with *Ano1*$^{n/+}$ sperm versus *Ano1*$^{+/+}$sperm.

To determine whether Ano1 modulates male fertility in vivo, we bred *Ano1*$^{n/+}$ and *Ano1*$^{+/+}$ male mice on a C57/Bl6J background with wild-type C57/Bl6J females. *Ano1*$^{n/+}$ mice produce significantly fewer (p<0.0001) offspring per litter (6.8 ± 1.7; n=37) compared to *Ano1*$^{+/+}$ controls (8.3 ± 1.4; n=40) (Figure 5C).

5.4 Discussion

Previous studies have demonstrated the presence of calcium-induced chloride currents in mouse and human sperm[9,13], but their molecular identity and functional importance in fertilization have not been fully characterized. A recent study used patch-

clamp of human sperm heads to characterize a calcium-induced chloride conductance that was sensitive to an ANO1-specific blocker, which also reduced ZP3-induced AR[13]. This previous study that used pharmacological inhibitors suggested that ANO1 is important for AR in isolated mature sperm. However, the localization of ANO1 and its *in vivo* function in mature sperm has not been described. In the current study, we determine the localization of ANO1 within mature mouse sperm and use a genetic approach to demonstrate for the first time the importance of ANO1 in regulating capacitation-associated processes, upstream of AR, and fertilization *in vivo* and *in vitro.*

The current study shows that ANO1 is expressed in the head and midpiece of normal mouse sperm and its reduction in *Ano1*$^{n/+}$ sperm altered their functional state. We report increased activation of capacitation-associated processes in the *Ano1*$^{n/+}$ sperm assessed by CTC staining and western blot analysis of protein tyrosine phosphorylation. Inhibition of another Cl^- channel, CFTR, has been previously associated with reduced frequency of the B pattern of CTC fluorescence, decreased tyrosine phosphorylation, HCO_3^- transport, fertilization and an inability to undergo the acrosome reaction [20–23]. In contrast, loss of ANO1 increased capacitation and spontaneous acrosome exocytosis, while still reducing fertilization ability, suggesting that different Cl^- transporters play different functional roles during capacitation and the AR.

ANO1 regulates the secretion of Cl^- in a variety of tissues[24]. Our data are consistent with a model in which ANO1 regulates capacitation via modulating Cl^- transport and intracellular Cl^- concentration. It has also been shown that intracellular Cl^- concentrations increase during capacitation and when Cl^- is removed from the sperm incubation media, capacitation-associated processes including tyrosine phosphorylation,

hyperpolarization, induced acrosome reaction and fertilization ability are reduced or abolished[8,25]. CFTR has been shown to regulate Cl^- transport during capacitation and there is evidence that other Cl^- channels are involved, but the mechanisms have not been fully characterized[7,25]. The kinase signaling during capacitation involves activation of PKA by $Ca^{2+}$and HCO_3^--dependent adenylyl cyclase and it has been suggested that the increased intracellular chloride concentration associated with capacitation promotes HCO_3^- entry [3,25,26]. Loss of ANO1 could remove an important mediator of Cl^- secretion and thereby increase intracellular Cl^-, facilitate HCO_3^- entry and membrane hyperpolarization in the sperm. This would promote capacitation-associated processes including activation of PKA and subsequent protein tyrosine phosphorylation.

The process of capacitation provides sperm with the competence to undergo the AR during fertilization[4] but it was surprising to see increases in both capacitation and spontaneous acrosome reaction in *Ano1*$^{n/+}$ mice. The results suggest that ANO1 plays different roles during capacitation and the AR in mouse sperm, which could be regulated by changes in intracellular Ca^{2+} concentration during these processes[4,27]. The function of ANO1 during the AR could also involve the ANO1-mediated regulatory volume decrease (RVD) that has been described in epithelial cells during swelling[28]. During the AR, it is thought that the RVD controls the distance between the outer acrosome membrane and plasma membrane after acrosome swelling [7,29]. Moreover, it has been shown that ANO1 regulates the exocytosis of mucins in the airway [30] and insulin secretion by pancreatic beta-cells[31,32]. ANO1 could be regulating the AR through its interaction with vesicle trafficking proteins including SNAREs and syntaxins[33], which are known to mediate acrosomal membrane fusion[34]. While the observed decrease in AR induction by

ionomycin in *Ano1*$^{n/+}$ mice is similar to the effects of ANO1 chemical blockers in human sperm on ZP-3-induced AR, the reduced Ionomycin-induced AR in *Ano1*$^{n/+}$ sperm could be a result of increased spontaneous acrosome reaction. These results suggest that genetic loss of Ano1 may have different effects on sperm function than acute treatment with chemical inhibitors ex vivo.

While completion of the AR is an absolute requirement for fertilization *in vivo*[5], our results suggest that premature acrosome exocytosis can be detrimental. In contrast, a previous study showed that accelerated AR progression in CD46 knockout male mice improved fertilization ability *in vivo* [35]. These findings suggest that the precise timing of AR progression is critical during fertilization. It was previously thought that the AR is triggered by direct binding to the zona pellucida but recent experiments have challenged this model [36,37]. A study that recorded videos of fertilization by mouse sperm expressing a green fluorescent protein reporter of acrosome status showed that the majority of fertilizing sperm had already completed the AR by the time they reached the zona pellucida[38]. Even though sperm may not need an intact acrosome when they reach the zona to fertilize, our results show that being twice as acrosome reacted prior to contact with cumulous was sufficient to reduce the overall fertilization rate by half. Thus, the early release of acrosome contents may reduce the ability of sperm to penetrate the cumulous oophorus. Future experiments should test the ability of *Ano1*$^{n/+}$ sperm to fertilize cumulous-free oocytes, which would clarify the importance of the AR as sperm penetrate through the cumulous.

When bred conventionally, *Ano1*$^{n/+}$ animals had a statistically significant reduction in the number of offspring produced per litter compared to controls. The

reduction in litter sizes was not as severe as the 50% decrease in fertilization *in vitro* but the results suggested that the augmented capacitation and spontaneous AR in *Ano1*$^{n/+}$sperm still decreased fertilization ability *in vivo*. Since the *Ano1*$^{n/+}$ sperm used in the study still have one functional allele of ANO1, it is unclear whether total loss of ANO1 expression would cause infertility. The premature mortality displayed by *Ano1*$^{n/n}$ mice has prevented such experiments from being conducted with this model[14]. In future studies, mice carrying conditional alleles of ANO1 in combination with spermatid-expressing Cre recombinase will be used to determine whether a greater reduction in ANO1 expression in sperm causes infertility.

The study demonstrates that ANO1 is expressed in elongated spermatids and mature mouse sperm. Reduced ANO1 expression in *Ano1*$^{n/+}$ sperm augmented capacitation-associated processes including tyrosine phosphorylation, increased the incidence of spontaneous AR and impaired their ability to fertilize oocytes *in vitro* and *in vivo*. Future studies should investigate the expression of ANO1 in human sperm and its functions during capacitation.

References

1. Kavanagh, J. P. Sodium, potassium, calcium, magnesium, zinc, citrate and chloride content of human prostatic and seminal fluid. *J. Reprod. Fertil.* **75,** 35–41 (1985).
2. Hernández-González, E. O. *et al.* Sodium and epithelial sodium channels participate in the regulation of the capacitation-associated hyperpolarization in mouse sperm. *J. Biol. Chem.* **281,** 5623–5633 (2006).
3. Visconti, P. E. Understanding the molecular basis of sperm capacitation through kinase design. *Proc. Natl. Acad. Sci.* **106,** 667–668 (2009).
4. Bailey, J. L. Factors Regulating Sperm Capacitation. *Syst. Biol. Reprod. Med.* **56,** 334–348 (2010).
5. Foster, J. A. & Gerton, G. L. Sperm Acrosome Biogenesis and Function During Fertilization. **220,** 15–33 (2016).
6. Buffone, M. G. *et al.* Heads or tails? Structural events and molecular mechanisms that promote mammalian sperm acrosomal exocytosis and motility. *Mol. Reprod. Dev.* **79,** 4–18 (2012).
7. Santi, C. M. *et al.* K+ and Cl- Channels and Transporters in Sperm Function. *Curr. Top. Dev. Biol.* **102,** 385–421 (2013).
8. Wertheimer, E. V. *et al.* Chloride is essential for capacitation and for the capacitation-associated increase in tyrosine phosphorylation. *J. Biol. Chem.* **283,** 35539–35550 (2008).
9. Espinosa, F. *et al.* Mouse sperm patch-clamp recordings reveal single Cl- channels sensitive to niflumic acid, a blocker of the sperm acrosome reaction. *FEBS Lett.* **426,** 47–51 (1998).

10. Yang, Y. D. *et al.* TMEM16A confers receptor-activated calcium-dependent chloride conductance. *Nature* **455,** 1210–1215 (2008).

11. Caputo, A. *et al.* TMEM16A, a membrane protein associated with calcium-dependent chloride channel activity. *Science* **322,** 590–4 (2008).

12. Schroeder, B. C., Cheng, T., Jan, Y. N. & Jan, L. Y. Expression cloning of TMEM16A as a calcium-activated chloride channel subunit. *Cell* **134,** 1019–1029 (2008).

13. Orta, G. *et al.* Human spermatozoa possess a calcium-dependent chloride channel that may participate in the acrosomal reaction. *J. Physiol.* **590,** 2659–75 (2012).

14. Rock, J. R., Futtner, C. R. & Harfe, B. D. The transmembrane protein TMEM16A is required for normal development of the murine trachea. *Dev Biol* **321,** 141–149 (2008).

15. Lybaert, P., Danguy, A., Leleux, F., Meuris, S. & Lebrun, P. Improved methodology for the detection and quantification of the acrosome reaction in mouse spermatozoa. *Histol. Histopathol.* **24,** 999–1007 (2009).

16. Ward, C. R. & Storey, B. T. Determination of the time course of capacitation in mouse spermatozoa using a chlortetracycline fluorescence assay. *Dev. Biol.* **104,** 287–296 (1984).

17. Feuer, S. K. *et al.* Use of a mouse in vitro fertilization model to understand the developmental origins of health and disease hypothesis. *Endocrinology* **155,** 1956–1969 (2014).

18. Schindelin, J. *et al.* Fiji: an open-source platform for biological-image analysis. *Nat Methods* **9,** 676–682 (2012).

19. Huang, F. *et al.* Calcium-activated chloride channel TMEM16A modulates mucin secretion and airway smooth muscle contraction. *Proc Natl Acad Sci U S A* **109,** 16354–16359 (2012).

20. Xu, W. M. *et al.* Cystic fibrosis transmembrane conductance regulator is vital to sperm fertilizing capacity and male fertility. *Proc. Natl. Acad. Sci. U. S. A.* **104,** 9816–21 (2007).

21. Li, C. Y. *et al.* CFTR is essential for sperm fertilizing capacity and is correlated with sperm quality in humans. *Hum. Reprod.* **25,** 317–327 (2010).

22. De La Vega-Beltran, J. L. *et al.* Mouse sperm membrane potential hyperpolarization is necessary and sufficient to prepare sperm for the acrosome reaction. *J. Biol. Chem.* **287,** 44384–44393 (2012).

23. Puga Molina, L. C. *et al.* Essential Role of CFTR in PKA-Dependent Phosphorylation, Alkalinization, and Hyperpolarization During Human Sperm Capacitation. *J. Cell. Physiol.* (2016). doi:10.1002/jcp.25634

24. Ousingsawat, J. *et al.* Loss of TMEM16A causes a defect in epithelial Ca2+-dependent chloride transport. *J. Biol. Chem.* **284,** 28698–703 (2009).

25. Hernández-González, E. O. *et al.* Involvement of cystic fibrosis transmembrane conductance regulator in mouse sperm capacitation. *J. Biol. Chem.* **282,** 24397–406 (2007).

26. Ickowicz, D., Finkelstein, M. & Breitbart, H. Mechanism of sperm capacitation and the acrosome reaction: role of protein kinases. *Asian J. Androl.* **14,** 816–21 (2012).

27. Darszon, A., Nishigaki, T., Beltran, C. & Treviño, C. L. Calcium Channels in the

Development, Maturation, and Function of Spermatozoa. *Physiol. Rev.* **91,** 1305–1355 (2011).

28. Almaça, J. *et al.* TMEM16 proteins produce volume-regulated chloride currents that are reduced in mice lacking TMEM16A. *J. Biol. Chem.* **284,** 28571–28578 (2009).

29. Zanetti, N. & Mayorga, L. S. Acrosomal swelling and membrane docking are required for hybrid vesicle formation during the human sperm acrosome reaction. *Biol. Reprod.* **81,** 396–405 (2009).

30. Huang, F. *et al.* Calcium-activated chloride channel TMEM16A modulates mucin secretion and airway smooth muscle contraction. *Proc. Natl. Acad. Sci. U. S. A.* **109,** 16354–9 (2012).

31. Edlund, A., Esguerra, J. L. S., Wendt, A., Flodström-Tullberg, M. & Eliasson, L. CFTR and Anoctamin 1 (ANO1) contribute to cAMP amplified exocytosis and insulin secretion in human and murine pancreatic beta-cells. *BMC Med.* **12,** 87 (2014).

32. Xu, Z. *et al.* Mapping of long-range INS promoter interactions reveals a role for calcium-activated chloride channel ANO1 in insulin secretion. *Proc. Natl. Acad. Sci. U. S. A.* **111,** 16760–16765 (2014).

33. Perez-Cornejo, P. *et al.* Anoctamin 1 (Tmem16A) Ca2+-activated chloride channel stoichiometrically interacts with an ezrin-radixin-moesin network. *Proc. Natl. Acad. Sci.* **109,** 10376–10381 (2012).

34. Belmonte, S. A., Mayorga, L. S. & Tomes, C. N. in *Advances in Anatomy Embryology and Cell Biology* **220,** 71–92 (2016).

35. Inoue, N. *et al.* Disruption of mouse CD46 causes an accelerated spontaneous acrosome reaction in sperm. *Mol. Cell. Biol.* **23,** 2614–22 (2003).

36. Yanagimachi, R. Mammalian sperm acrosome reaction: where does it begin before fertilization? *Biol. Reprod.* **85,** 4–5 (2011).

37. Avella, M. A. & Dean, J. Fertilization with acrosome-reacted mouse sperm: Implications for the site of exocytosis. *Proc. Natl. Acad. Sci.* **108,** 19843–19844 (2011).

38. Jin, M. *et al.* Most fertilizing mouse spermatozoa begin their acrosome reaction before contact with the zona pellucida during in vitro fertilization. *Proc. Natl. Acad. Sci. U. S. A.* **108,** 4892–4896 (2011).

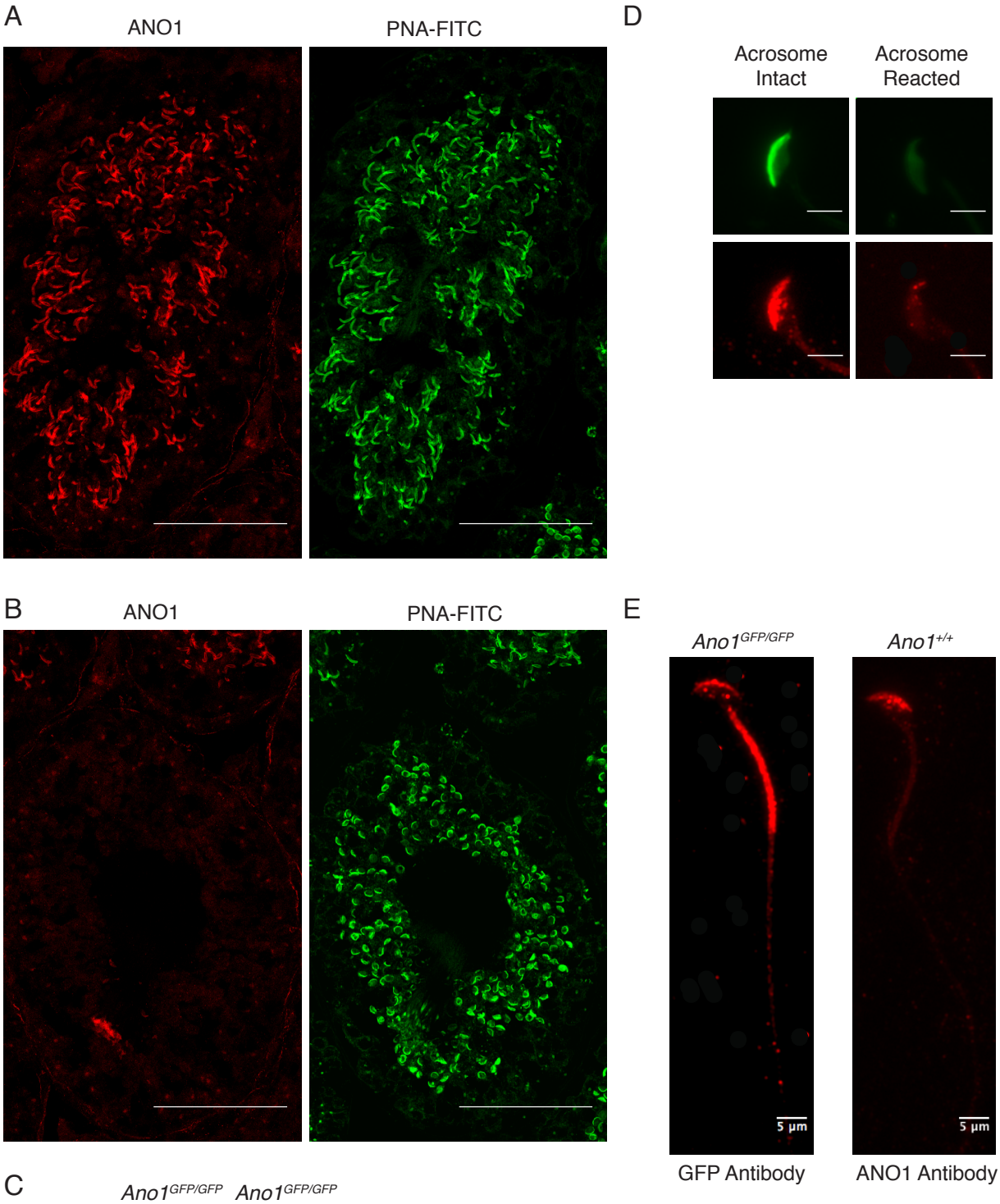
A
ANO1
PNA-FITC
B
ANO1
PNA-FITC
C
Ano1GFP/GFP
Ano1GFP/GFP
ANO1
GFP
D
Acrosome Intact
Acrosome Reacted
E
Ano1GFP/GFP
Ano1+/+
5 µm
5 µm
GFP Antibody
ANO1 Antibody

Figure 1. ANO1 is expressed in the midpiece and head of mature mouse sperm

(A) Representative image captured by confocal microscopy of a seminiferous tubule containing elongated spermatids shows ANO1 (red) and PNA-FITC (green). (B) Representative lumen containing round spermatids. Scale bars are 20μm (C) Western blot analysis of sperm proteins from an *Ano1*$^{GFP/GFP}$ mouse with Ano1 and GFP antibodies (D) Representative images of acrosome intact and reacted sperm co-labelled with PNA-FITC and Ano1. Scale bars are 5μm. (E) Representative images of *Ano1*$^{GFP/GFP}$ sperm labelled with a GFP antibody and *Ano1*$^{+/+}$ sperm labelled with an Ano1 antibody. Scale bars are 5μm.

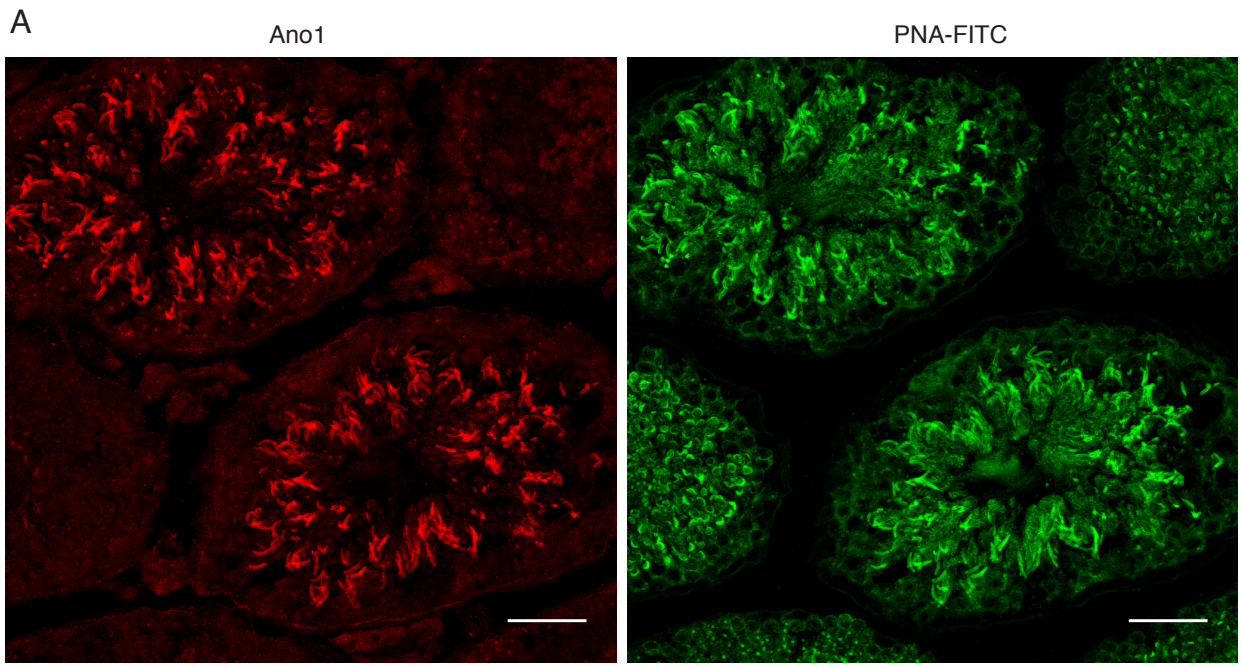
A
Ano1
PNA-FITC

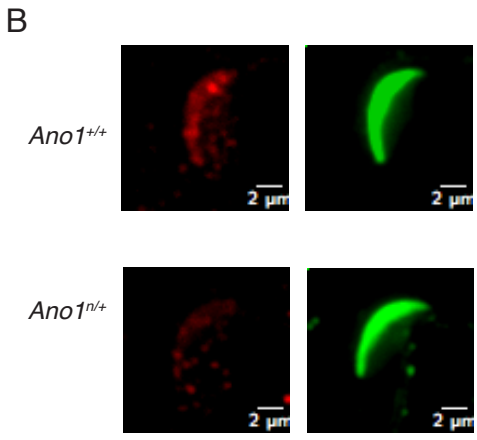
B
Ano1+/+
Ano1n/+
2 µm
2 µm
2 µm
2 µm

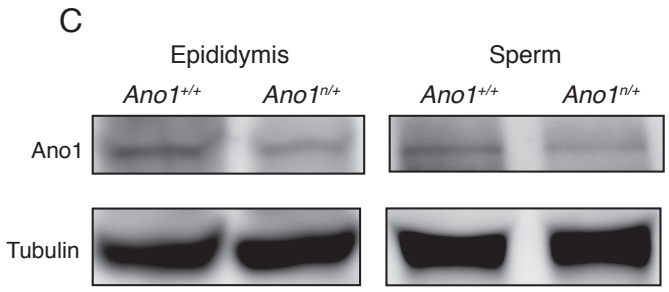
C
Epididymis
Sperm
Ano1+/+
Ano1n/+
Ano1+/+
Ano1n/+
Ano1
Tubulin

Figure 2. ANO1 expression is reduced in sperm from *Ano1*$^{n/+}$ mice

(A) Representative image of seminiferous tubule lumen from *Ano1*$^{n/+}$ mouse co-labelled with PNA-FITC (green) and ANO1 antibody (red). Scale bars are 20μm. (B) Immunohistochemistry experiments with isolated sperm using ANO1 antibody (red) and PNA-FITC (green). Scale bars are 2μm. (C) Western blot analysis of proteins from *Ano1*$^{n/+}$ and *Ano1*$^{+/+}$ littermate. An anti-acetylated tubulin antibody served as loading control.

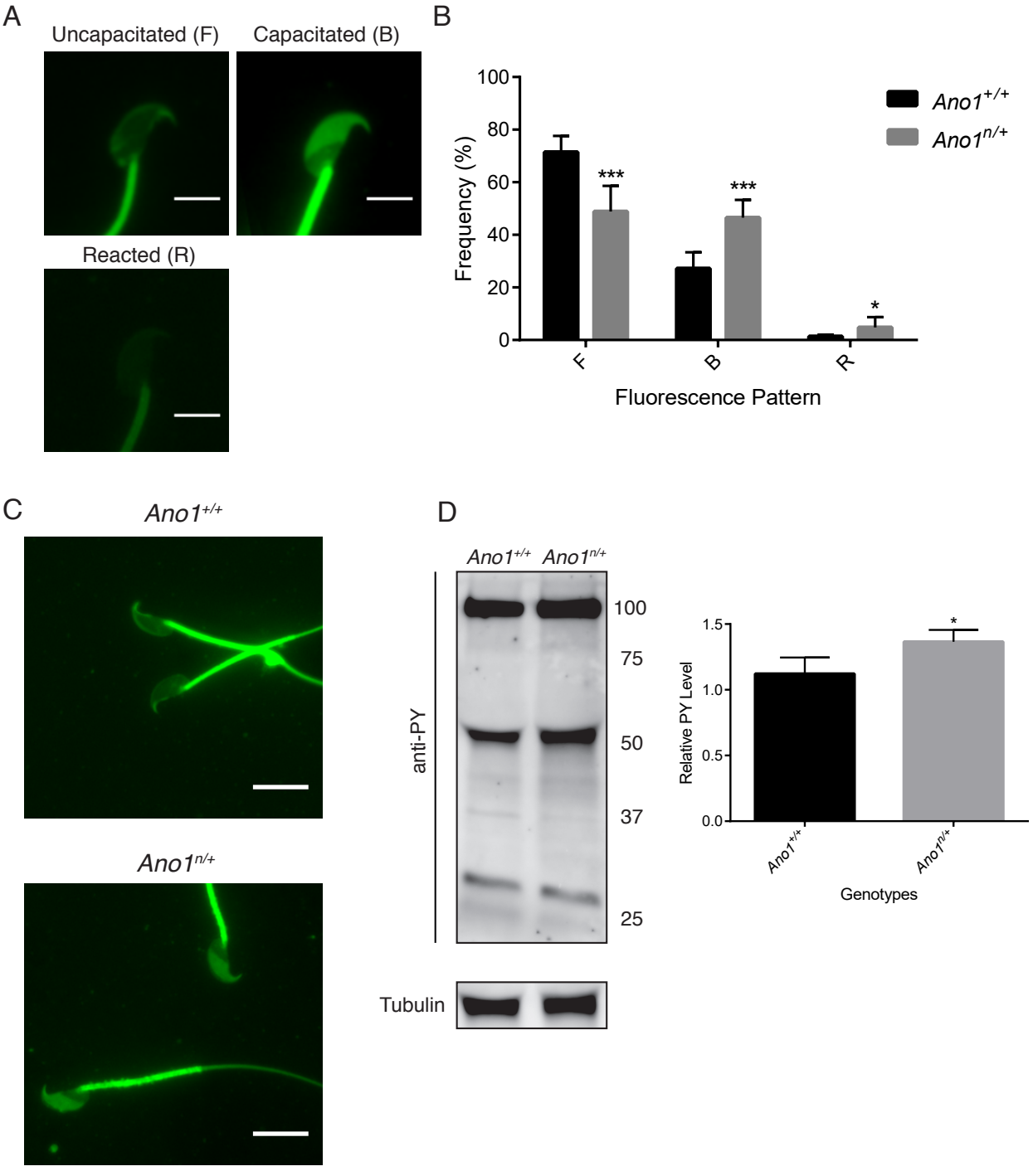
A
Uncapacitated (F)
Capacitated (B)
Reacted (R)
B
Frequency (%)
100
80
60
40
20
0
***
***
*
F
B
R
Fluorescence Pattern
Ano1+/+
Ano1n/+
C
Ano1+/+
Ano1n/+
D
Ano1+/+
Ano1n/+
anti-PY
100
75
50
37
25
Tubulin
Relative PY Level
1.5
1.0
0.5
0.0
*
Genotypes

Figure 3. Increased activation of capacitation-associated processes in *Ano1*$^{n/+}$ sperm

(A) Representative images of the three patterns of chlortetracycline (CTC) staining observed in mouse sperm. Scale bars are 5μm (B) The frequencies of the three different sperm head fluorescence patterns were quantified in *Ano1*$^{n/+}$ and *Ano1*$^{+/+}$ littermate control. (C) Representative images of common CTC fluorescence patterns observed in *Ano1*$^{n/+}$ and *Ano1*$^{+/+}$ mice. Scale bars are 10μm. (D) Left image shows western blot of tyrosine phosphorylated proteins in sperm lysates from *Ano1*$^{n/+}$ and *Ano1*$^{+/+}$ mice. Protein sizes in kDa are shown. An anti-acetylated tubulin antibody was used as loading control. Right graph shows quantification of phosphotyrosine level normalized to tubulin. Graphs show mean ± SD. * represents $p<0.05$ and *** represents $p<0.0001$.

A

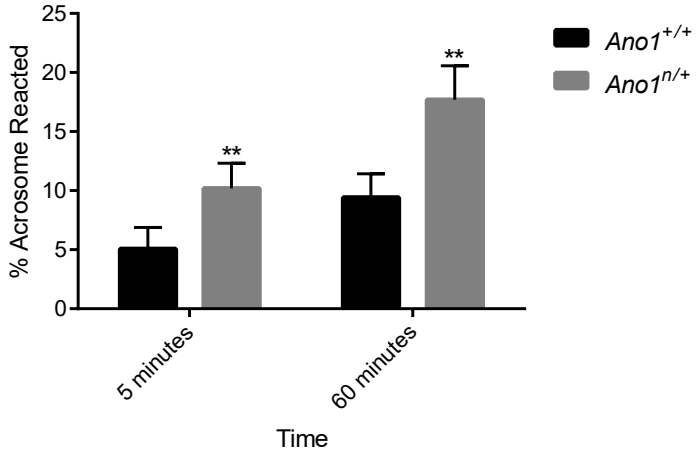
% Acrosome Reacted
25
20
15
10
5
0
**
**
5 minutes
60 minutes
Time
Ano1+/+
Ano1n/+

B

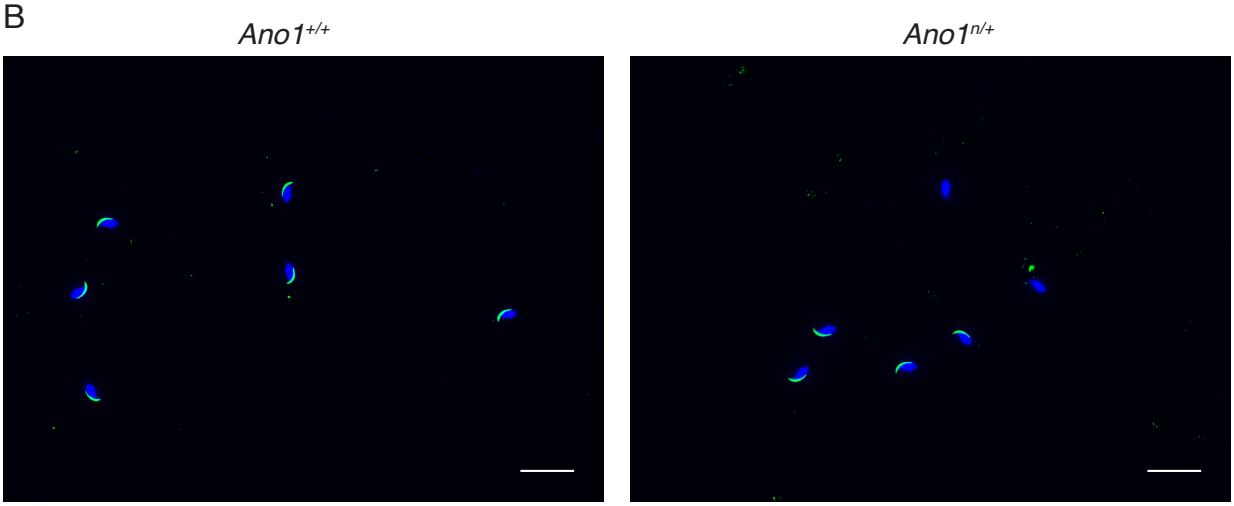
Ano1+/+
Ano1n/+

C

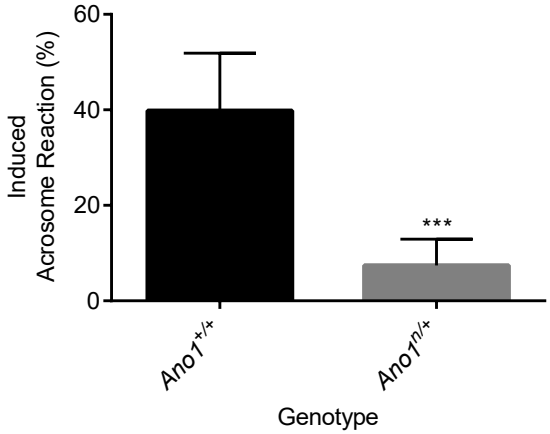
Induced Acrosome Reaction (%)
60
40
20
0
***
Ano1+/+
Ano1n/+
Genotype

Figure 4. Increased spontaneous acrosome reaction in *Ano1*$^{n/+}$ sperm

(A) PNA-FITC staining was analyzed by fluorescence microscopy to quantify the number of acrosome reacted *Ano1*$^{n/+}$ and *Ano1*$^{+/+}$ sperm following 5 minute and 60 minute incubations. (B) Representative images of sperm from *Ano1*$^{n/+}$ and *Ano1*$^{+/+}$ mice showing PNA-FITC label in green and DAPI nuclear stain in blue. Scale bars show 20μm. (C) Ionomycin-induced acrosome reaction in *Ano1*$^{n/+}$ and *Ano1*$^{+/+}$ animals was assessed by PNA-FITC staining. Graphs show mean ± SD. * represents significance cutoff of $p<0.05$.

A

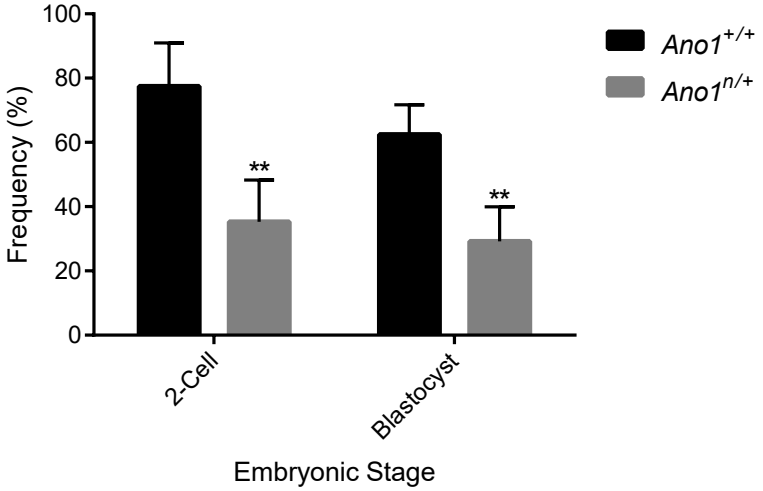
100
80
60
40
20
0
Frequency (%)
**
**
2-Cell
Blastocyst
Embryonic Stage
Ano1+/+
Ano1n/+

B

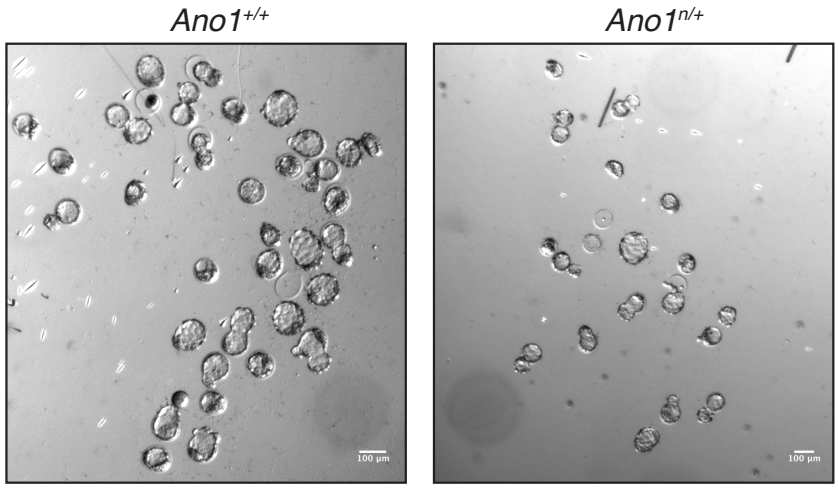
Ano1+/+
Ano1n/+
100 µm
100 µm

C

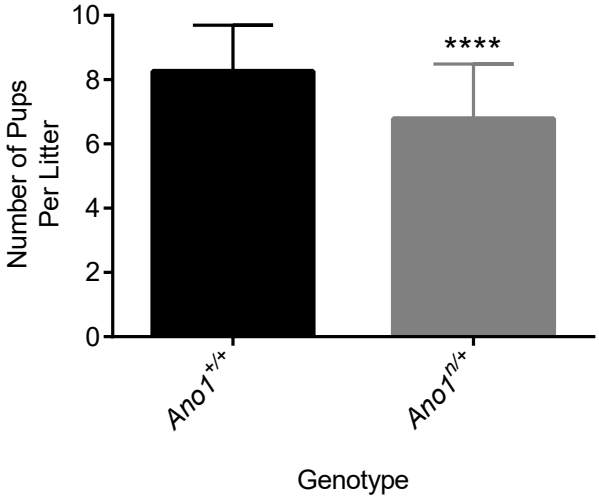
10
8
6
4
2
0
Number of Pups Per Litter
****
Ano1+/+
Ano1n/+
Genotype

Figure 5. Decreased fertilization capacity of *Ano1*$^{n/+}$ sperm

(A) The frequencies of 2-cell embryos and blastocysts were counted after *in vitro* fertilization of oocytes with *Ano1*$^{n/+}$ and *Ano1*$^{+/+}$ sperm. (B) Representative images of embryos 4 days after insemination of oocytes with *Ano1*$^{n/+}$ and *Ano1*$^{+/+}$ sperm. (C) Analysis of the number of offspring produced by breeding *Ano1*$^{n/+}$ and *Ano1*$^{+/+}$ males conventionally. Graphs show means ± SD. **** represents $p<0.0001$ and * represents $p<0.005$.

Chapter 6: Conclusion

Since the identification of ANO1 as providing an essential component of calcium-induced chloride currents, its expression in a diversity of tissues known to exhibit CaCC activity has been confirmed[1]. The early postnatal mortality of ANO1 knockout mice suggests that ANO1 may be required for diverse physiological functions *in vivo*. So far it has been shown that the comorbidities in these mice include secretory and gastrointestinal motility defects and tracheal malformations[2,3]. Experiments in adult mice using tissue-specific conditional knockout approaches have also demonstrated that ANO1 regulates salivary gland and kidney secretion[4,5]. However, the physiological functions of ANO1 within other organs are currently unknown.

In the first study, we used an inducible Cre recombinase allele that expresses within the ICC population to disrupt ANO1 expression throughout the gastrointestinal tract and determine whether ANO1 expression is required GI slow waves. Reducing ANO1 in the GI tract delayed total transit and restricted gastric emptying. Slow waves were absent from the gastric antrum in animals lacking ANO1 expression in ICCs, while the small intestine from most animals displayed slow waves despite reduced ANO1 levels. Our results support previous findings that ANO1 is required for slow wave generation in GI organs but the gastric antrum is more sensitive to loss of ANO1 expression. We also for the first time show that ANO1-mediated slow waves regulate gastrointestinal motility *in vivo*.

While lactating mammary glands express ANO1 and display CaCC activity, the expression and localization of ANO1 during MG development has not been explored. In the second study, we determined that ANO1 is expressed within the luminal-facing membrane of MG ducts and that reducing its expression with MMTV-Cre delays mammary gland development through decreased ductal outgrowth and branching. It was notable that the defects

were only observed in mammary glands isolated from 8-week old animals and that the delay dissipated by 8-weeks of age. The restriction of the delay to a brief period midway through puberty could have been caused by intrinsic variation that results from using mice on a mixed background. Future experiments should use pure background mice to reduce the influence of strain-related differences on MG development and confirm these findings.

In the third study, we investigated whether ANO1 promotes growth of *MMTV-PyMT* tumors. We first showed that ANO1 is expressed in primary tumors, lung metastasis and a *MMTV-PyMT* cell line. We demonstrate that reducing ANO1 expression abrogates growth of a *MMTV-PyMT* cell line *in vitro* and *in vivo*. The results also showed that ANO1-mediated *MMTV-PyMT* growth involves activation of an EGFR-dependent signaling pathway because treatment with chemical inhibitors of ANO1 and EGFR together does not synergistically reduce growth. These findings support previous studies which have established that EGFR and ANO1 cooperate to promote the growth of HNSCC and breast cancers. Furthermore, the study establishes that the MMTV-PyMT mouse model should be utilized in future studies to explore the functional role of ANO1 during different stages of tumorigenesis in spontaneously growing tumors *in vivo*.

In the fourth study, we described the localization and functions of ANO1 within sperm using mice heterozygous for the null allele. We showed that ANO1 is normally expressed within the heads and midpiece of mature sperm but not developing spermatids. Reducing ANO1 expression in sperm from *Ano1*$^{n/+}$ mice promotes capacitation, accelerates the spontaneous acrosome reaction and impairs fertilization *in vitro* and *in vivo*. The study demonstrates a novel role for ANO1 in regulating capacitation-associated processes and for the first time shows that genetic loss of ANO1 reduces fertilization ability of mouse sperm. These findings should

encourage future experiments to determine the mechanistic role for ANO1 during these processes.

These four studies advance our knowledge of the diverse physiological functions of ANO1. Future experiments using tissue-specific knockout approaches in adult mice will continue to establish its functions in additional tissues. Collectively, these findings will have important clinical implications since ANO1 is a suggested therapeutic target in numerous disease states.

References

1. Huang, F. *et al.* Studies on expression and function of the TMEM16A calcium-activated chloride channel. (2009).

2. Hwang, S. J. *et al.* Expression of anoctamin 1/TMEM16A by interstitial cells of Cajal is fundamental for slow wave activity in gastrointestinal muscles. *J Physiol* **587,** 4887–4904 (2009).

3. Ousingsawat, J. *et al.* Loss of TMEM16A causes a defect in epithelial Ca2+-dependent chloride transport. *J. Biol. Chem.* **284,** 28698–28703 (2009).

4. Buchholz, B. *et al.* Anoctamin 1 induces calcium-activated chloride secretion and proliferation of renal cyst-forming epithelial cells. *Kidney Int.* **85,** 1–10 (2013).

5. Catalan, M. A. *et al.* A fluid secretion pathway unmasked by acinar-specific Tmem16A gene ablation in the adult mouse salivary gland. *Proc. Natl. Acad. Sci. U. S. A.* **112,** 2263–2268 (2015).

Publishing Agreement

It is the policy of the University to encourage the distribution of all theses, dissertations, and manuscripts. Copies of all UCSF theses, dissertations, and manuscripts will be routed to the library via the Graduate Division. The library will make all theses, dissertations, and manuscripts accessible to the public and will preserve these to the best of their abilities, in perpetuity.

Please sign the following statement:

I hereby grant permission to the Graduate Division of the University of California, San Francisco to release copies of my thesis, dissertation, or manuscript to the Campus Library to provide access and preservation, in whole or in part, in perpetuity.

David Parks
Author Signature

12/26/2016
Date